AD-A188 450 TRACTION MODEL DEVELOPMENT(U) MRC BEARINGS-SKF AEROSPACE KING OF PRUSSIA PA J I MCCOOL SEP 87 AFWAL-TR-87-4079 F33615-84-C-5028 1/2

UNCLASSIFIED F/G 11/8 NL

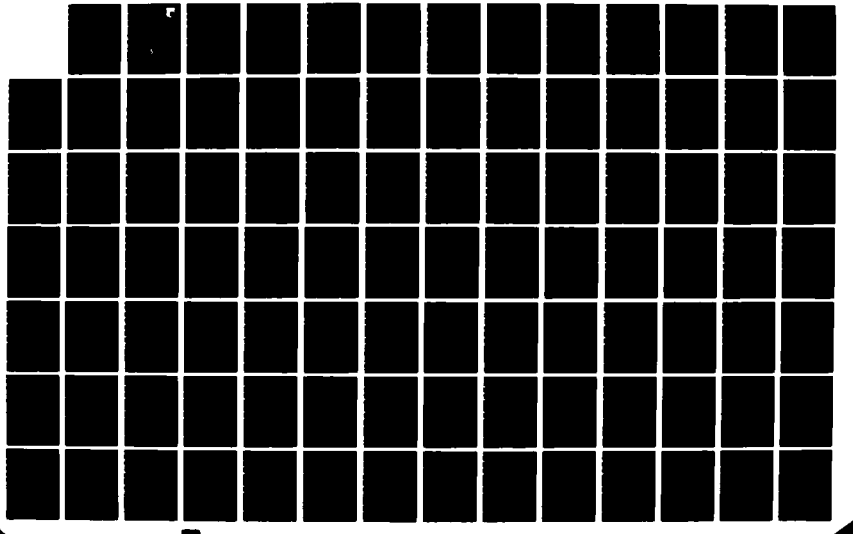

MICROCOPY RESOLUTION TEST CHART

AFWAL-TR-87-4079

TRACTION MODEL DEVELOPMENT

J. I. McCool

MRC Bearings-SKF Aerospace
Tribonetics
1100 First Avenue
King of Prussia PA 19406-1352

September 1987

Final Technical Report *for Period:* 28 September 1984 - 31 March 1987

Approved for public release; distribution is unlimited

MATERIALS LABORATORY
AIR FORCE WRIGHT AERONAUTICAL LABORATORIES
AIR FORCE SYSTEMS COMMAND
WRIGHT-PATTERSON AIR FORCE BASE OH 45433-6533

UNCLASSIFIED
SECURITY CLASSIFICATION OF THIS PAGE

A178 450

REPORT DOCUMENTATION PAGE

1a. REPORT SECURITY CLASSIFICATION UNCLASSIFIED	1b. RESTRICTIVE MARKINGS None
2a. SECURITY CLASSIFICATION AUTHORITY	3. DISTRIBUTION/AVAILABILITY OF REPORT Approved for public release; distribution is unlimited.
2b. DECLASSIFICATION/DOWNGRADING SCHEDULE	
4. PERFORMING ORGANIZATION REPORT NUMBER(S) NA	5. MONITORING ORGANIZATION REPORT NUMBER(S) AFWAL-TR-87-4079
6a. NAME OF PERFORMING ORGANIZATION MRC BEARINGS-SKF AEROSPACE 6b. OFFICE SYMBOL (If applicable)	7a. NAME OF MONITORING ORGANIZATION Air Force Wright-Aeronautical Laboratories Materials Laboratory (AFWAL/MLBT)
6c. ADDRESS (City, State and ZIP Code) 1100 First Avenue King of Prussia PA 19406-1352	7b. ADDRESS (City, State and ZIP Code) Wright-Patterson AFB, OH 45433-6533
8a. NAME OF FUNDING/SPONSORING ORGANIZATION 8b. OFFICE SYMBOL (If applicable)	9. PROCUREMENT INSTRUMENT IDENTIFICATION NUMBER F33615-84-C-5028
8c. ADDRESS (City, State and ZIP Code)	10. SOURCE OF FUNDING NOS. PROGRAM ELEMENT NO. 62102F; PROJECT NO. 2421; TASK NO. 01; WORK UNIT NO 36
11. TITLE (Include Security Classification) Traction Model Development	
12. PERSONAL AUTHOR(S) John I. McCool	
13a. TYPE OF REPORT Final	13b. TIME COVERED FROM 840928 TO 870331
14. DATE OF REPORT (Yr., Mo., Day) September 1987	15. PAGE COUNT 163
16. SUPPLEMENTARY NOTATION	

17. COSATI CODES		
FIELD	GROUP	SUB. GR.
9	2	
11	8	

18. SUBJECT TERMS (Continue on reverse if necessary and identify by block number)
Traction, Modelling, Traction Model

19. ABSTRACT (Continue on reverse if necessary and identify by block number)

This report provides the theoretical background, the numerical procedures and a comparison with test results for a PC-based computer program for computing traction force components and torque in an elastohydrodynamically lubricated contact. The program provides a comprehensive tribological assessment of a general lubricated, concentrated contact under combined rolling, spinning and sliding. The joint effect of 34 input variables can be considered in the descriptive characteristics of the contact.

(Keywords: —

20. DISTRIBUTION/AVAILABILITY OF ABSTRACT UNCLASSIFIED/UNLIMITED ☒ SAME AS RPT. ☐ DTIC USERS ☐	21. ABSTRACT SECURITY CLASSIFICATION UNCLASSIFIED
22a. NAME OF RESPONSIBLE INDIVIDUAL Dr. K. J. Eisentraut	22b. TELEPHONE NUMBER (Include Area Code) (513) 255-4860 22c. OFFICE SYMBOL AFWAL/MLBT

DD FORM 1473, 83 APR EDITION OF 1 JAN 73 IS OBSOLETE.

UNCLASSIFIED
SECURITY CLASSIFICATION OF THIS PAGE

TABLE OF CONTENTS

TABLE OF CONTENTS (Concluded)

LIST OF FIGURES

LIST OF FIGURES (Concluded)

LIST OF TABLES

1.0 INTRODUCTION

This report provides the theoretical background, the numerical procedures, a user's description and a comparison with test results for a PC based computer program for computing traction force components and torque in an elastohydrodynamically lubricated contact. The program is dubbed McFRIC because it was designed primarily to compute **FRIC**tion, including the effect of **Mc**roContacts. The program in fact provides a comprehensive tribological assessment of a general lubricated, concentrated contact under combined rolling, spinning and sliding. It reflects the joint effect of 34 input variables in computing the following descriptive characteristics of the contact:

1. The contact ellipse dimensions and area.

2. The elastohydrodynamic (EHD) film thickness both at the plateau and at the constriction that forms at the rear of a lubricated, concentrated contact under fully flooded (unstarved) and isothermal lubricant inlet conditions.

3. A film thickness correction factor accounting for a viscosity decrease of the oil in the contact inlet due to shear heating.

4. A film thickness correction factor accounting for lubricant starvation in the contact inlet.

5. The apportionment of the applied load between the asperities and the lubricant film, using the Greenwood-Williamson microcontact model with parameters estimated from the ordinary output of a stylus profile device.

6. The estimated mean square curvature of the composite surface roughness profile, the density of surface summits and the mean asperity tip radius.

7. The mean number of asperity contacts and the real contact area, i.e., the total contact area of the elastically deformed asperities.

8. The average number of microcontacts which have undergone plastic flow within the contact area at the computed surface separation.

9. An index of surface fatigue behavior based on the number and area of plastic microcontacts.

10. The magnitude of the spin torque and the magnitude and direction of the tractive force transmitted between the contacting bodies by the combined effects of (i) shearing of the fluid film and (ii) coulomb friction between contacting asperities. This computation may be performed isothermally or thermally. With the thermal option the heat generated by both types of interfacial

friction raises the temperature of the fluid film and the surfaces and alters the lubricant properties. The computed torque and force components are printed and optionally plotted as a function of sliding velocity in the rolling direction.

11. The average and maximum value of the temperature of the lubricant film and the surfaces, when the thermal option is elected.

12. The power transmitted by the contact and the power dissipated in friction. This is printed and optionally plotted as a function of sliding speed.

Section 2.0 is a narrative outline of the scope of the traction prediction problem as it is addressed in this report.

Section 3.0 is a summary of the computational procedures used for computing the thickness of the lubricant film separating the contacting bodies, accounting for the effects of lubricant film starvation and inlet heating. The relationships employed to compute the dimensions of the contact ellipse, the total elastic approach of the contacting bodies, and the contact pressure are summarized.

Section 4.0 is a description of the methodology employed to calculate the load sharing between the pressurized lubricant film and the elastically deformed surface asperities which penetrate

it. The analysis yields the density of microcontacts, the mean real and mean apparent pressure due to asperity deformation, the density of plastic microcontacts, and the mean real elastically deformed area of contact. These quantities are computed as functions of the plateau film thickness and the RMS profile height and slope of the two contacting bodies using the assumption that the surface roughness processes are isotropic and that the spectrum of the composite roughness is a power function of spatial frequency. The computation of the asperity contribution to the total traction torque and force components is developed postulating coulomb friction at the microcontacts.

Section 5.0 is a description of a nonlinear Maxwell rheological model adopted for computing fluid traction. The Trachman-Cheng constitutive law is used as the nonlinear viscous component. It is shown how the model is capable of accounting for viscous, elastic and plastic fluid behavior as appropriate.

The numerical scheme used to solve for the components of the fluid shear stress as a function of the position within the contact ellipse is outlined in Section 6.0. The fluid viscosity is taken to vary with pressure in accordance with Barus' equation. The fluid's limiting shear strength is taken to be proportional to pressure. Both of these fluid properties are therefore spatially variable over the contact ellipse via the Hertzian distribution of pressure. The integration of the shear stress

components over the contact ellipse to yield the traction force components, torque and power loss is also described.

The iterative analysis whereby the steady state solid and film mean plane temperatures are computed is described in Section 7.0. Fluid shearing and asperity friction combine to form the heat source. This heat is dissipated by the mechanisms of conduction and convection. The analysis accounts for the mean effect of temperature in the film on the lubricant viscosity and limiting shear strength.

The organization and logic flow of McFRIC is given in Section 8.0 along with a detailed description of the iterative thermal solution. This section contains instructions for installing the program and for the preparation of input data. A sample program input file and the corresponding program output are given.

Section 9.0 contains a description of the traction tests conducted at AFML including lubricant selection, specimen and test rig description the choice of test variables and the specific test matrices used for each lubricant.

Lubricant specific rules for the computation of six physical properties as a function of temperature are described for each of the three test fluids. Computation of the limiting shear strength of the fluid and of the shear modulus of the composite system comprising the lubricant and the near surface layers of the contacting bodies, is discussed.

Reduction of the traction test data and the compilation of a traction data base is described in Section 10.0. These data are used as input to McFRIC in an effort to predict the experimental traction curves. The data showed that the thermal effect was overpredicted when the limiting shear strength was taken to vary inversely with absolute temperature. With this dependence removed the relatively minor thermal effects exhibited by the data were well explained with a thermally dependent viscosity.

Fits were found to be acceptably good for all cases in which the Deborah number computed at the mean Hertzian pressure via Barus' Law exceeded unity. This included all of the data for two of the oils and roughly half of the data for the third. For the cases in which the Deborah number was less than unity the predicted curves approached their asymptotic value with increasing strain rate too slowly. An approach is adopted for these cases of using an empirical viscosity value to bring the prediction into accord with the experimentally observed traction curve slopes. This approach though successful is shown to be equivalent to simply increasing the Deborah number. It is suggested that the Trachman-Cheng model may need to be supplemented with a further lubricant dependent parameter that governs the speed of convergence to the limiting shear strength as shear rate increases.

In the concluding part of Section 10.0 regression fits to the limiting shear strength and elastic modulus values for the three

oils are listed. Using these approximate equations one may use McFRIC for conditions of load, speed, contact ellipse aspect ratio and temperature for which traction tests are not available.

Numerous contributions were made in the early stages of this work by Gail Hadden and Lea Sheynin. Robert Aman compiled the traction data base and authored the program MATPROP. Mark Ragen converted McFRIC to run on a PC and developed the input data structure. He also provided the information for program users given in Section 8.0. John Walsh and Monica Friday conducted most of the McFRIC runs and reruns and performed the data plotting. Advice and many valuable suggestions offered in technical discussions with Dr. Luc Houpert of SKF during the course of this work, are gratefully acknowledged.

2.0 PROBLEM STATEMENT

The subject being addressed herein is the lubricated contact of two moving elastic bodies, focusing on the problem of predicting the resultant forces and torque due to the tangential stresses distributed over their interface.

The forces are known as friction or traction forces; the torque as spinning moment or spinning torque.

The bodies are assumed to be bounded by surfaces of revolution with their separation in the vicinity of a point of deformationless contact, assumed to be adequately approximable as a second degree polynomial in a system of coordinates having its origin at the contact point. With this assumption, and in the absence of a lubricant, the equations of Hertz apply for the calculation of 1) the mutual approach of the bodies under a load P 2) the dimensions a and b respectively, of the semimajor and seminor axes of the elliptical interfacial contact area and 3) the elliptically paraboloid distribution of interfacial normal pressure. Figure 2.1 shows the contact and relevant velocities and dimensions. The two surfaces are presumed to move with respective velocities u_1 and u_2 in a direction coincident with one of the principal axes of the contact ellipse. The average velocity in that direction is denoted $u = (u_1 + u_2)/2$. u is customarily termed the rolling or longitudinal velocity. The difference $\Delta u = u_1 - u_2$ is known as the sliding or slipping velocity.

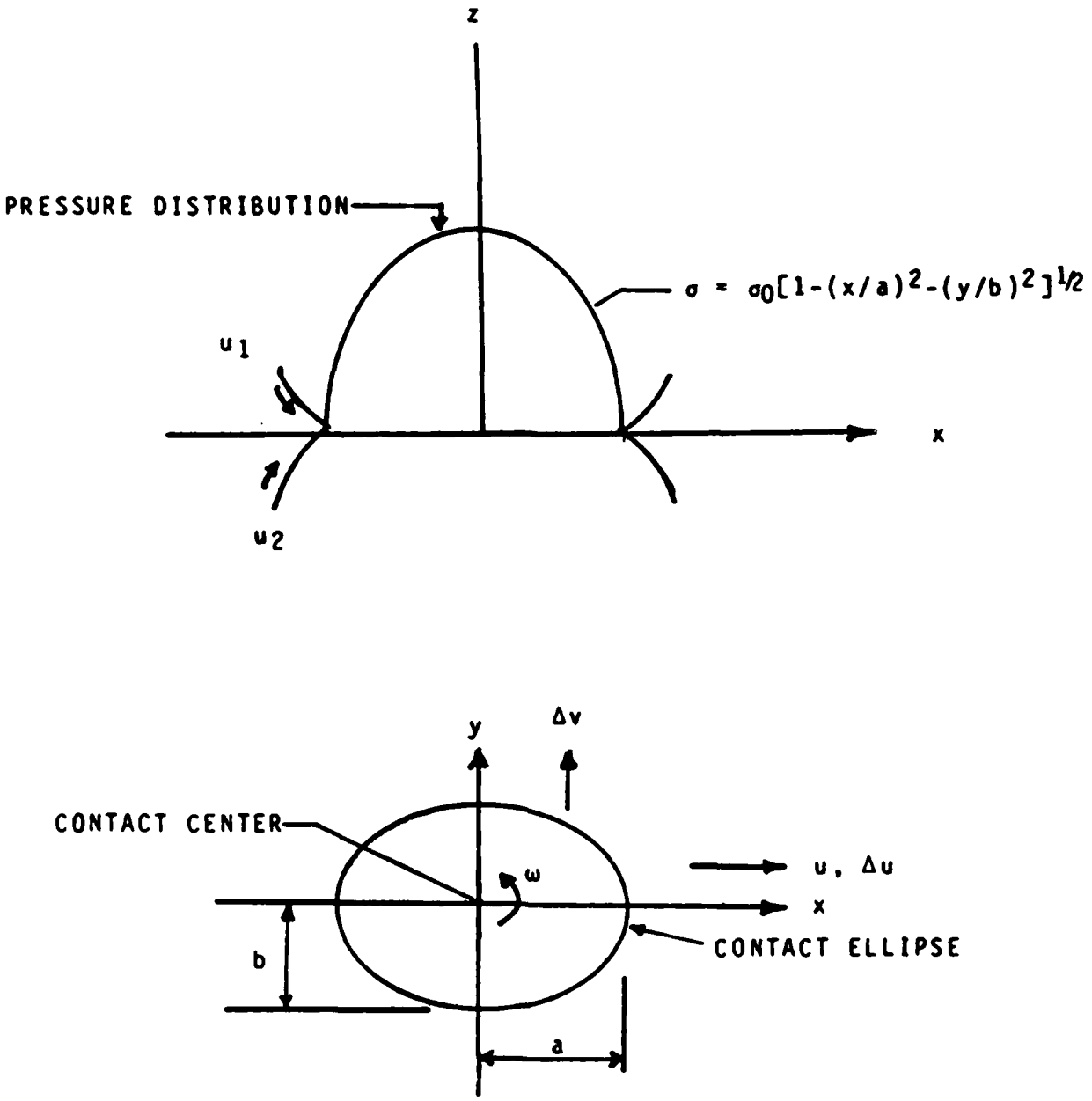

Fig. 2.1 MOVING BODIES IN DRY CONTACT

Δv denotes the velocity difference in the direction orthogonal to u. It is known as the transverse sliding velocity or side slip. Finally, a relative rotational velocity known as spin may act about an axis perpendicular to the contact ellipse and through its center.

Figure 2.1(b) shows the distribution of interfacial pressure and its equation expressed in an orthogonal coordinate system established at the contact center and with the x-axis coincident with the semimajor axis of the contact ellipse. This pressure integrates over the contact area to a force equal to the applied normal force P.

If a viscous lubricant is introduced and adheres to the surfaces as they approach the converging inlet to the contact region, a fluid pressure builds and, for the class of fluids typically used as lubricants, the viscosity increases and the surfaces separate and deform to allow the fluid to pass through the contact region or 'nip' as it is referred to in some literature.

Figure 2.2 shows the consequences of the introduction of the lubricant on the dry contact pressure distribution and shape of the gap between the contacting bodies. The pressure distribution is extended forward in front of the dry contact ellipse. The gap is relatively flat except for a constriction near the exit end of the contact. A large 'spike' in the pressure distribution precedes the exit constriction as shown.

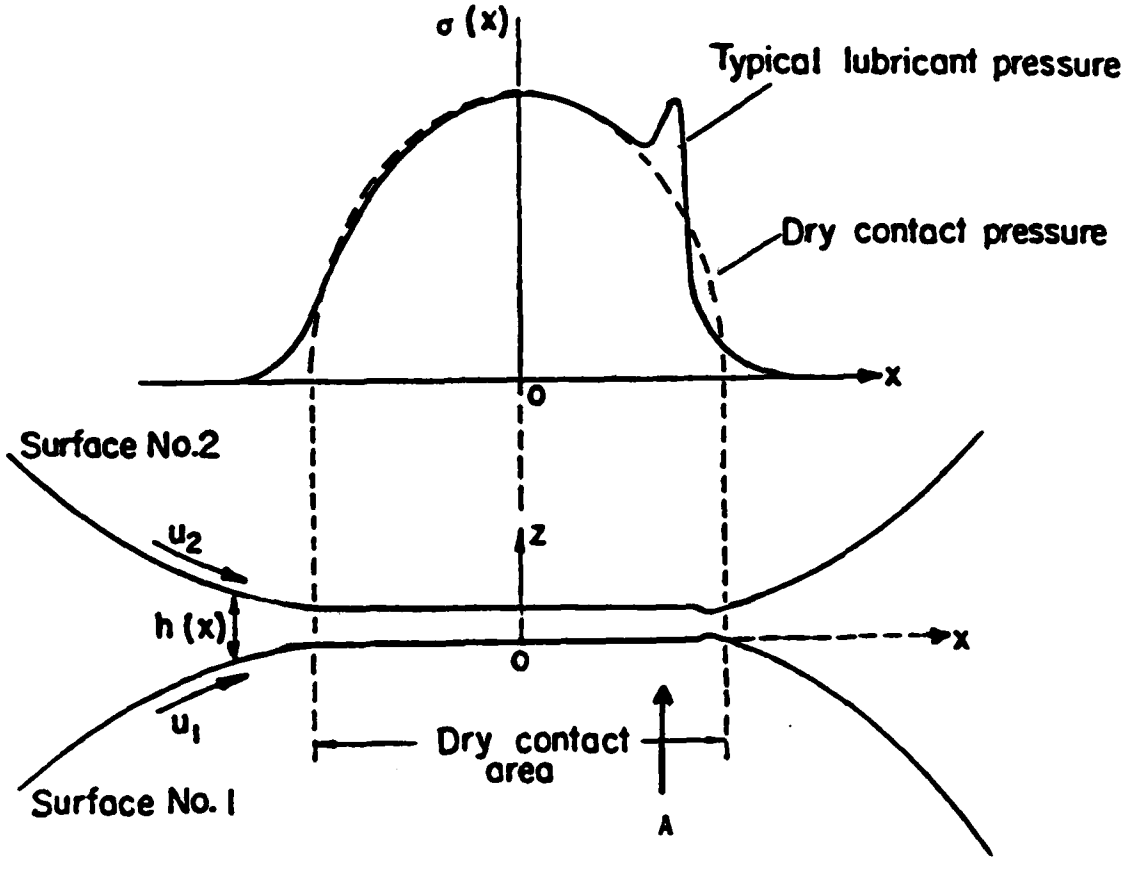

Fig. 2.2 FILM SHAPE AND PRESSURE DISTRIBUTION

The exact thickness and slope of the lubricant film is determined by the joint solution of the Reynold's equation of hydrodynamics and the deformation equations of contact elasticity. The film separating the surfaces is consequently known as an elastohydrodynamic (EHD) film.

The thickness of the lubricant film separating the surfaces is small (typically 0.1 - 1 μm) and is frequently of the same order as the microscale roughness of the contact bodies. The bodies cannot, therefore, in general be considered to be fully separated by the lubricating film. Instead there will be a random number of microcontacts taking place through the lubricant film as shown in Figure 2.3. The expected number of such contacts will depend for a given contact size upon the ratio of the mean film thickness to the root mean square value of the lubricant gap separating the surfaces. This ratio is often termed the film parameter and is designated by the symbol Λ. For $\Lambda > 3$ the expected number of such contacts is negligible. This state of affairs is known as the full film regime. For $\Lambda < 3$ one refers to a partial film or mixed lubrication regime.

In this work we address both the full film and the partial film regimes.

We may now state the problem being considered.
Given the following variables:

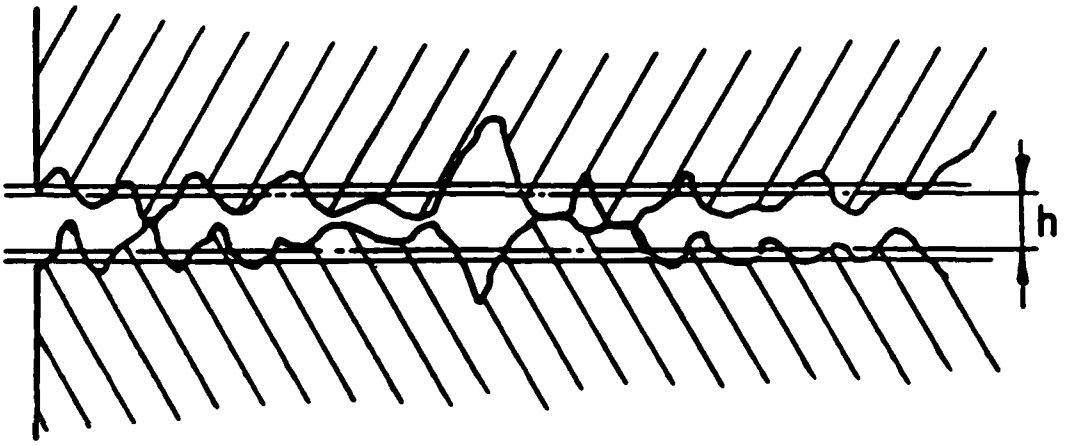

Fig. 2.3 ASPERITY CONTACTS THROUGH PARTIAL OIL FILM

1. The size and shape of the contacting bodies.
2. The material of the contacting bodies.
3. The characteristics of the surface roughness of the contacting bodies.
4. The ambient temperature.
5. The lubricant properties as functions of pressure and temperature.
6. The imposed kinematic conditions u_1, u_2, Δv and ω,

calculate the magnitude and direction of the shear force τ at each point within the contact region considering the locally variable conditions of relative velocity, pressure, temperature and gap width at each point. Sum (integrate) these forces to give the orthogonal components F_x and F_y of the total traction force and the total traction or spin moment M.

In the above statement of the problem the kinematics have been considered known. In implementation, e.g. in an analysis of bearing dynamics, the converse problem is met i.e. it is necessary to determine the velocities (e.g. Δu) for which the resultant traction force provides equilibrium. A series of solutions are therefore usually wanted giving, e.g., the traction force F_x in the rolling direction or perhaps the traction coefficient F_x/P as a function of Δu or, more often, as a function of the slip-to-roll ratio $\Delta u/u$. Thus, a full solution of the traction prediction problem should include the facility of varying the

kinematics systematically and calculating the associated traction force components and spinning moment.

The solution of the traction prediction problem involves making the appropriate choice of a relationship between the conditions at each point (pressure, relative velocity, temperature, gap thickness, etc.) and the shear stress and in deducing the constants and properties which are embodied in that relationship.

3.0 FILM SHAPE, CONTACT DIMENSIONS AND PRESSURE DISTRIBUTION

In this section the method adopted for the computation of key variables which affect the solution of the traction prediction problem is outlined. These variables are 1) the thickness and shape of the lubricant film that separates the surfaces, 2) the shape and dimensions of the interfacial contact area between the surfaces and 3) the magnitude, shape and location of the interfacial pressure distribution.

3.1 Film Shape

As noted, the introduction of lubrication has the effect of separating the contacting surfaces by a film of virtually constant thickness over a central plateau region while providing a somewhat smaller film separation over a narrow constriction that forms at the rear of the contact. As is customary in traction calculations, the film shape will be taken to be constant with thickness equal to the computed plateau thickness.

Highly accurate solutions for the plateau film thickness have been developed by Hamrock and Dowson [1] for the fully flooded condition where a copious lubricant supply is available and for the 'starved' case where the lubricant meniscus is at a finite distance X_b, forward of the contact center as shown in Figure 3.1. The value of X_b responds to the method of lubricant supply. By specification of X_b it will be possible for the user of the

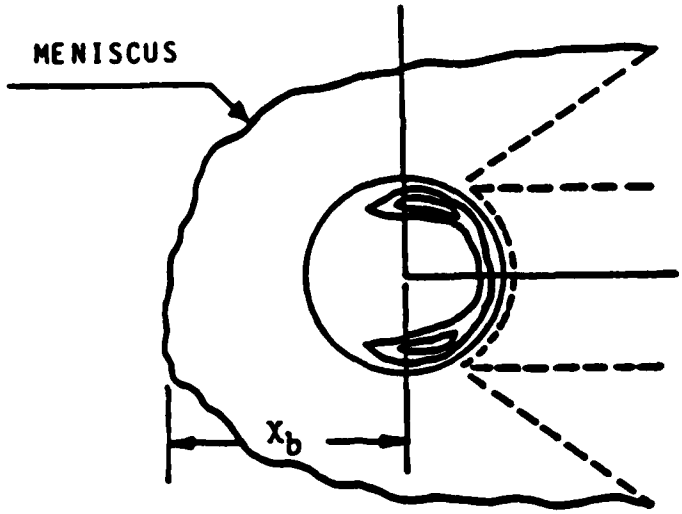

(a)

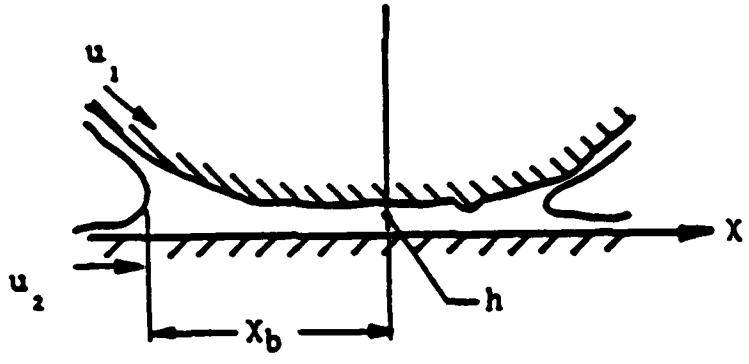

(b)

Fig. 3.1 EHD FILM SHAPE AND INLET MENISCUS GEOMETRY

traction model to account quantitatively for the effect of lubricant supply rate on the traction condition. Heating in the inlet will increase the inlet temperature above ambient, thus lowering the viscosity and hence the EHD film. A multiplicative reduction factor is used to account for this effect as discussed below:

3.1.1 Fully Flooded Central Film Thickness

The plateau or central film thickness that develops in a lubricated contact under flooded conditions, i.e. conditions of copious lubricant supply, is calculated according to the formula developed by Hamrock and Dowson [1].

$$h_{c,f} = 2.69\ R_x\ V^{0.67} G1^{0.53} W^{-0.067} (1-0.61e^{-0.73b/a}) \qquad (3.1)$$

where

$$V = \eta_0\ u/(E' R_x)$$

$$W = P/(E' R^2_x)$$

$$G1 = E'\alpha$$

η_0 = absolute viscosity at ambient pressure and temperature

u = entrainment velocity, i.e., the average surface velocity in the rolling direction

$$E' = 2\ [((1-\nu^2_1)/E_1 + (1-\nu^2_2)/E_2)]^{-1} \qquad (3.2)$$

E_1, E_2 = Young's moduli of two contacting bodies

ν_1, ν_2 = Poisson's ratio for the two contacting bodies

R_x = effective radius in rolling direction

α = pressure viscosity coefficient

a,b = contact ellipse semi-axes in the direction of and transverse to the rolling direction

This formula was developed by curve fitting to the results obtained in full computer solutions of the equations of elasticity and hydrodynamics. The results were obtained for cases with b > a, i.e. with the contact ellipse major axis transverse to the rolling direction but, as stated by Hamrock and Dowson, remain plausible for a > b.

3.1.2 Starved Central Film Thickness

The starved central film thickness $h_{c,s}$ is calculated by multiplying the fully flooded central thickness $h_{c,f}$ by the 'starvation' factor $\varphi_{s,c}$. $\varphi_{s,c}$ is computed as

$$\varphi_{s,c} = \left[\frac{(X_b/a - 1)}{(m^* - 1)}\right]^{0.29} \quad ; \quad X_b/a < m^* \qquad (3.3)$$

$$= 1.0 \quad ; \quad X_b/a > m^*$$

$$m^* = 1 + 3.06\,[(R_x/a)^2\,(h_{c,f}/R_x)]^{0.58} \qquad (3.4)$$

Formulas comparable to Eqs. (3.1) and (3.3) have been developed for the constriction film thickness as well. These are also incorporated in McFRIC and the constriction film thickness is printed for reference.

3.1.3 Film Reduction Due to Inlet Heating

Convergence of the lubricant film in the EHD contact inlet results in heating of the inlet oil with a consequent loss in viscosity and thinning of the lubricant film. Murch and Wilson [2] have analyzed this problem and derived a multiplicative factor φ_t which may be applied to the isothermally calculated film to correct for this effect. The factor is given by

$$\varphi_t = 1/(1 + 0.108A^{0.62}) \tag{3.5}$$

where

$$A = 4\eta_0 \beta u^2/k \tag{3.6}$$

and

k = heat conductivity of the oil

β = temperature viscosity coefficient $(°R)^{-1}$ defined through Reynold's viscosity-temperature relation

$$\eta = \eta_0 e^{-\beta(T-T_0)}$$

T = temperature

η_0 = viscosity at temperature T_0 and ambient pressure

u = entrainment velocity

3.2 Contact Ellipse Dimensions and Pressure

The calculation of elastic contact ellipse dimensions and the contact pressure follows classical Hertzian theory [3].

Figure 3.2 shows the assumed undeflected forms and dimensions of the bodies that comprise the type of contacts that are being considered. Prior to deflecting under the load P, the boundaries of the bodies in the vicinity of contact are surfaces of revolution. The principal planes, i.e., the orthogonal planes in which the radii of curvature are largest or smallest are assumed to coincide. The principal radius for Body I in Plane 1 is denoted r_{I1}. Correspondingly, the principal radius for Body II in Plane 1 is denoted r_{II1}. The principal radii in Plane 2 are denoted r_{I2} and r_{II2}, respectively.

Under the action of the load P, the surfaces will deflect and the region of contact will expand from a point to an elliptical area. The axes of the contact ellipse will be parallel to the principal planes. Whether the major axis of the contact ellipse is parallel to Plane 1 or to Plane 2 depends upon the relative magnitudes of the principal radii.

It is possible to consider a somewhat more general contact situation in which the principal planes for Bodies I and II make

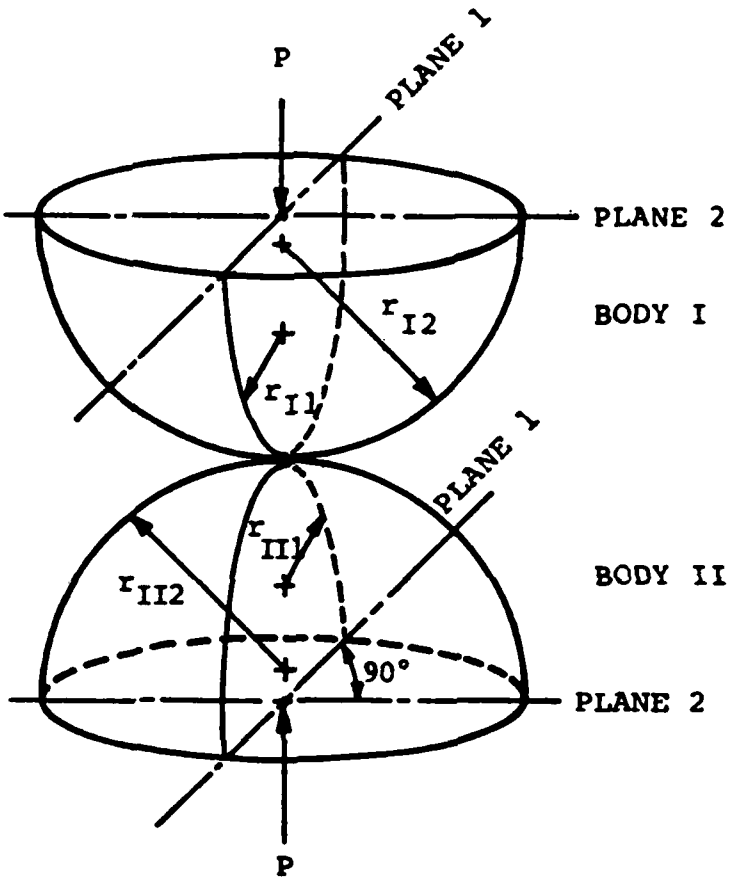

Fig. 3.2 PRINCIPAL PLANES & RADII FOR CONTACTING BODIES

an arbitrary angle with each other. However, inasmuch as the most complete state-of-the-art film thickness and fluid traction models assume that the rolling direction is parallel to one of the axes of the contact ellipse, we limit consideration to the geometry of Figure 3.2.

We define the principal curvatures ρ_1, ρ_2 of a body as the reciprocals of the principal radii r_1, r_2. The curvature associated with a given direction is taken to be algebraically positive if the body is convex in that direction and negative if concave. The curvature sum for a contact is defined as:

$$\Sigma\rho = \rho_{I1} + \rho_{I2} + \rho_{II1} + \rho_{II2} \tag{3.7}$$

The auxiliary quantity $F(\rho)$ is defined as:

$$F(\rho) \equiv \frac{(\rho_{I1} + \rho_{II1}) - (\rho_{I2} + \rho_{II2})}{\Sigma\rho} \tag{3.8}$$

If $F(\rho) > 0.0$, the major axis of the contact ellipse is parallel to Plane 2 in Figure 3.2. If $F(\rho) < 0.0$, it is parallel to Plane 1.

The ratio κ of the major to minor axes of the contact ellipse is found by solving the transcendental equation

$$ABS(F(\rho)) = \frac{(\kappa^2+1)\ E(\kappa)-2F(\kappa)}{(\kappa^2-1)\ E(\kappa)} \tag{3.9}$$

where ABS(•) denotes the absolute value function and $F(\kappa)$ and $E(\kappa)$ denote the complete elliptical integrals of the first and second kinds defined, respectively, by:

$$F(\kappa) = \int_0^{\pi/2} [1-(1-\kappa^{-2})\sin^2\phi]^{-1/2}\, d\phi \qquad (3.10)$$

and

$$E(\kappa) = \int_0^{\pi/2} [1-(1-\kappa^{-2})\sin^2\phi]^{1/2}\, d\phi \qquad (3.11)$$

The major axis ℓ_1 may be calculated as

$$\ell_1 = \left(\frac{6\kappa^2 E(\kappa)}{E'\pi\ \Sigma\rho} P\right)^{1/3} \qquad (3.12)$$

where

P = applied load

$$E' = 2\left[\frac{1-\nu^2 I}{E_I} + \frac{1-\nu_{II}^2}{E_{II}}\right]^{-1}$$ reduced elastic modulus

$E_{I,II}$ = elastic moduli of Bodies I and II

$\nu_{I,II}$ = Poisson's ratio

The minor axis is computed as

$$\ell_2 = a/\kappa \qquad (3.13)$$

The contact area A is

$$A = \pi\ \ell_1\ell_2 \qquad (3.14)$$

The total distance δ through which remote points within the contacting bodies move under the action of the load P, is

$$\delta = F(\kappa) \bullet \left[\frac{9(\Sigma\rho)}{2E(\kappa)} (P/\pi\kappa E')^2\right]^{1/3} \qquad (3.15)$$

The maximum pressure σ_0 acting on the contact ellipse is

$$\sigma_0 = 1.5\ P/A \qquad (3.16)$$

The average pressure p is simply,

$$p = P/A \tag{3.17}$$

3.3 Pressure Shift

As noted, the presence of the lubricant redistributes the interfacial pressure from its dry contact, Hertzian, shape. Tevaarwerk and Johnson [4] suggested that to a first approximation this effect could be modelled as a forward shift δ_x of the dry contact pressure distribution. The dry contact center still serves as the axis of spin since that is kinematically determined.

The displacement δ_x of the load center due to the redistribution of Hertzian pressure by the lubricant film as shown in Figure 3.3, is calculable by the formula developed by Hamrock and cited in Tevaarwerk and Johnson [4].

$$\delta_x = 4.25\ a\ (g_1)^{0.022}\ (g_2)^{-0.35}\ (b/a)^{0.91} \tag{3.18}$$

where g_1 and g_2 are the following dimensionless variables:

$$g_1 = \frac{\alpha P^3}{\eta_0 u^2 E' R_x^4} \tag{3.19}$$

$$g_2 = \left\{\frac{P}{\eta_0^3 u^3 E' R_x^5}\right\}^{2/3} \tag{3.20}$$

As noted, the magnitude of the contact ellipse dimensions and pressure distribution are calculated using the Hertz equations.

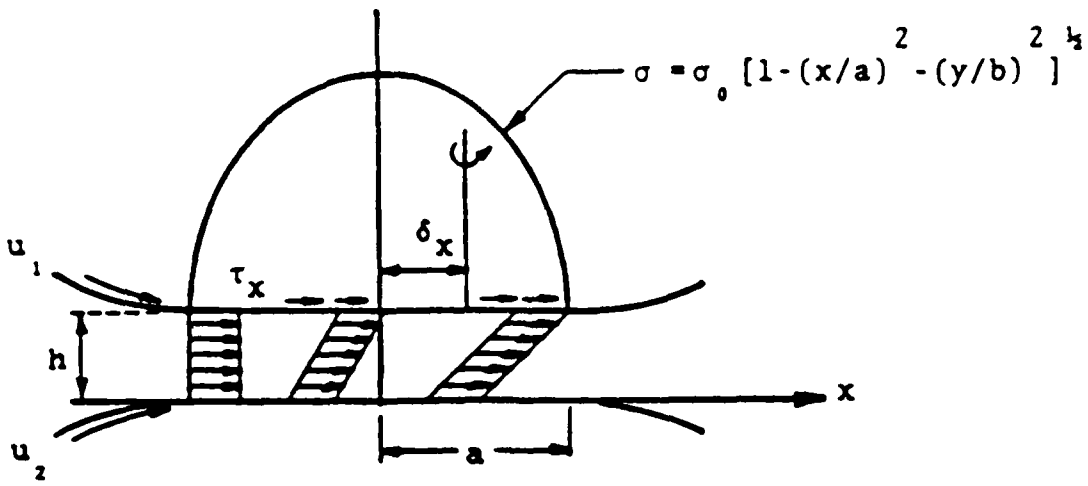

(a) OIL FILM SHEARING

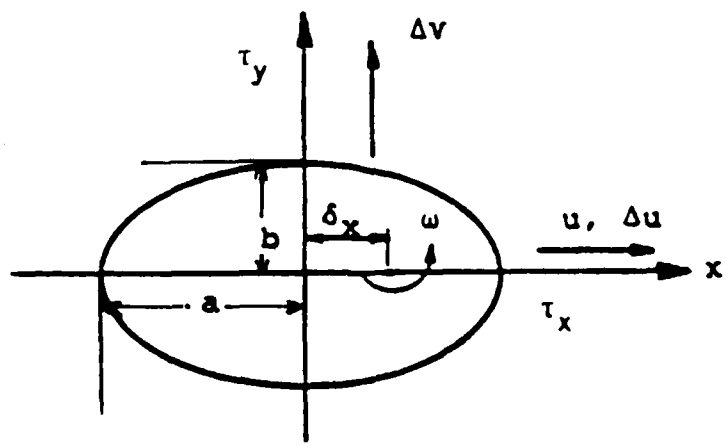

(b) CONTACT GEOMETRY

Fig. 3.3 IDEALIZED EHD CONTACT GEOMETRY AND KINEMATICS WITH SHIFTED PRESSURE DISTRIBUTION

Figure 3.3 shows the shifted pressure distribution and interfacial area over which the shear stresses are appreciable.

3.4 Deborah Number

As discussed in depth below in Section 5.0, the Deborah number plays a key role as a determinant of whether a fluid behaves viscously or elastically as it deforms under sliding conditions. For an isoviscous fluid, the Deborah number is defined as

$$T = \eta u/aG \tag{3.21}$$

where η, u and a as defined previously are the viscosity, entrainment velocity and contact ellipse semi axis in the rolling direction. G is the shear modulus of the elastic composite formed by the fluid and the contacting bodies.

Inasmuch as the viscosity varies with pressure through the contact, the Deborah number is a point function of the spatial coordinates within the contact region. To compute a representative number one could use a value of the viscosity averaged by means of an appropriate pressure viscosity law over the contact pressure distribution. As a simple approach in computing the Deborah number, the average viscosity is approximated as the viscosity at the average pressure computed using the Barus relation. That is,

$$\eta = \eta_o \, e^{\alpha \bar{p}} \tag{3.22}$$

where $\bar{p}$, the average pressure is

$$\bar{p} = 2/3 \, \sigma_o \tag{3.23}$$

and η_o is the viscosity at ambient pressure.

If the Barus' equation applies over the full contact, the average viscosity will substantially exceed the viscosity computed in this manner. Nevertheless the value thus computed is indicative, in that it responds to changes in pressure and ambient viscosity. Quantitative interpretation of T, i.e., classifying fluid behavior based on the value of T is discussed in Section 10.0.

4.0 ASPERITY CONTACT TRACTION MODEL AND SURFACE FATIGUE INDEX

As indicated in Section 2.0, considering the partial EHD regime brings the added complexity of asperity contact into the traction prediction problem. Bair and Winer [5] show curves of traction force against the film parameter Λ, in which a six fold increase of traction occurs as Λ decreases from 1.0 to 0.3. Clearly the role of asperity contact cannot be ignored.

The approach taken within program McFRIC is to use the Greenwood-Williamson (GW) microcontact model [6] to determine the average force acting at a contacting asperity, the number of microcontacts per unit area and the real contact area as a function of the apparent area. A summary of the GW model is given in Section 4.1 below.

The three GW model parameters are deduced in terms of the RMS height and RMS slope using the spectral estimation approach proposed by McCool [7]. This method is summarized in Section 4.3.

Assuming that coulomb friction with a known friction coefficient acts at the deformed asperities the statistical expectation of the net traction force components and torque is computed as described in Section 4.4.

4.1 The Greenwood-Williamson Microcontact Model

The Greenwood-Williamson microcontact model applies to the contact of a rough surface and a smooth plane. It is based on the assumptions that:

1. Asperities have spherically capped summits of constant radius **R** irrespective of their height.

2. Asperities are mechanically independent, i.e. the load they support depends on their height and not upon the load supported by neighboring asperities.

3. Asperities deform elastically in accordance with the Hertzian relations between deflection, load and contact area.

4. Summit height expressed as a deviation from the mean plane of the summits is a random variable and follows a gaussian probability distribution with standard deviation σ_s.

Comparisons of the Greenwood-Williamson model with more comprehensive models that relax many of its seemingly restrictive assumptions, show that it is nonetheless astonishingly accurate in its predictions [8]. In view of this and its simplicity to use, it has been adopted as the microcontact model for use within McFRIC.

The GW model requires three input parameters:

D_{SUM} : the surface density of summits

σ_s : the standard deviation of the probability distribution of summit heights and

R : the deterministic (non-random) radius of the spherical summit caps.

Given the values of these parameters, the contact density ZNCON, the total asperity supported force TOTF, the total real area of contact per unit nominal area, TOTA, and the average asperity supported force AVF, are computed as:

$$ZNCON = D_{SUM} \bullet F_0(d/\sigma_s) \tag{4.1}$$

$$TOTA = \pi D_{SUM} R \sigma_s F_1(d/\sigma_s) \tag{4.2}$$

$$TOTF = 1.333 A_0 D_{SUM} E' R^{1/2} \sigma_s^{3/2} F_{3/2}(d/\sigma_s) \tag{4.3}$$

and

$$AVF = 1.333 E'R^{1/2} \sigma_s^{3/2} F_{3/2}(d/\sigma_s)/F_0(d/\sigma_s) \tag{4.4}$$

The density N_p of plastic contacts, i.e., of contacts which have experienced some degree of subsurface plastic flow is given by

$$N_p = D_{SUM} \bullet F_0 (d/\sigma_s + w_p^*) \tag{4.5}$$

The elastically computed microcontact area, A_p, of the plastically deformed contacts, per unit nominal area A_0, is given by:

$$A_p/A_0 = D_{SUM} \bullet F_1 \ (d/\sigma_s + w_p^*) \tag{4.6}$$

where

$$E' = [(1-\nu^2_1)/E_1 + (1-\nu_2{}^2)/E_2]^{-1} \tag{4.7}$$

E_1, E_2 = Young's modulus for the rough and smooth surfaces

ν_1, ν_2 = Poisson's ratios for the rough and smooth surfaces

$$w_p^* \equiv 6.4R(Y/E')^2/\sigma_s \tag{4.8}$$

Y = Yield strength of rough surface in simple tension

$F_o(\bullet), F_1(\bullet), F_{3/2}(\bullet)$ = Functions defined in terms of the standard gaussian density function. Values are tabled e.g. in [8]. Piecewise approximations to these functions are employed within McFRIC.

4.2 Fatigue Index

If the microcontact area is denoted **A**, the number of plastic contacts acting over this area, ZNPLAS, is given by:

$$ZNPLAS = N_p \bullet A \tag{4.9}$$

The mean area APLAS of a plasticized asperities is

$$APLAS = A_p/A_0 \bullet A/ZNCON \tag{4.10}$$

An index of fatigue behavior ϕ, proposed in [19], is the product of the number and average area of plastic contacts i.e.,

$$\phi = \text{ZNPLAS} \bullet \text{APLAS} \tag{4.11}$$

It is reasoned that the higher the value of ϕ, the greater the opportunity for surface initiated fatigue failure. No studies have yet been performed to quantify the relation between fatigue life and ϕ. It is nonetheless a reasonable index to use to gauge relative performance of a number of surface/lubricant combinations.

4.3 Relating the GW Parameters to Spectral Moments

In work subsequent to the development of Greenwood and Williamson's model, it was found that the GW parameters could be expressed in terms of 3 quantities, m_0, m_2 and m_4, known as spectral moments. These values may be determined from a profile $z(x)$ as

$$m_0 = \text{AVG}\ (z^2(x)) \tag{4.12}$$

$$m_2 = \text{AVG}\ [(dz(x)/dx)^2] \tag{4.13}$$

$$m_4 = \text{AVG}\ [(d^2z(x)/dx^2)^2] \tag{4.14}$$

where $z(x)$ represents the profile height deviation from the surface mean plane at some position **x**, relative to an arbitrary origin. m_0 is, of course, R_q^2 and is frequently called σ^2 in the Tribology literature. m_2 is the mean square slope and m_4 is, very nearly, the mean square curvature.

Under the assumption that $z(x)$ is a gaussian random variable the summit density, D_{SUM}, is given by Longuet-Higgins [9] as

$$D_{SUM} = (m_4/m_2)/6\pi\sqrt{3} \qquad (4.15)$$

Bush et al [10] suggest that the radius **R** may be approximated as the reciprocal of the average summit curvature and give the expression

$$R = 0.375\ (\pi/m_4)^{1/2} \qquad (4.16)$$

Bush et al also express the summit height standard deviation σ_s as

$$\sigma_s = (1-0.8968/\alpha)^{1/2}\ m_0^{1/2} \qquad (4.17)$$

where α, termed the bandwidth parameter, is defined as:

$$\alpha \equiv (m_0 m_4)/m_2^2 \qquad (4.18)$$

It is more usual in Tribology to use the profile mean plane as a reference than the summit mean plane used by the GW model. Figure 4.1 shows that a smooth surface whose height above the summit mean plane is **d**, is situated at a distance $h = d + \bar{z}$ above the profile mean plane. The difference in mean planes is expressible as (Bush et al [10])

$$\bar{z} = 4(m_o/\pi\alpha)^{1/2} \qquad (4.19)$$

Using Eqs. (4.17) and (4.19) the film parameter Λ i.e., the ratio $h/R_q \equiv h/\sigma$ is found to be linearly related to d/σ_s as:

$$d/\sigma_s = [(h/\sigma) - 4/(\pi\alpha)^{1/2}]/(1-0.8968/\alpha)^{1/2} \qquad (4.20)$$

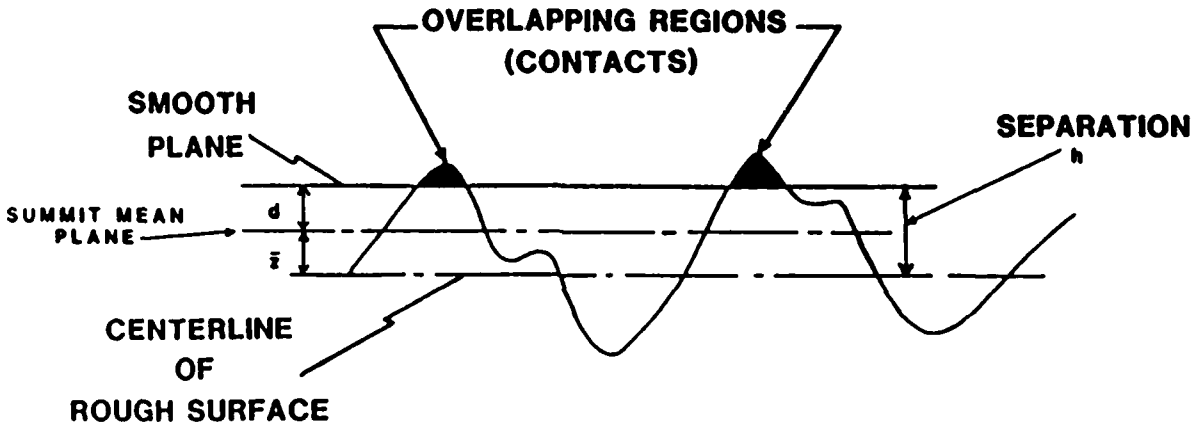

Fig. 4.1 RELATION BETWEEN SUMMIT AND SURFACE MEAN PLANES

For a specified h/σ value and given values of m_0, m_2 and m_4, one may use Eq. (4.20) to find d/σ_s and thereafter, Eqs. (4.1) to (4.4) to compute the microcontact conditions at that h/σ value. When both surfaces are rough an equivalent smooth and rough surface is considered in which the values of m_0, m_2 and m_4 are summed for the two rough surfaces, i.e.:

$$m_0 = (m_0)_1 + (m_0)_2 \tag{4.21}$$

$$m_2 = (m_2)_1 + (m_2)_2 \tag{4.22}$$

$$m_4 = (m_4)_1 + (m_4)_2 \tag{4.23}$$

where $(m_n)_i$ denotes the n-th spectral moment for profile i ($i=1,2$). The m_n values computed from Eqs. (4.21) to (4.23) are referred to as <u>composite</u> values. When surfaces are anisotropic there exist two orthogonal directions, called principal directions, along which the profile value of m_2 is a minimum and a maximum. According to [11], the value of m_2, designated $(m_2)_e$, for an equivalent isotropic surface may be constructed as the harmonic mean:

$$(m_2)_e = (m_{2max} \bullet m_{2min})^{1/2} \tag{4.24}$$

The m_4 values in the same two principal directions are combined in the same way to give $(m_4)_e$. In principle m_0 is independent of tracing direction. If m_0 is measured in two directions along with m_2 and m_4, the ordinary arithmetic average and not the harmonic mean should be used to combine the two values of m_0.

4.4 Estimating m_4 from Stylus Profile Equipment Output

As shown above, the GW model is completely specified if we know m_0, m_2 and m_4 for the composite and for the equivalent isotropic surface. These quantities may be computed directly from a profile as the finite difference approximations to Eqs. (4.12) to (4.14). Alternatively, m_0, m_2 and m_4 may be computed in terms of the spectrum s(f) of a profile if the spectrum is known or estimated. Roughly speaking the spectrum is a function that expresses how the various frequencies present in a random profile contribute to the overall profile variability.

It has been found empirically that the spectrum of a roughness profile most always plots nearly linearly on a set of logarithmic scales with perhaps spikes at frequencies which correspond to the spacing of grinding furrows, chatter or other nearly periodic features. It is postulated, therefore, that the spectrum is of the form $s(f) \sim f^{-k}$ where **k**, termed the spectral exponent, is the magnitude of the slope of a plot of log **s** against log **f**. Introducing a proportionality constant '**c**' gives

$$s(f) = cf^{-k} \tag{4.25}$$

It is further postulated that the spatial frequencies present in the profile are confined to a passband ranging from a lower frequency f_1 to an upper frequency f_2. The lower frequency f_1 is associated with the long wave cutoff of a profile instrument.

The upper frequency f_2 is determined by the electronic filter of the stylus instrument or by the finite stylus radius, whichever results in a lower frequency value.

The n-th spectral moment m_n is given in terms of the spectrum by:

$$m_n = (2\pi)^n \int_{f_1}^{f_2} f^n \bullet s(f)df \tag{4.26}$$

Using Eqs. (4.25) and (4.26) gives the results tabled below for the values corresponding to n=0, 2 and 4, needed for the GW microcontact analysis.

$$\begin{aligned} m_0 &= c\ell n(f_2/f_1);k=1 \\ &= [c/(1-k)][f_2{}^{1-k}-f_1{}^{1-k}];k\neq 1 \end{aligned} \tag{4.27}$$

$$\begin{aligned} m_2 &= c(2\pi)^2\ell n(f_2/f_1);k=3 \\ &= [c(2\pi)^2/(3-k)][f_2{}^{3-k}-f_1{}^{3-k}];k\neq 3 \end{aligned} \tag{4.28}$$

$$\begin{aligned} m_4 &= c(2\pi)^4\ell n(f_2/f_1);k=5 \\ &= [c(2\pi)^2/(5-k)][f_2{}^{5-k}-f_1{}^{5-k}];k\neq 5 \end{aligned} \tag{4.29}$$

The quantities R_q and Δq provided by current generation profile instruments are related to m_0 and m_2:

$$R_q = m_0{}^{1/2} \tag{4.30}$$

$$\Delta q = m_2{}^{1/2} \tag{4.31}$$

Thus, using Eqs. (4.27) and (4.28) the ratio $R_q/\Delta q$ may be expressed as:

$$R_q/\Delta q = 1/2\pi \left\{ \frac{(3-k)}{(1-k)} \frac{[f_2^{1-k} - f_1^{1-k}]}{[f_2^{3-k} - f_1^{3-k}]} \right\}^{1/2} ; \; k \neq 1 \text{ or } 3 \qquad (4.32)$$

For specified f_1 and f_2 and measured values of R_q and Δq, one may solve Equation (4.32) numerically for **k**. With **k** thus determined, one may then express the ratio m_4/m_0 from Eqs. (4.27) and (4.28) in terms of f_1, f_2 and **k** and thereby estimate m_4 as:

$$m_4 = (2\pi)^4 \frac{(1-k)}{(5-k)} \left[\frac{f_2^{5-k} - f_1^{5-k}}{f_2^{1-k} - f_1^{1-k}} \right] \bullet m_0 \; ; \; (k \neq 1 \text{ or } 3) \qquad (4.33)$$

Having thus determined m_0, m_2 and m_4, the GW parameters are computed from Eqs. (4.15) to (4.17).

In using Eq. (4.32) to find k, the composite R_q and Δq values are formed following Eqs. (4.21) and (4.22) as:

$$R_q^2 = R_{q1}^2 + R_{q2}^2 \qquad (4.34)$$

$$\Delta q^2 = \Delta q_1^2 + \Delta q_2^2 \qquad (4.35)$$

where the subscripts 1 and 2 refer to the respective surfaces.

The individual surface values are input to McFRIC. If a surface is anisotropic the equivalent Δq value should be input. This is computed from the maximum and minimum values using Eq. (4.24) as:

$$\Delta q_e = [(\Delta q)_{MAX} \bullet (\Delta q)_{MIN}]^{1/2} \qquad (4.36)$$

4.5 Expected Values of Traction Force Components and Torque at Asperities

The contact ellipse dimensions are assumed to have their dry contact values. The fluid pressure at a general position within the contact ellipse is assumed to be reduced by asperity loading but to remain proportional to the dry contact pressure:

$$\sigma'(x,y) = \theta\sigma_o\,[1-(x/a)^2 - (y/b)^2]^{1/2} \qquad (4.37)$$

where θ is a constant of proportionality.

The value of θ is determined by requiring that the sum of the load supported by elastic asperity deformation (TOTF) and the fluid pressure equilibrate the applied load P, i.e.

$$(2/3\ \theta\sigma_o + TOTF)\pi ab = P \qquad (4.38)$$

so that

$$\theta = 1.5\ [P/\pi ab - TOTF]/\sigma_o \qquad (4.39)$$

The solution requires, of course, that $P > TOTF \bullet \pi ab$ and may be invalid for thin films and light loads.

For lubricant films that are thick relative to the surface roughness TOTF = 0 and $\theta = 1.0$.

We assume further that a Coulomb friction law governs at the contact of a pair of asperities on the two mating bodies undergoing macro-EHD contact. It is not implied that a Coulomb model is literally true; micro-EHD effects may actually be the basis for the thin film increase of traction. Wedeven [12] has shown experimentally that micro-EHD effects can be responsible for a 20% variation in traction. At the present state of understanding a more refined model is unwarranted.

Consider an asperity contact located at coordinates (x,y) within the contact ellipse. The friction force at this asperity will act in the direction of the resultant sliding velocity vector at x,y. The components of the sliding velocity vector are

$$v_x = \Delta u - \omega y \tag{4.40}$$

$$v_y = \Delta v + \omega\ (x-\delta_x) \tag{4.41}$$

The magnitude of the force vector is the product of a Coulomb friction coefficient, **f**, and the normal force on the asperity pair. The normal force consists of the sum of the integrated pressure at that point in the contact ellipse and the force to deform the asperity pair elastically by the amount by which they interfere at the computed film thickness.

The force of elastic deformation is a random variable having a mean value AVF over all contacting asperities. The probability of an asperity contact occurring within a differential area dxdy

within the macrocontact ellipse, is, to a first approximation, independent of coordinate position.

This probability is the product of the number of contacts per unit area ZNCON and the differential area dxdy, i.e.

$$\text{PROB [Contact in dxdy]} = (\text{ZNCON})\ dxdy \tag{4.42}$$

The expected normal force due to elastic deformation at (x,y) is thus

$$E(N) = (\text{AVF} \bullet \text{ZNCON})\ dxdy \tag{4.43}$$

The expected friction force at position (x,y) is thus

$$E(F(x,y)) = f\ [\text{AVF} \bullet \text{ZNCON} + \text{TOTA} \bullet \theta\sigma\ (x,y)]\ dxdy \tag{4.44}$$

where $\sigma(x,y)$ is the Hertzian pressure distribution. θ is the fluid pressure reduction factor and TOTA is the total asperity area per unit nominal area.

The x component of the total expected friction force is found by integrating the x projection of E(F(x,y)) over the contact ellipse, i.e.

$$E(F_x) = \iint f\ [\text{AVF} \bullet \text{ZNCON} + \text{TOTA} \bullet \theta\sigma(x,y)]\{v_x/(v^2{}_x + v_y{}^2)^{1/2}\}dxdy \tag{4.45}$$

The y component is similarly defined but with v_y replacing v_x in the numerator of the integrand.

The expected spinning torque due to asperity contact is

$$E(T) = \iint x \bullet I(x,y)\ v_y\ d_x d_y - \iint y \bullet I(x,y) v_x\ dxdy \qquad (4.46)$$

where

$$I(x,y) = f\ [AVF \bullet ZNCON + TOTA \bullet \theta\sigma\ (x,y)]\ /\ (v_x^2 + v_y^2)^{1/2} \qquad (4.47)$$

These expected asperity traction forces and moments are added to the fluid film values computed as if the surfaces were smooth.

5.0 RHEOLOGICAL MODEL FOR FLUID TRACTION

5.1 One Dimensional Maxwell Model

A survey of the literature on traction in concentrated contacts was made in conjunction with this project, and a summary account is given in the Interim Report [13]. A pivotal paper in the traction literature, noted therein, is that of Johnson and Roberts [14], in which it was ingeniously established experimentally that a fluid in a concentrated contact can deform elastically at sufficiently high pressures and rolling velocities. The key to this demonstration is the fact that a lateral force develops in the presence of spin with an elastic fluid, but not if the fluid deforms viscously. This lateral force was shown by Gentle and Bonesс [15] to be essential for correctly predicting the steady state ball rotational axis in angular contact ball bearings.

To account for the viscoelastic response, Johnson and Roberts proposed that the lubricant be regarded as a Maxwell fluid in which, on the application of a shear rate $\dot{\gamma}$, the fluid shear stress τ varies with time t in accordance with the differential equation:

$$(1/G)\, d\tau/dt + \tau/\eta = \dot{\gamma} \qquad (5.1)$$

Essentially, this model regards the strain rate $\dot{\gamma}$ as consisting of two components: an elastic strain rate $\dot{\gamma}_e$ given by

$$\dot{\gamma}_e = 1/G \; d\tau/dt \tag{5.2}$$

and a viscous component $\dot{\gamma}_v$ corresponding to ordinary Newtonian viscous behavior

$$\dot{\gamma}_v = \tau/\eta \tag{5.3}$$

in which $\dot{\gamma}$ is linear with τ.

Referring to Figure 3.3(a), wherein the lubricant passes through the contact with velocity $u = (u_1 + u_2)/2$, the elastic component of shear rate can be written

$$\dot{\gamma}_e = (1/G)(d\tau/dx)(dx/dt) = (u/G)\, d\tau/dx \tag{5.4}$$

Using Eq. (5.4), and assuming constant lubricant properties, the solution of Eq. (5.1) is,

$$\tau(x) = \eta\dot{\gamma}[1-\exp(-G(x+a)/\eta u)] \tag{5.5}$$

wherein the initial condition $\tau=0$ at $x=-a$ has been used. The shear stress at the contact center, $\tau(x=0)$ approximates the average shear stress over the contact. It has the value,

$$\tau(0) = \eta\dot{\gamma}[1-\exp[-aG/\eta u]] \tag{5.6}$$

$$= \eta\dot{\gamma}[1-\exp(-1/T)] \tag{5.7}$$

where $T \equiv \eta u/aG$ is known as the Deborah number. For small T

$$\tau(0) \approx \eta\dot{\gamma} \tag{5.8}$$

that is, the fluid behaves as a purely viscous Newtonian fluid.

For large T,

$$\exp(-1/T) \cong 1-1/T \tag{5.9}$$

and Eq. (5.7) reduces to

$$\tau(0) = \eta\dot{\gamma}/T = a\,G\,\dot{\gamma}/u \tag{5.10}$$

i.e. the fluid acts purely elastically.

For intermediate **T** values the fluid behaves viscoelastically, but in any case, according to Eq. (5.6), shear stress and hence traction force increases linearly with shear rate $\dot{\gamma}$. The Deborah number is usually interpreted as the ratio of two time intervals: 1) the relaxation time of the fluid, η/G, and 2) the transit time, i.e., the time u/a for the fluid to travel a contact half width. Large **T** values represent the case where the relaxation time, i.e., the time to achieve the Newtonian shear stress is large compared with travel time through the contact.

Johnson and Roberts recognized that the Maxwell model of Eq. (5.1) would only apply at low strain rates since the shape of experimental traction curves invariably shows a nonlinearity with shear rate.

5.2 Nonlinear One-Dimensional Maxwell Model

Subsequently, Johnson and Tevaarwerk [16] employed the Ree-Eyring nonlinear viscous relation in lieu of the linear

Newtonian form within a Maxwell model. They thus deduced a constitutive relationship that was capable of explaining 1) the nonlinear behavior of experimental traction curves taken at various values of the Deborah number, and 2) the existence of a traction force transverse to the rolling direction in the presence of superimposed spin.

Johnson and Tevaarwerk noted that the diminishing rate of increase of traction force with sliding speed at high Deborah numbers "strongly suggests an elastic/plastic solid". The Eyring model, however, does not reach an asymptote with increased sliding, and in [4], Tevaarwerk and Johnson proposed instead the use for high Deborah numbers of an elastic/plastic model under which shear stress increases with sliding velocity in a linear elastic manner until reaching a limiting shear stress τ_c.

At low shear rates the Eyring based model exhibits Newtonian viscous behavior, while the elastic/plastic model exhibits purely elastic behavior.

At high shear rates the elastic/plastic model yields a constant limiting shear stress; while the shear stress under the Eyring model continues to increase with increasing shear rate. In Section 5.3 below, the nonlinear viscous model of Trachman and Cheng [17] is used in the same manner as Johnson and Tevaarwerk employ the Ree-Eyring model. The result is a single model capable of representing elastic, plastic, linear viscous (Newtonian) and nonlinear viscous fluid response.

5.3 The Trachman-Cheng Nonlinear Viscous Model

Trachman and Cheng [17,18] proposed a nonlinear viscous model which varies smoothly between Newtonian behavior in which shear stress and strain rate are proportional, to a limiting value of shear stress τ_c achieved at high strain rates. The model is:

$$\dot{\gamma} = \tau/\eta(1-\tau/\tau_c) \; ; \; \tau < \tau_c \tag{5.11}$$

where

$\dot{\gamma}$ = strain rate

η = viscosity

τ = shear stress

τ_c = limiting shear stress

Expressing τ in terms of $\dot{\gamma}$, the model becomes,

$$\tau = \eta\dot{\gamma}/(\eta\dot{\gamma}/\tau_c + 1) \tag{5.12}$$

For a Newtonian fluid

$$\tau = \eta\dot{\gamma} \tag{5.13}$$

The T-C model thus gives a lower shear stress value than Newtonian for all strain rates but approaches Newtonian behavior as $\dot{\gamma}$ approaches zero.

Dividing through by $\eta\dot{\gamma}$, Eq. (5.12) becomes

$$\tau = (1/\tau_c + 1/\eta\dot{\gamma})^{-1} \tag{5.14}$$

In this form it is seen that for $\dot{\gamma}$ large, τ approaches τ_c.

Thus, of itself, the T-C model accommodates Newtonian behavior at low strain rates and plastic behavior at large strain rates.

For an elastic fluid as we have seen

$$\dot{\gamma} = (U/G)\, d\tau/dx \tag{5.15}$$

5.4 The Nonlinear One-Dimensional Maxwell Model Using the Trachman-Cheng Viscous Component

Following Tevaarwerk and Johnson, we express the total strain rate $\dot{\gamma}$ as the sum of an elastic strain rate $\dot{\gamma}_E$ and a (nonlinear) viscous strain rate $\dot{\gamma}_V$:

$$\dot{\gamma} = \dot{\gamma}_E + \dot{\gamma}_V \tag{5.16}$$

Using Eq. (5.15) for $\dot{\gamma}_E$ and the T-C model, Eq. (5.11), for $\dot{\gamma}_V$ leads after rearrangement to the following differential equation for τ

$$d\tau/dx = G\dot{\gamma}/u - G\tau_c/u\eta \bullet \tau/(\tau_c-\tau) \tag{5.17}$$

5.5 Application to a Line Contact

In order to evaluate the model implications, a line contact (or a strip across an elliptical contact) of width 2a and with an x coordinate established at the contact center is now considered

as shown in Figure 3.3a. As with the linear Maxwell model, the lubricant properties are taken as constant for this purpose.

Separating the variables in Eq. (5.17), and integrating gives the relation between $\tau = \tau(x)$ and the coordinate x.

$$\int_0^{\tau(x)} \frac{d\tau}{[G\dot{\gamma}/u - G\tau\ \tau_c/u\eta(\tau_c-\tau)]} = \int_{-a}^{x} dx = x + a \qquad (5.18)$$

Integration of the left hand side gives, after rearrangement:

$$\frac{u\eta}{G(\eta\dot{\gamma}/\tau_c+1)^2}\ \ell n\left[\frac{1}{(1-\tau/\tau_c)-(\tau/\tau_c)/(\eta\dot{\gamma}/\tau_c)}\right] \qquad (5.19)$$

$$+\ \frac{u\eta(\tau/\tau_c)}{G[\eta\dot{\gamma}/\tau_c+1]} = x+a$$

Introducing the dimensionless distance $X = x/a$ and the following dimensionless variables:

$$T = u\eta/aG \qquad (5.20)$$

and

$$W = \eta\dot{\gamma}/\tau_c \qquad (5.21)$$

Eq. (5.19) becomes

$$(T/(W+1)^2)\ell n\ [1/\{(1-\tau/\tau_c)-(\tau/\tau_c)/W\}] + T(\tau/\tau_c)/(W+1)$$
$$= X + 1 \qquad (5.22)$$

The dimensionless variable T is, of course, the Deborah number.

Eq. (5.22) has been solved to yield the dimensionless shear stress τ/τ_c as a function of dimensionless shear rate **W** for various values of **T** and coordinate position **X**. Integrating across the contact, i.e. with respect to **X**, yields the average value $\bar{\tau}/\tau_c$ as a function of **W** with **T** as a parameter. Figures 5.1 and 5.2 show $\bar{\tau}/\tau_c$ as a function of **W** and of W/T, respectively. It is of interest to show how certain limiting forms, viz. the Newtonian viscous, the pure elastic and the pure plastic models appear on these grids.

Newtonian Viscous Model

For a Newtonian purely viscous model,

$$\tau = \eta\dot{\gamma} \tag{5.23}$$

so that

$$\tau/\tau_c = \eta\dot{\gamma}/\tau_c = W \tag{5.24}$$

represents a Newtonian viscous model. Since under this model τ/τ_c does not depend on **x**, the average value, $\bar{\tau}/\tau_c$ is also equal to **W**. The value of $\bar{\tau}/\tau_c$ for a Newtonian viscous model thus plots against **W** as a line of unit slope. This Newtonian limit is shown in Figure 5.1. On a plot of $\bar{\tau}/\tau_c$ against W/T, a Newtonian viscous model will appear as a straight line with a slope equal to the Deborah number. The curve for T = 0.001 in Figure 5.2 is sufficiently straight to suggest nearly Newtonian viscous behavior.

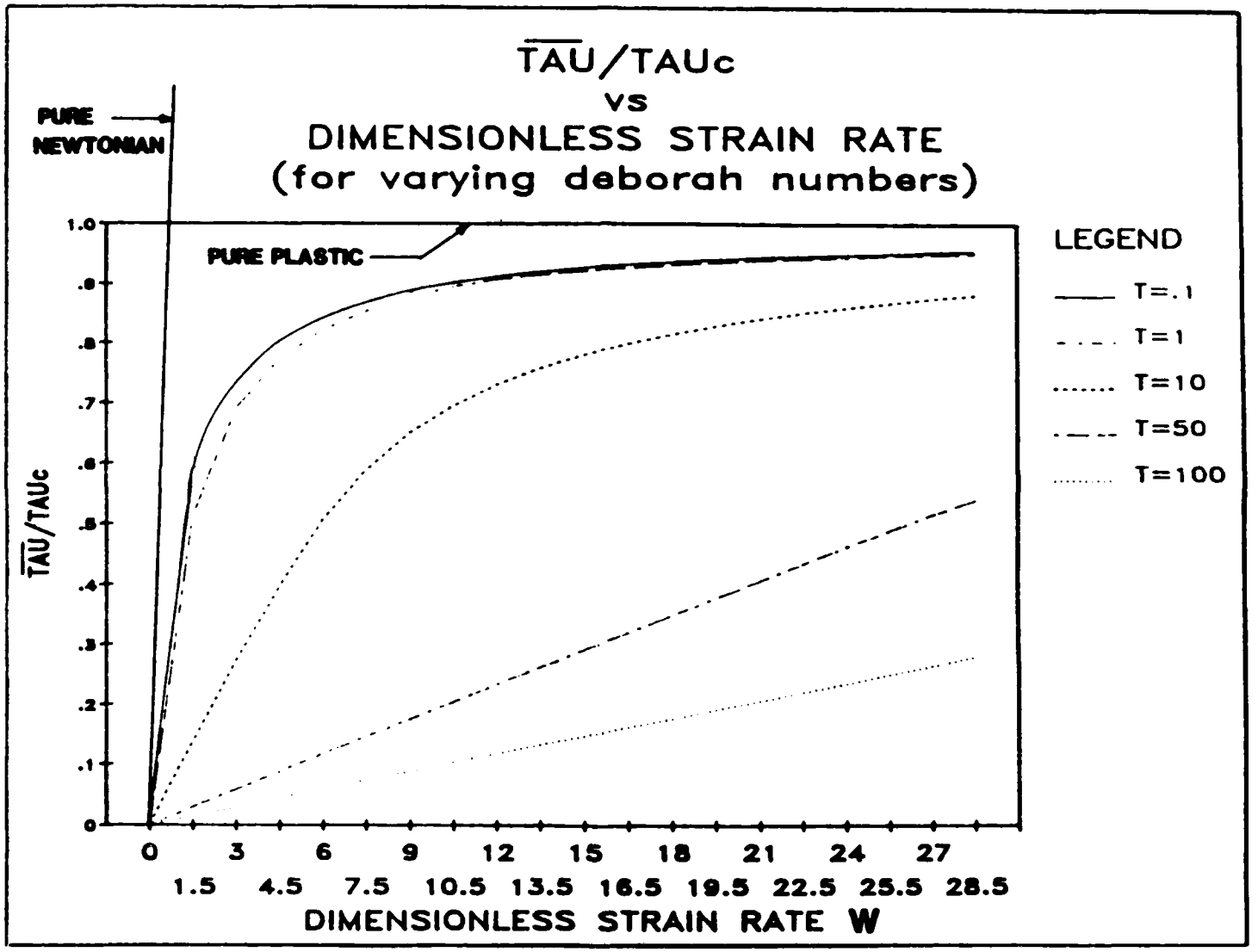

Fig. 5.1

$\bar{\tau}/\tau_c$ VS. DIMENSIONLESS STRAIN RATE

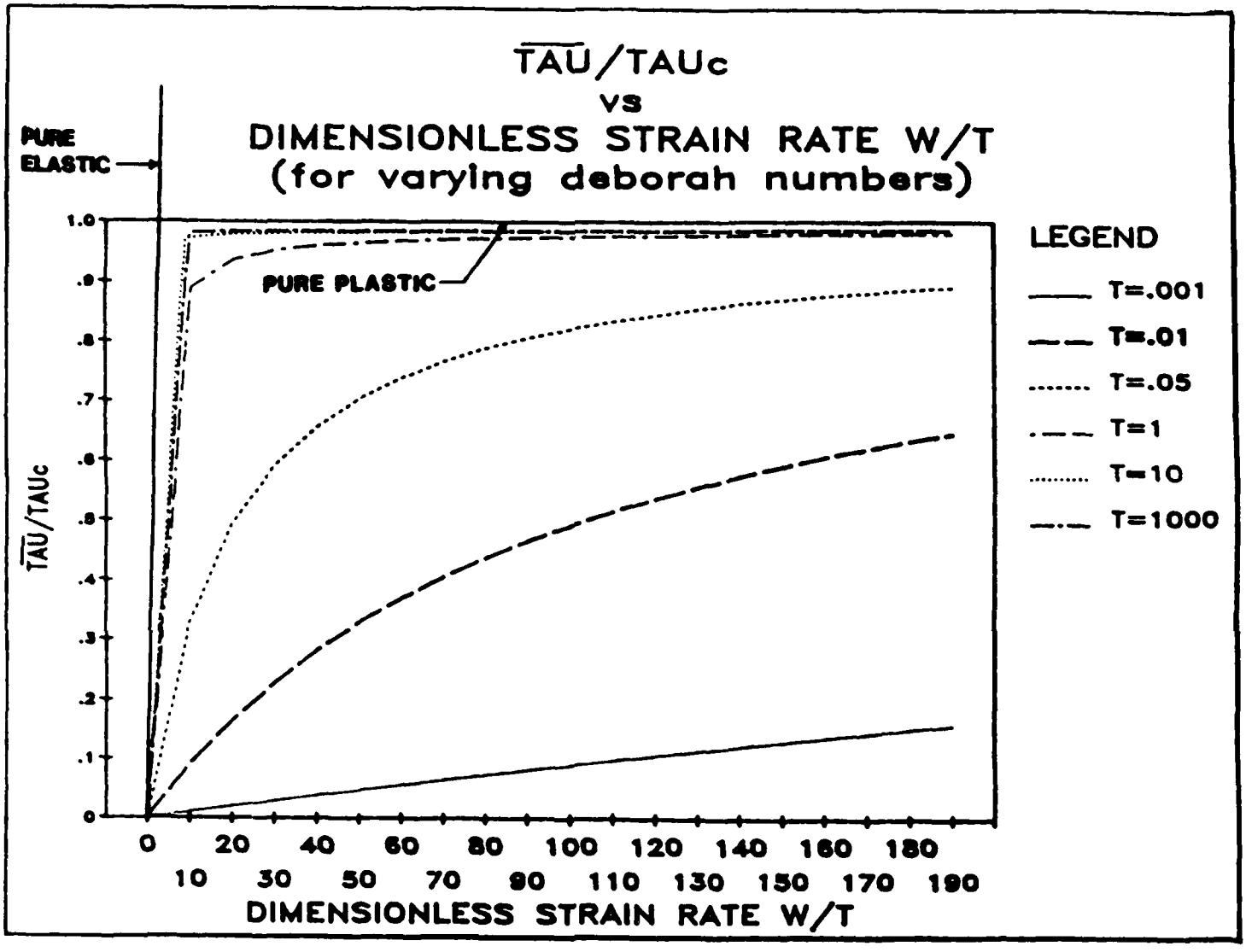

Fig. 5.2

$\bar{\tau}/\tau_c$ VS. DIMENSIONLESS STRAIN RATE W/T

Purely Plastic Model

A purely plastic model is represented by

$$\tau = \tau_c$$

or $$\tau/\tau_c = 1.0 = \bar{\tau}/\tau_c \qquad (5.25)$$

This line is shown on Figures 5.1 and 5.2.

Purely Elastic Model

For a purely elastic model one may integrate Eq. (5.14) to give:

$$\tau = G\dot{\gamma}aX + c/u \qquad (5.26)$$

where **c** is a constant of integration.

Using the initial condition $\tau = 0$ at $X = -1$, gives

$$\tau/\tau_c = G\dot{\gamma}a/u\tau_c\ (X+1) = (W/T)(X+1) \qquad (5.27)$$

Since this expression is linear in **X**, $\bar{\tau}/\tau_c$ is equal to τ/τ_c at the average value of **X**, i.e. at $X = 0$.

Thus,

$$\bar{\tau}/\tau_c = W/T \qquad (5.28)$$

In a plot of $\bar{\tau}/\tau_c$ against W/T, the pure elastic model will thus have unit slope. This pure elastic limit line is shown drawn on Figure 5.2.

In a plot against **W**, the pure elastic model is a straight line of slope 1/T. The curve shown in Figure 5.1 for T = 50 appears straight to within graphical accuracy and thus represents primarily elastic behavior.

Bidimensional Constitutive Law

Following Johnson and Tevaarwerk [16], the lubricant film in the contact in which shear stresses are developed, is assumed to be uniform and thin.

The flow due to the pressure gradient in the EHD contact is ignored as negligible over the high pressure region, with the consequence (from the momentum equation) that the shear stress in the **x** and **y** directions does not vary across the thickness of the film. In these circumstances the bidirectional version of the constitutive relation that was adopted for the one dimensional case in Section 5.0, becomes the coupled system of differential equations:

$$\frac{ud\tau_x}{Gdx} + \frac{\tau_x}{\tau_e} \bullet \frac{\tau_e}{\eta(1-\tau_e/\tau_c)} = \dot{\gamma}_x \qquad (5.29)$$

$$\frac{ud\tau_y}{Gdx} + \frac{\tau_y}{\tau_e} \bullet \frac{\tau_e}{\eta(1-\tau_e/\tau_c)} = \dot{\gamma}_y \qquad (5.30)$$

where τ_x and τ_y are the orthogonal components of the interfacial shear stress. τ_e, the equivalent shear stress, is defined as:

$$\tau_e = (\tau_x^2 + \tau_y^2)^{1/2} \tag{5.31}$$

The orthogonal components of shear rate, $\dot{\gamma}_x$ and $\dot{\gamma}_y$ are given by

$$\dot{\gamma}_x = (\Delta u - \omega y)/h \tag{5.32}$$

$$\dot{\gamma}_y = [\Delta v + \omega(x - \delta_x)]/h \tag{5.33}$$

Introducing the dimensionless stresses

$$\hat{\tau}_x = \tau_x/\tau_c, \quad \hat{\tau}_y = \tau_y/\tau_c, \quad \hat{\tau}_e = \tau_e/\tau_c \tag{5.34}$$

and the dimensionless strain rates,

$$W_x = \dot{\gamma}_x \eta/\tau_c \qquad W_y = \dot{\gamma}_y \eta/\tau_c \tag{5.35}$$

the dimensionless coordinates

$$X = x/a \qquad Y = y/b$$

and the Deborah number,

$$T = u\eta/Ga \tag{5.36}$$

gives the transformed equations,

$$T(d\hat{\tau}_x/dX) + (\hat{\tau}_x\hat{\tau}_e)/\hat{\tau}_e(1-\hat{\tau}_e) = W_x \tag{5.37}$$

$$T(d\hat{\tau}_y/dX) + (\hat{\tau}_y\hat{\tau}_e)/\hat{\tau}_e(1-\hat{\tau}_e) = W_y \tag{5.38}$$

6.0 SOLUTION SCHEME FOR CONSTITUTIVE EQUATIONS

Figure 6.1 shows the contact ellipse with semiaxes **a** and **b** aligned with the rolling and transverse directions, respectively. The contact is divided into strips parallel to the **x** direction and of thickness Δy. Each strip in turn is divided into rectangular elements of length Δx. A general strip with midline at coordinate location y has a half width a(y) given by:

$$a(y) = a[1-(y/b)^2]^{1/2} \tag{6.1}$$

The pressure at coordinate position x,y is

$$p(x,y) = \sigma_o\ [1-(x/a)^2-(y/b)^2]^{1/2} \tag{6.2}$$

where σ_o is the maximum Hertzian pressure.

At a fixed slice, i.e., at a fixed **y** coordinate, the maximum pressure occurs at x = 0, i.e.,

$$p_{max}(y) = \sigma_o[1-(y/b^2)]^{1/2} \tag{6.3}$$

The distribution over that strip can be written as

$$p(x,y) = p_{max}(y) \bullet [1-(x/a(y))^2]^{1/2} \tag{6.4}$$

since using (6.1) and (6.3) in (6.4) reproduces (6.2).

In solving the constitutive equations we focus on strips such as that shown in Figure 6.1 and use the local dimensionless **x** coordinate X = x/a(y) and the global dimensionless **y** coordinate

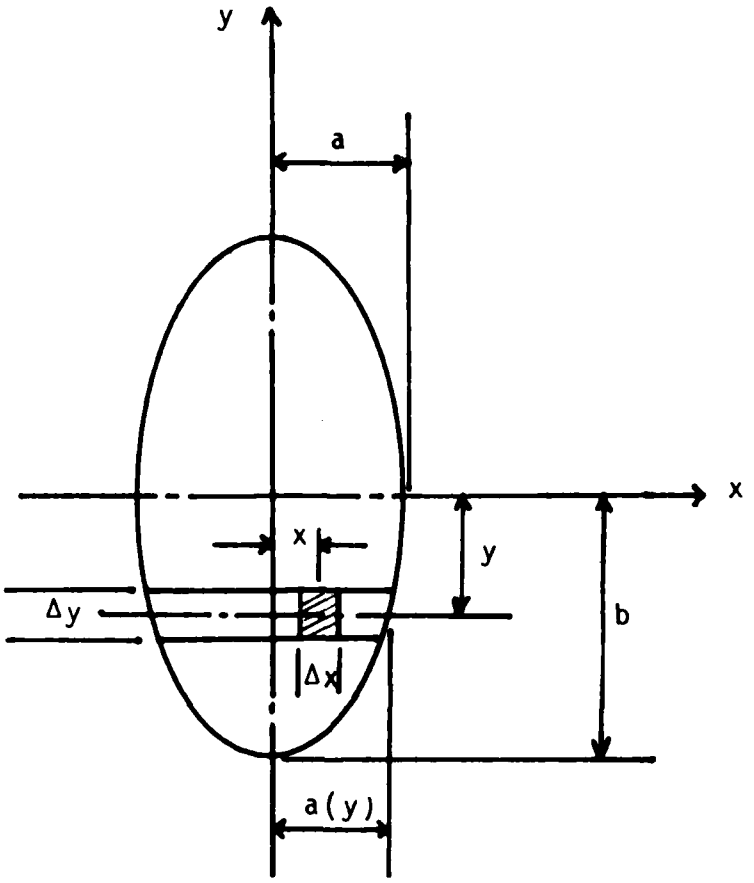

Fig. 6.1 CONTACT ELLIPSE COORDINATE SYSTEM

$Y = y/b$. The equations are solved for τ_x and τ_y along each strip. These stresses are then integrated over the strip to give the differential contribution of the strip to the force component and the torque acting over the whole contact.

The solution scheme follows an ad hoc approach developed by Houpert [20] in conjunction with a different constitutive relationship. The derivatives $d\hat{\tau}_x/dX$ and $d\hat{\tau}_y/dX$ are written in finite difference form:

$$d\hat{\tau}_x/dX = (\hat{\tau}_x - \hat{\tau}_x^*)/\Delta X \tag{6.5}$$

$$d\tau_y/dX = (\tau_y - \tau_y^*)/\Delta X \tag{6.6}$$

where τ_x, τ_y are the current values at position X and τ_x^*, τ_y^* are the values at the previous area element at coordinate position $X-\Delta X$. Substituting into Eqs. (5.37) and (5.38) gives, after rearrangement:

$$W_x + T\,\hat{\tau}_x^*/\Delta X = \hat{\tau}_x[T/\Delta X + 1/(1-\hat{\tau}_e)] \tag{6.7}$$

$$W_y + T\,\hat{\tau}_y^*/\Delta X = \hat{\tau}_y[T/\Delta X + 1/(1-\hat{\tau}_e)] \tag{6.8}$$

Dividing (6.7) by (6.8) gives,

$$\hat{\tau}_x/\hat{\tau}_y = A = \frac{W_y + T\,\hat{\tau}_y^*/\Delta X}{W_x + T\,\hat{\tau}_x^*/\Delta X} \tag{6.9}$$

Eq. (6.9) is used to compute the ratio **A** at each new position in terms of the values at the previous **X** position and modified by the values of the strain rates Wx and Wy at the new position.

Thus,

$$\hat{\tau}_x = \hat{\tau}_y \bullet A \tag{6.10}$$

Also,

$$\hat{\tau}_e = [\hat{\tau}_x^2 + \hat{\tau}_y^2]^{1/2} = \hat{\tau}_x[1+A^2]^{1/2} = \hat{\tau}_x \bullet B \tag{6.11}$$

Using Eq. (6.11) to eliminate τ_x in the original differential equation, Eq. (5.37) gives,

$$T\, d\hat{\tau}_e/dX + \hat{\tau}_e/(1-\hat{\tau}_e) = BW_x \tag{6.12}$$

Separating variables gives

$$Td\hat{\tau}_e = [BW_x - \hat{\tau}_e/(1-\hat{\tau}_e)]dX \tag{6.13}$$

$$Td\hat{\tau}_e/BW_x - \hat{\tau}_e/(1-\hat{\tau}_e) = dX \tag{6.14}$$

Integrating over the interval $X^* = X - \Delta X$ to X gives

$$\int_{\tau_e^*}^{\hat{\tau}_e} Td\hat{\tau}_e/[BW_x - \hat{\tau}_e/(1-\hat{\tau}_e)] = \int_{X-\Delta X}^{X} dX = \Delta X \tag{6.15}$$

The left hand side integrates to

$$F(\hat{\tau}_e)\Big|_{\hat{\tau}_e^*}^{\hat{\tau}_e} = F(\hat{\tau}_e) - F(\hat{\tau}_e^*) \tag{6.16}$$

where

$$F(\hat{\tau}_e) = T/(BW_x+1)^2 \ \ell n \ [1-(1+1/BW_x)\hat{\tau}_e] + \hat{\tau}_e T/(BW_x+1) \qquad (6.17)$$

Given τ_e^* at the abscissa value X^*, the next successive value is found by numerically solving:

$$F(\hat{\tau}_e) - F(\hat{\tau}_e^*) = \Delta X \qquad (6.18)$$

A golden section search technique is used to implement the solution. Having thus found $\hat{\tau}_e$, τ_e is found as

$$\tau_e = \tau_c \bullet \hat{\tau}_e \qquad (6.19)$$

$\hat{\tau}_x$ and $\hat{\tau}_y$ are then computed as

$$\hat{\tau}_x = \hat{\tau}_e/B \qquad (6.20)$$

$$\hat{\tau}_y = \hat{\tau}_x/A \qquad (6.21)$$

The solution scheme starts with $\tau_e=0$ at the inlet end of the strip and bootstraps across the strip length solving for the stress on the next successive element located at the distance ΔX further down the strip. Inasmuch as the lubricant properties depend on the local pressure and temperature at each successive location, they are adjusted to the local conditions of each element using properties relationships discussed further below.

The actual stresses τ_x and τ_y are obtained by multiplying $\hat{\tau}_x$ and $\hat{\tau}_y$ by the locally variable value of τ_c. The differential torque contribution at location x,y is

$$DT(x,y) = \tau_x \bullet y - \tau_y (X-\delta x) \tag{6.22}$$

τ_x, τ_y and $dT(x,y)$ are integrated over the strip at position y to yield the differential force components $dF_x(y)$, $dF_y(y)$ and the differential torque contribution of the strip $dT(y)$.

$$dF_x(y) = \int_{-a(y)}^{a(y)} \tau_x dx \tag{6.23}$$

$$dF_y(y) = \int_{-a(y)}^{a(y)} \tau_y dx \tag{6.24}$$

$$dT(y) = \int_{-a(y)}^{a(y)} dT(x,y)dx \tag{6.25}$$

Once these quantities are evaluated for each strip of the contact ellipse they are integrated across the strips to give the total fluid force and torque components:

$$F_x = \int_{-b}^{b} dF_x(y)dy \tag{6.26}$$

$$F_y = \int_{-b}^{b} dF_y(y)dy \tag{6.27}$$

$$T = \int_{-b}^{b} dT(y)dy \tag{6.28}$$

The combined fluid and asperity friction forces are obtained by summing the fluid force components and spinning torque from Eqs. (6.26)-(6.28) and the corresponding expected coulomb friction values from Eqs. (4.45) and (4.46). Denote these sums F_x, F_y and T.

The combined frictional power loss (EL) may then be computed as

$$EL = F_x \bullet \Delta u + F_y \bullet \Delta v + T \bullet \omega \qquad (6.29)$$

For some applications, most notably traction drives, the power transmitted (ET) through the contact is of critical importance. This is

$$ET = F_x \bullet u \qquad (6.30)$$

The loss factor (LF) is computed as the ratio of the power loss to the power transmitted, i.e.

$$LF = EL/ET \qquad (6.31)$$

7.0 HEAT GENERATION AND THERMAL ANALYSIS

7.1 Heat Generation

The heat generated per unit volume is computed point-by-point along each strip in the contact area. The total heat input per unit volume, Q, is the sum of the contribution due to shearing of the fluid, Qf, and due to the coulomb friction at the asperities, Qa.

7.1.1 Fluid Shear Heat

The fluid contribution is computed as the product of the resultant shear stress

$$\tau_e = [\tau_x^2 + \tau_y^2]^{1/2} \tag{7.1}$$

and the viscous component of the shear rate $\dot{\gamma}_v$. The recoverable elastic shear is thus not included in computing fluid heat generation. Using Eq. (5.11) gives

$$\dot{\gamma}_v = \tau_e/\eta(1-\tau_e/\tau_c) \tag{7.2}$$

so that

$$Q_f = \tau_e \bullet \dot{\gamma}_v \tag{7.3}$$

Since $\dot{\gamma}_v$ must not exceed $\dot{\gamma}$, a numerical check is made. If $\dot{\gamma}_v > \dot{\gamma}$, Q_f is computed as

$$Q_f = \tau_e \bullet \dot{\gamma} \qquad (7.4)$$

7.1.2 Heat Generated at Asperities

As noted in Section 4.0, the quantity TOTF computed using the Greenwood-Williamson microcontact model is the asperity load per unit area of apparent contact. With a coulomb friction coefficient μ, the traction force per unit area is μTOTF. Multiplying by the resultant sliding velocity and dividing by film thickness **h** gives the asperity generated heat per unit apparent volume, i.e.

$$Q_a = \mu TOTF[v_x^2 + v_y^2]^{1/2}/h = \mu \bullet TOTF \bullet \dot{\gamma} \qquad (7.5)$$

where v_x and v_y are the sliding velocity components:

$$v_x = \Delta v - \omega y \qquad (4.40)$$

$$v_y = \Delta v + \omega(x - \delta x) \qquad (4.41)$$

7.2 Thermal Analysis

7.2.1 Temperature Distribution in Solid and Film

It is assumed that heat generated within the film along a strip in the **x** direction as shown in Fig. 6.1 is conducted to the two surfaces and carried by convection in the direction of rolling. Conduction in the **y** direction is neglected as negligible. This permits the independent analysis of the strips which comprise the total contact.

It is also assumed that both the solids bounding the lubricant film have the same thermal properties and the same ambient temperature ϑ_o. The maximum film temperature thus occurs on and is symmetrical about the center plane. The common temperature of the bounding solid $\theta_s(x)$ varies with coordinate **x** and may be expressed as the sum of the ambient temperature and the increase $\Delta\vartheta s(x)$ caused by heating in the contact. The maximum film temperature ϑc, in turn is expressed as the sum of the solid temperature at the given coordinate position and the increase $\Delta\theta c(x)$ of the center film temperature over the solid temperature, i.e.:

$$\vartheta c(x) = \vartheta_s(x) + \Delta\vartheta_c(x) \tag{7.6}$$

$$\vartheta c(x) = \vartheta_o + \Delta\theta_s(x) + \Delta\theta_c(x) \tag{7.7}$$

Fig. 7.1 shows the temperature profile of the solids as a function of coordinate position **x** and the temperature profile across the film at a specific **x** position. Following Houpert [20,21] we assume that the temperature profile across the film has a nearly triangular shape. With this assumption, Jaeger's equation [22] for computing $\Delta\theta s(x)$ becomes

$$\Delta\vartheta s(x) = [\pi\rho_m c_m k_m \mu]^{-1/2} \int_{-a(y)}^{x} -2k\Delta\theta_c / h[x-\psi]^{1/2} d\psi \tag{7.8}$$

where

ρ = density

c = specific heat

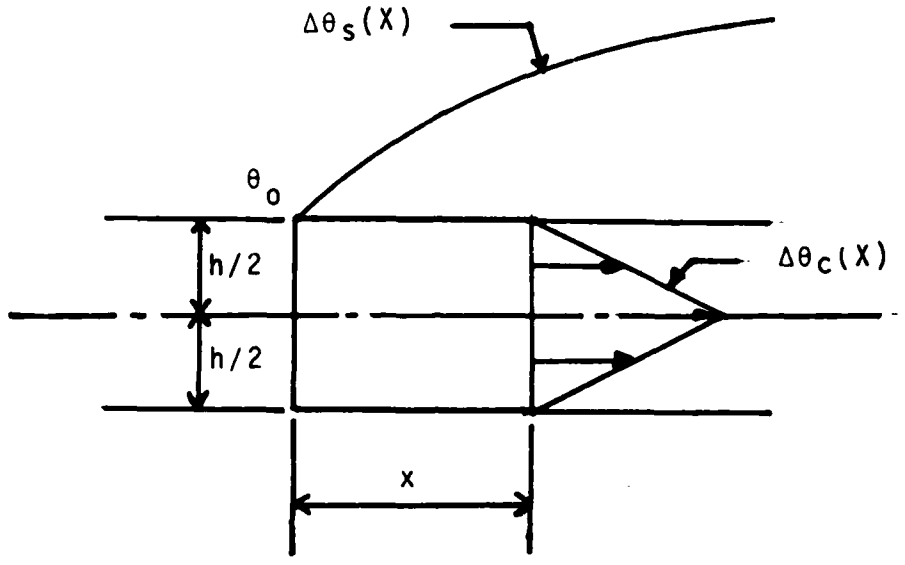

Fig. 7.1 SURFACE AND FILM TEMPERATURE PROFILES

k = thermal conductivity

h = film thickness

a(y) = half width of contact zone at coordinate position y

The subscript '**m**' indicates that the property is that of the solid.

Houpert's finite difference approximation for the mean plane temperature, accounting for conduction and convection is

$$\Delta\theta c(x) = \frac{[\{Q/k-\rho cu/k(\Delta\theta_s-\Delta\theta_s^*)/\Delta x\}h^2/8 + E\Delta\theta_c^*]}{1 + E} \qquad (7.9)$$

where

$$E \equiv \rho cuh^2/12k\Delta x \qquad (7.10)$$

and ρ,c and **k** are fluid properties.

Like τ_x^*, $\Delta\theta^*s$ and $\Delta\theta^*c$ refer to the previous interval. **Q**, the power dissipated in the film at position **x** is computed as described in Sections 7.1.1 and 7.1.2.

Eqs. (7.8) and (7.9) must be solved iteratively until mutually consistent functions $\theta s(x)$ and $\theta c(x)$ are found. A further issue is that the generated heat **Q** depends on the lubricant properties which themselves depend on the temperature distribution in the film and, through the pressure, on the position x,y.

7.2.2 Temperature and Pressure Dependence of Lubricant Properties

The shear modulus G was assumed constant at its average value, independent of pressure and temperature. The lubricant viscosity was initially assumed to vary with temperature θ and pressure **p** as

$$\eta(\theta,p) = \eta_o \exp[-\beta(\theta-\theta_o) + \alpha p] \qquad (7.11)$$

where η_o is the viscosity at ambient temperature θo and at ambient pressure. α is the pressure-viscosity index and β is the temperature-viscosity index. Eq. (7.11) may be written as

$$\eta(\theta,p) = \eta_\theta \exp[\alpha p] \qquad (7.12)$$

where

$$\eta_\theta = \eta_o \exp[-\beta(\theta-\theta_o)] \qquad (7.13)$$

In this form Eq. (7.12) is known as Barus' equation.

The viscosity averaged across the film at position **x** is:

$$\bar{\eta} = 2/h \int_o^{h/2} \eta[\theta(z)]dz \qquad (7.14)$$

Considering a triangular temperature distribution across the film, this yields:

$$\bar{\eta}_\theta = \eta_o \exp[-\beta\Delta\theta_s] \times [1-\exp[-\beta\Delta\theta_c]]/\beta\Delta\theta_c \qquad (7.15)$$

The critical shear stress was taken to be proportional to pressure following Tevaarwerk and Johnson [4] and, following Lingard [26], to be inversely proportional to the absolute temperature of the lubricant. This may be expressed as:

$$\tau_c = \varsigma p/T_o \tag{7.16}$$

where ς is a constant of proportionality, and $T_o = \theta o+460$ is the absolute ambient temperature. At constant temperature, the average value of τc is

$$\bar{\tau}_c = \varsigma \bar{p}/T_o \tag{7.17}$$

Knowing $\bar{\tau}_c$ at ambient temperature one may compute ς as:

$$\varsigma = \bar{\tau}_c/\bar{p} \bullet T_o \tag{7.18}$$

Letting $T_s = \theta_s+460$ be the absolute temperature of the solid at position **x** and $T_c = \theta c+460$ the corresponding absolute temperature of the center of the film, the mean value of τ_c assuming a linear temperature distribution across the film is

$$\bar{\tau}_c = \bar{\tau}_{co}[T_o/(T_c-T_s)]\ell n[T_c/T_s] \tag{7.19}$$

This expression was initially used within McFRIC but it was found that the thermal effect on traction was over predicted using this expression. Taking τ_c to be a function of pressure only resulted in greatly improved fits (cf. Section 10.0).

In the numerical solution for temperature, an initial film temperature rise $\Delta\theta c(x)$ was assumed by neglecting convection in

Eq. (7.9) and taking the heat generation rate **Q** to be the product of τ_c and $\Delta u/h$.

This gives

$$\Delta\theta c(x) = \tau_c \Delta\mu h/8 \qquad (7.20)$$

and τ_c varies with **x** because of its dependence on $p = p(x,y)$. This expression is used in Eq. (7.8) to yield $\Delta\theta s(x)$. Eq. (7.8) contains a singularity at $\psi = x$. In the implementation the first two values of $\Delta\theta_s(x)$ on each strip are taken to be zero.

For the third point, the following approximate expression developed by Houpert [24] is used:

$$\Delta\theta_s(x) = A[23.0\Delta\theta_c(x-\Delta x)-5.878\Delta\theta_c(x-2\Delta x)]k(\Delta x)^{1/2}/3h \qquad (7.21)$$

where

$$A \equiv [\pi\rho_m\, c_m\, k_m\, u]^{-1/2} \qquad (7.22)$$

For the fourth point,

$$\Delta\theta_s(x) = A[0.5773\Delta\theta_c(x-3\Delta x)-1.17\Delta\theta_c(x-2\Delta x) + 11\Delta\theta_c(x-\Delta x)] \times 2k(\Delta x)^2/3h \qquad (7.23)$$

For subsequent points

$$\Delta\theta_s(x) = A[I+10\Delta\theta_c(x-\Delta x)-4\Delta\theta_c(x-2\Delta x)2k(\Delta x)^{1/2}/3h \qquad (7.24)$$

where

$$I = \int_{-a(y)}^{x-\Delta x} \frac{-\Delta\theta_c(\psi)}{\sqrt{x-\psi}}\, d\psi \qquad (7.25)$$

is evaluated numerically using Simpson's rule.

Expressions (7.21) and (7.22) are found by integrating by parts over the singularity. Following the computation of $\Delta\theta s(x)$ the lubricant propertis are corrected, and the generated heat recomputed. Eq. (7.9) is then used to recompute $\Delta\theta c(x)$, now allowing for convection.

8.0 PROGRAM DESCRIPTION, ORGANIZATION LOGIC FLOW AND USERS INFORMATION

8.1 Description of Computer Program

The McFRIC program computes the components of sliding traction in the rolling direction and the transverse direction (orthogonal to the rolling direction) as well as the spinning torque for a general elastohydrodynamic (EHD) contact that experiences rolling, sliding and spinning. It calculates the power transmitted and the power lost for each kinematic condition. The lubricant shear force is modelled as viscoelastic/plastic with temperature and pressure dependent viscosity and limiting shear stress. Asperity friction is assumed to be Coulombic and is proportional to the asperity load computed via the Greenwood-Williamson microcontact model.

The program solution can be isothermal or it can consider the generation of heat due to fluid shear and asperity friction and its conduction through the film and convection along the rolling direction. For the thermal case, the program computes film mean plane and surface temperature distributions and outputs their average and maximum values over the contact.

In addition to traction related output, the program computes the contact dimensions, pressure, deflection, film thickness, including the effects of starvation and inlet heating, Deborah number and a surface fatigue index.

8.2 Program Organization

Computer program McFRIC is organized into 9 modules and comprises, in aggregate, a main routine, 15 subroutines and 17 function subprograms. The module names and their associated function and subroutine names are listed in Table 8.1. The input data comprises 34 elements of variable data and 17 run control variables. These input data elements are contained in an input file prepared and named by the user by editing a sample file supplied with the program disk. The input data is discussed further in Section 8.4.3 below.

8.3 Program Logic Flow

Figure 8.1 shows the overall logic flow for computer program McFRIC. On execution, the program requests that the name of an input data file be typed from the console. This file is then read and echoed in the printed output. The program calculates the contact parameters using subroutine HERTZ, the film thickness (starved, unstarved, constriction and plateau) using subroutine FILM and Deborah number (subroutine DEBORA). The microcontact parameters are computed using subroutine GW and a surface fatigue index is computed within the main program. The program enters a loop in which the sliding velocity is varied over a user specified range.

For each value of the sliding velocity the fluid traction forces and torque are computed through subroutine TRACT and its

Table 8.1 MODULES, FUNCTIONS AND SUBROUTINE NAMES FOR MCFRIC

MODULE	FUNCTION	SUBROUTINE
MCFRIC	INTEG, SIMPS, F1	MCFRIC (MAIN) PLOT
	F2, F3, FI	OUTPUT
INPOUT		OUTPUT INPUT PRINT
EHD	SOLN	HERTZ ELINT FILM
GW	FUNO, ERFC, FUN11 FUN321, FUN1, FUN32 ANORM, SPECEX, FUNC SPEC4	GW DEBORA
TRACT		TRACT
STRESS	FUN	STRESS XSTRESS
FTINT		FTINT
MAXAV		MAXAV
HEAT		HEAT

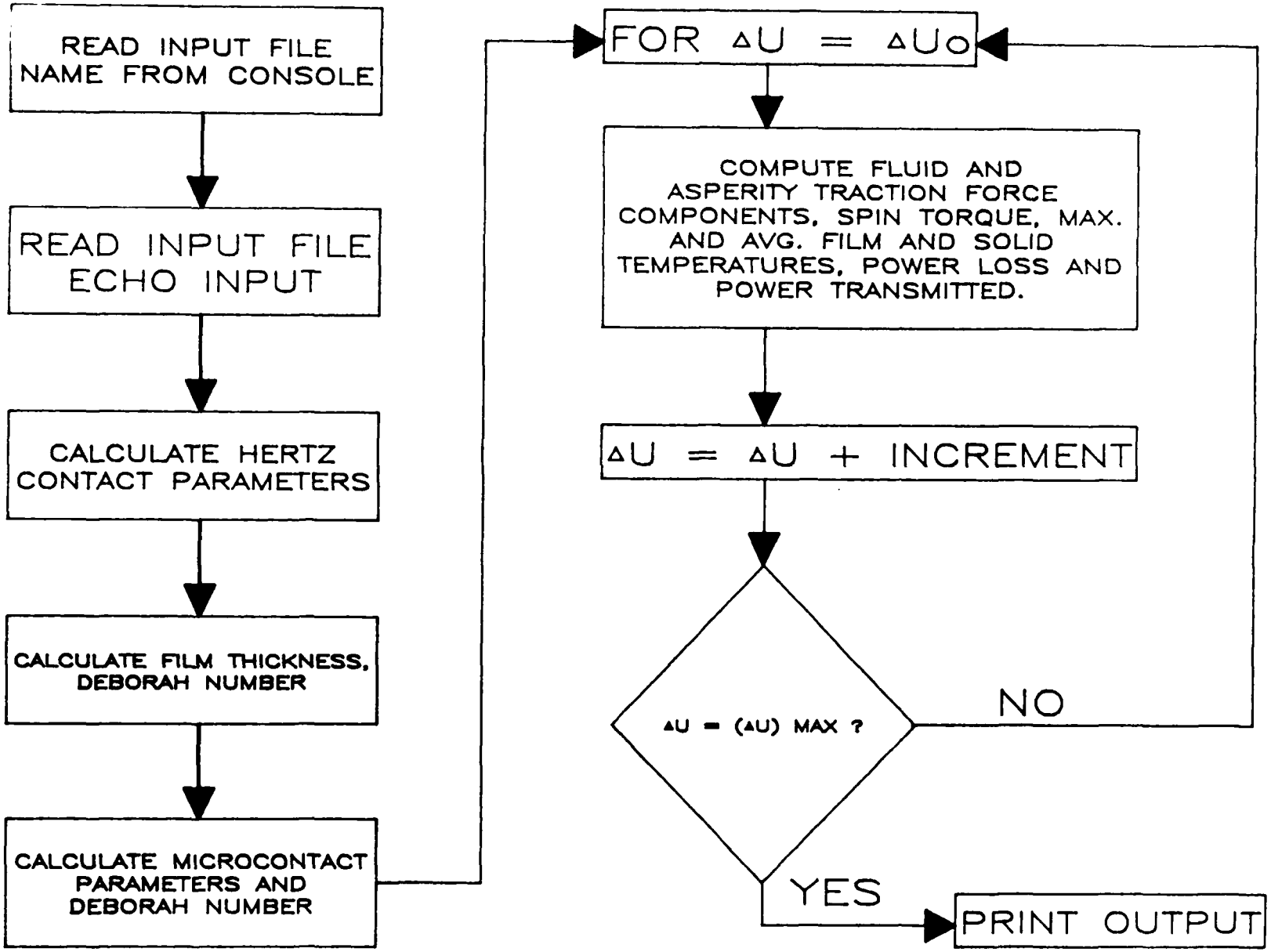

Fig. 8.1 — OVERALL FLOW DIAGRAM FOR PROGRAM McFRIC

subsidiary subroutines. TRACT is discussed in more detail below. At the completion of the traction computational loop, the remaining program output is printed. At the user's option printer plots may be specified in which up to 12 traction related variables may be plotted against sliding speed.

Figure 8.2 is a detailed flow diagram for subroutine TRACT. As noted, it computes fluid traction point-by-point over the contact area, at a specified value of the sliding velocity Δu. The contact ellipse is divided into NY strips of thickness $\Delta y = 2\,b/NY$. The index "I" references the individual strips. For each strip the half width a(y) and maximum pressure p(y) are computed along with the step length in the **x** direction $\Delta x = 2a(y)/NX$ (NX = number of elements on each strip).

The index "J" references each of the NX individual rectangular elements along a strip, in the **x** direction. The pressure at each element determines the viscosity $\eta(p)$ and the limiting shear $\tau_c(p)$. The shear rates $\dot{\gamma}_x$ and $\dot{\gamma}_y$ are functions of the location of each element, i.e., the x,y coordinates or, equivalently the I and J indices. The stress components τ_x and τ_y and the torque contribution of the element are then found as a function of the lubricant properties and shear rates using subroutine STRESS which implements the solution scheme outlined in Section 6.0. At this point, for an isothermal solution ITHERM = 0, TRACT increments the index J, i.e., it moves to the next adjacent element along the Ith strip.

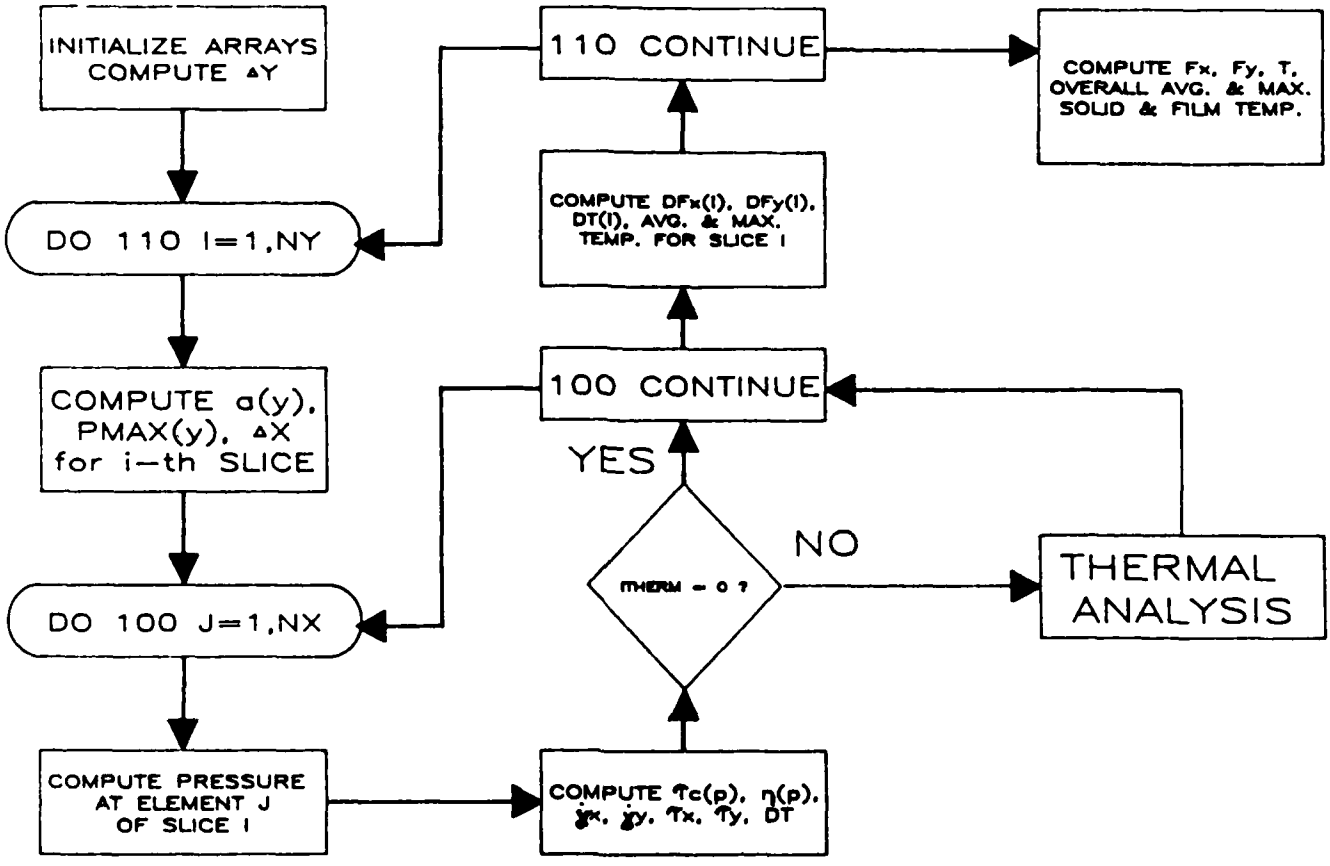

Fig. 8.2 — LOGIC DIAGRAM FOR SUBROUTINE TRACT

For a thermal solution (ITHERM=1), TRACT calls subroutine HEAT (cf. Fig. 8.2.1) to calculate the generated heat at the element location (I,J) due to fluid shear (Q_f) and asperity friction Q_c. An initial guess of the maximum film temperature rise $\Delta\theta_c$ is made and given the temporary variable name DTETA1. A second temporary variable DTETAS1 is set to zero. The surface temperature at location J is now estimated as outlined in Section 7.0 and then set equal to the variable DTETAS2. Iteration counters ITER1 and ITER2 are maintained for convergence of the surface and film temperatures, respectively. They have limiting values MAXIT1 and MAXIT2 presently set within the program to 50. The fluid properties averaged over the film temperature are next computed as outlined in Section 7.0. The shear stresses, torque contribution and heat are then recomputed using the modified properties. A new value of $\Delta\theta_c(J)$ is then computed and set equal to the temporary variable DTETA2. DTETA1 and DTETA2 are compared. If they differ by more than the value EPS1 (EPS1 = 0.001 and EPS2 = 0.1 are the values presently hard coded in the program), DTETA1 is set to DTETA2 and another iteration is performed for $\Delta\theta_c(x)$. When convergence is achieved, $\Delta\theta_c(J)$ is set to the last value of DTETA2. Convergence of the surface temperature is then checked by comparing DTETAS2 and DTETAS1. If it has not occurred, DTETAS1 is set to DTETAS2 and another iteration is performed. Convergence failure messages are printed to the screen if the maximum number of iterations is exceeded in either loop, but,

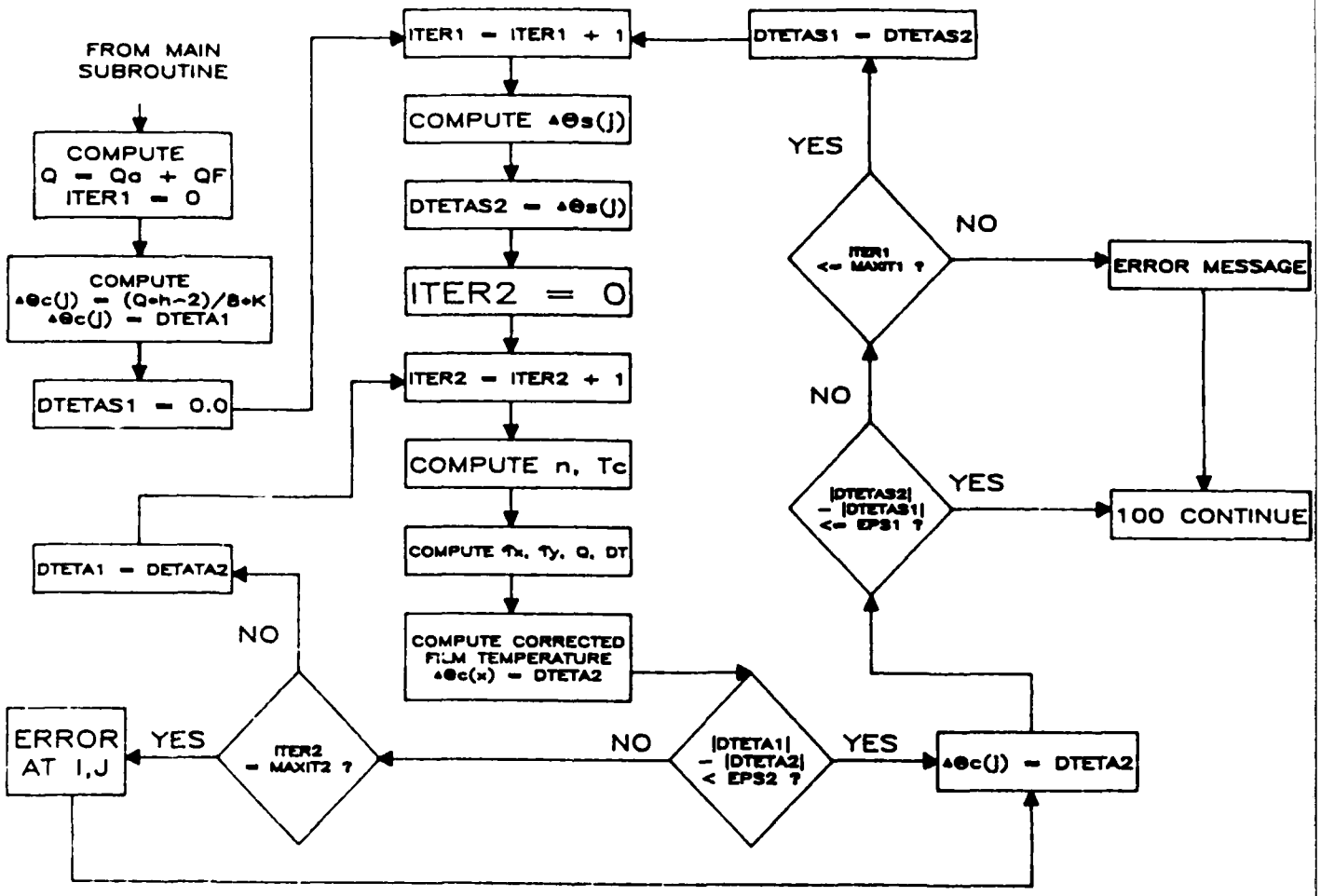

Fig 8.2.1 THERMAL ANALYSIS

computation proceeds as indicated. (In such cases, the user must then exercise discretion in using the results. Convergence failure has not, however, been a problem in the test evaluations of McFRIC discussed in Section 10.0).

When convergence is achieved for each element of a given slice, the shear stresses and differential torque are integrated to give the contributions DFX(I), DFY(I) and DT(I) of the slice to the traction force components FX and FY and to the torque T. A subroutine MAXAV is also used to find the average and maximum solid and film temperature at the slice. When all slices are complete, an integration is performed over the slices to give the resultant values of FX, FY and T. MAXAV is then reinvoked to give the overall average and maximum values of the solid and film temperatures.

8.4 User's Information

Section 8.4 is a detailed description of how to use the McFRIC program. Topics in this section include instructions for loading and executing the program, and a discussion of the output data for a sample case. The information is intended to be sufficient to permit a user to successfully run and interpret the results of the McFRIC program.

8.4.1 Installing the Program

McFRIC is written in the FORTRAN language and is executable on IBM-PC-XT or AT computers using the DOS operating system. It

is recommended that the program be executed on a computer which has the appropriate Math Co-processor chip (8087 or 80287) installed.

The program is delivered on two floppy diskettes. The first diskette (Diskette No. 1) contains the following files:

MCFRIC.EXE - Executable code for McFRIC program

MCF.BAT - Batch file for executing McFRIC program

SAMPLE.DAT - Sample problem data file

The second diskette (Diskette No. 2) contains source code files (.FOR) for the modules making up the McFRIC program: MCFRIC, INPOUT, EHD, GW, TRACT, STRESS, FTINT, MAXAV, and HEAT.

It is recommended for ease and speed of execution that the program be installed on the IBM-PC hard disk. To copy the program onto the hard disk, use the following procedure:

1. Turn on the computer and set the default drive to C:
2. Insert Diskette No. 1 into Drive A
3. Issue the command COPY A:*.*

When the copy operation is completed, remove the floppy diskette and store it in a safe location. If desired, Diskette No. 2 can be copied onto the hard disk using the same procedure. However, the files on Diskette No. 2 will only be needed if the program is to be modified.

8.4.2 Executing the Program

Once the program has been copied onto the hard disk, it may be executed as follows:

1. Set default drive to C (C>)
2. Issue the following command: MCF

The program should begin execution by displaying a heading on the screen and prompting the user for the name of an input data file. By typing SAMPLE.DAT, the sample case data file can be used to verify that the program is executing properly. A listing of the sample case data file is given as Fig. 8.3. The corresponding program output is included as Fig. 8.4. Section 8.4.3 below contains instructions for creating an input data file in the format required by the program.

8.4.3 Creating an Input Data File

The McFRIC program has been set up to read the input data from a standard ASCII file which can reside on the hard disk (C:___) or on a floppy disk (A:___ or B:___). The recommended technique for creating a new data file is as follows:

1. Use the DOS COPY command to copy an old data file into a new file. For example, by issuing the command COPY C:SAMPLE.DAT C:CASE1.DAT, a new file named CASE1.DAT will be created on the hard disk containing the sample case data.

```
THREE TITLE LINES DESCRIBING THE RUN:
-------------------------------------------------------------
---------
TEST CASE CREATED FROM WPAFB TEST DATA FILE M18N9g0
LOAD = 140.1 LBS, ROLLING VELOCITY = 748 IN/SEC
AMBIENT TEMPERATURE = 183 DEG. F

MATERIAL DATA:
-------------------------------------------------------------
---------
ELASTIC MODULUS OF BODY I                          (lb/in**2)
[EMOD(1)] ..    29.5E6
ELASTIC MODULUS OF BODY II                         (lb/in**2)
[EMOD(2)] ..    29.5E6
POISSON'S RATIO FOR BODY I
[PRAT(1)] ..     0.30
POISSON'S RATIO FOR BODY II
[PRAT(2)] ..     0.30
TENSILE YIELD STRESS OF SOFTER MATERIAL            (lb/in**2)
[SIGMAE] ...    3.62E5
COULOMB FRICTION COEFFICIENT
[EF] .......     0.06
DENSITY                                            (lb/in**3)
[ROM] ......     0.284
SPECIFIC HEAT                                (Btu/lbm-deg. F)
[CM] .......     0.11
THERMAL CONDUCTIVITY                          (lb/sec-deg. F)
[AKM] ......     7.34

GEOMETRY AND ENVIRONMENTAL DATA:
-------------------------------------------------------------
---------
RADIUS OF BODY I  TRANSVERSE TO ROLLING DIRECTION   (in)
[RI1] ......    0.71
RADIUS OF BODY I  IN ROLLING DIRECTION              (in)
[RI2] ......    0.75
RADIUS OF BODY II TRANSVERSE TO ROLLING DIRECTION   (in)
[RII1] .....    0.71
RADIUS OF BODY II IN ROLLING DIRECTION              (in)
[RII2] .....    0.75
VELOCITY OF BODY I  IN ROLLING DIRECTION        (in/sec)
[UI] ....... 748.18
VELOCITY OF BODY II IN ROLLING DIRECTION        (in/sec)
[UII] ...... 748.18
TRANSVERSE DIRECTION SLIDING VELOCITY           (in/sec)
[DELV] .....    0.0
SPINNING VELOCITY                          (radians/sec)
[OMEGA] ....    0.0
MENISCUS DISTANCE                                   (in)
[EXB] ......    1.0
CONTACT NORMAL LOAD                            (lbs) [P]
........ 140.1
AMBIENT TEMPERATURE                            (deg. F)
[TAMB] ..... 183.0
```

Fig. 8.3 INPUT FILE - SAMPLE.DAT

```
LUBRICANT DATA:
-------------------------------------------------------------
---------
KINEMATIC VISCOSITY AT OPERATING TEMPERATURE        (cst)
[VISCS] ....  1.31
SPECIFIC GRAVITY
[SPGR] .....  1.7627
TEMPERATURE VISCOSITY COEFFICIENT              (1/deg. R)
[BETA] .....  1.01E-2
PRESSURE VISCOSITY INDEX                       (in**2/lb)
[ALPHA1] ...  7.14E-5
THERMAL CONDUCTIVITY                     (lb/sec-deg. F)
[CON] ......  0.0086
SPECIFIC HEAT                           (Btu/lbm-deg. F)
[CF] .......  0.200
AVERAGE SHEAR MODULUS                          (lb/in**2)
[GBAR] ..... 2443.69
LIMITING SHEAR STRESS                          (lb/in**2)
[TAUC] .....12603.41

SURFACE DATA:
-------------------------------------------------------------
---------
RMS SURFACE HEIGHT FOR BODY I                 (microinch)
[RQ1] ......   2.0
RMS SURFACE HEIGHT FOR BODY II                (microinch)
[RQ2] ......   2.0
RMS PROFILE SLOPE FOR BODY I
[DELQ1] ....   0.035
RMS PROFILE SLOPE FOR BODY II
[DELQ2] ....   0.035
LOWER FREQUENCY LIMIT                             (1/in)
[FR11] .....  50.0
UPPER FREQUENCY LIMIT                             (1/in)
[FR21] .....10000.0

RUN CONTROL DATA:
-------------------------------------------------------------
---------
INCREMENT FOR DELTAU = UI - UII                  (in/sec)
[UINC] ..... 1.0
MAXIMUM VALUE FOR DELTAU                         (in/sec)
[UMAX] ..... 10.0
TYPE OF ANALYSIS <0 = ISOTHERMAL, 1 = THERMAL>
[ITHERM] ...0
PLOT SELECTION ARRAY <0 = NO PLOT, 1 = PLOT> :
  PLOT FLUID SHEAR FORCE IN ROLLING DIRECTION (FX)?
[IVEC(1)] ..1
  PLOT FLUID SHEAR FORCE IN TRANSVERSE DIRECTION (FY)?
[IVEC(2)] ..0
  PLOT TORQUE DUE TO FLUID SHEAR (T)?
[IVEC(3)] ..0
  PLOT EXPECTED ASPERITY TRACTION FORCE
```

```
            - IN ROLLING DIRECTION (E(FX))?
[IVEC(4)] ..0
            - IN TRANSVERSE DIRECTION (E(FY))?
[IVEC(5)] ..0
  PLOT EXPECTED TORQUE DUE TO ASPERITY FRICTION (E(T))?
[IVEC(6)] ..0
  PLOT TOTAL TRACTION FORCE
            - IN ROLLING DIRECTION (FX+E(FX))?
[IVEC(7)] ..0
            - IN TRANSVERSE DIRECTION (FY+E(FY))?
[IVEC(8)] ..0
  PLOT TOTAL TRACTION TORQUE (T+E(T))?
[IVEC(9)] ..0
  PLOT COMBINED FRICTIONAL POWER LOSS (EL)?
[IVEC(10)] .0
  PLOT POWER TRANSMITTED THROUGH CONTACT (ET)?
[IVEC(11)] .0
  PLOT LOSS FACTOR (LF)?
[IVEC(12)] .0
NUMBER OF DIVISIONS OF CONTACT ELLIPSE
          - IN ROLLING DIRECTION
[NXDIV] ....41
          - IN TRANSVERSE DIRECTION
[NYDIV] ....41
```

```
*********************************************
*                                           *
*          McFRIC COMPUTER PROGRAM          *
*                                           *
*  VERSION : 1.0    RELEASE DATE : 8-15-86  *
*                                           *
*  SKF TRIBONETICS     KING OF PRUSSIA, PA  *
*                                           *
*********************************************
```

TEST CASE CREATED FROM WPAFB TEST DATA FILE M18N9g0
LOAD = 140.1 LBS, ROLLING VELOCITY = 748 IN/SEC
AMBIENT TEMPERATURE = 183 DEG. F

INPUT DATA FILE : SAMPLE.DAT

I. M A T E R I A L V A R I A B L E S

EMOD(1) - YOUNG'S MODULUS FOR BODY I = 2.950000E+07 LB/IN**2

EMOD(2) - YOUNG'S MODULUS FOR BODY II = 2.950000E+07 LB/IN**2

PRAT(1) - POISSON'S RATIO FOR BODY I = 3.000000E-01

PRAT(2) - POISSON'S RATIO FOR BODY II = 3.000000E-01

SIGMAE - TENSILE YIELD STRENGTH = 3.620000E+05 LB/IN**2

EF - COULOMB FRICTION COEFFICIENT = 6.000000E-02

ROM - DENSITY = .284000E+00 LB/IN**3

CM - SPECIFIC HEAT = .110000E+00 BTU/LBM-DEG. F

AKM - THERMAL CONDUCTIVITY = .734000E+01 LB/SEC-DEG. F

Fig. 8.4 McFRIC OUTPUT FOR FILE SAMPLE.DAT

TEST CASE CREATED FROM WPAFB TEST DATA FILE M18N9g0
LOAD = 140.1 LBS, ROLLING VELOCITY = 748 IN/SEC
AMBIENT TEMPERATURE = 183 DEG. F

1. GEOMETRY AND ENVIRONMENTAL VARIABLES

RI1 - RADIUS OF BODY I (TRANSVERSE TO ROLLING DIRECTION)	=	7.10000E-01 INCHES
RI2 - RADIUS OF BODY I (IN ROLLING DIRECTION)	=	7.50000E-01 INCHES
RII1 - RADIUS OF BODY II (TRANSVERSE TO ROLLING DIRECTION)	=	7.10000E-01 INCHES
RII2 - RADIUS OF BODY II (IN ROLLING DIRECTION)	=	7.50000E-01 INCHES
UI - VELOCITY OF BODY I (IN ROLLING DIRECTION)	=	7.48180E+02 INCHES/SEC
UII - VELOCITY OF BODY II (IN ROLLING DIRECTION)	=	7.48180E+02 INCHES/SEC
DELV - TRANSVERSE DIRECTION SLIDING VELOCITY	=	.00000E+00 INCHES/SEC
OMEGA - SPINNING VELOCITY	=	.00000E+00 RADIANS/SEC
EXB - MENISCUS DISTANCE	=	1.00000E+00 INCHES
P - LOAD	=	1.40100E+02 LBS
TAMB - AMBIENT TEMPERATURE	=	.18300E+03 DEG. F

TEST CASE CREATED FROM WPAFB TEST DATA FILE M18N9g0
LOAD = 140.1 LBS, ROLLING VELOCITY = 748 IN/SEC
AMBIENT TEMPERATURE = 187 DEG. F

III. L U B R I C A N T V A R I A B L E S

VISCS - OIL VISCOSITY AT OPERATING TEMPERATURE	= 1.310000E+00	CENTISTOKES
SPGR - SPECIFIC GRAVITY OF OIL	= 1.762700E+00	
ETA0 - ABSOLUTE VISCOSITY	= 3.348248E-07	LB-SEC/IN**2
BETA - TEMPERATURE VISCOSITY COEFFICIENT	= 1.010000E-02	1/DEG. R
ALPHA1 - PRESSURE VISCOSITY INDEX	= 7.140000E-05	IN**2/LB
CON - THERMAL CONDUCTIVITY OF LUBRICANT	= 8.600000E-03	LB/SEC-F
GBAR - AVERAGE SHEAR MODULUS	= 2.443690E+03	LBS/IN**2
TAUC - LIMITING SHEAR STRESS	= 1.260341E+04	LBS/IN**2
CP - SPECIFIC HEAT	= .200000E+00	BTU/LBM-DEG. F

AD-A188 458 TRACTION MODEL DEVELOPMENT(U) MRC BEARINGS-SKF 2/2
AEROSPACE KING OF PRUSSIA PA J I MCCOOL SEP 87
AFWAL-TR-87-4079 F33615-84-C-5028

UNCLASSIFIED F/G 11/8 NL

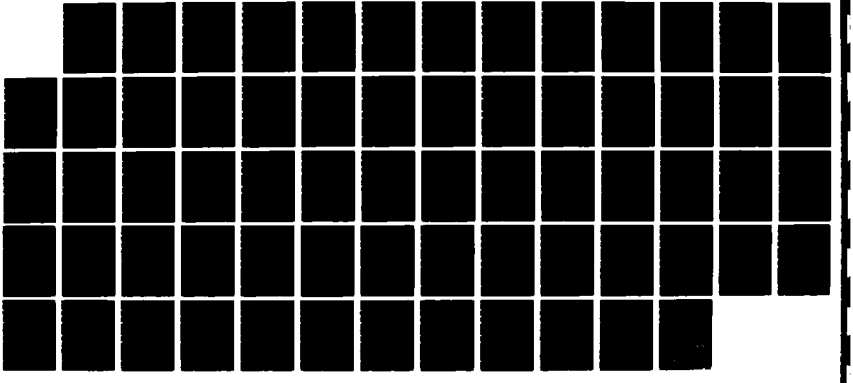

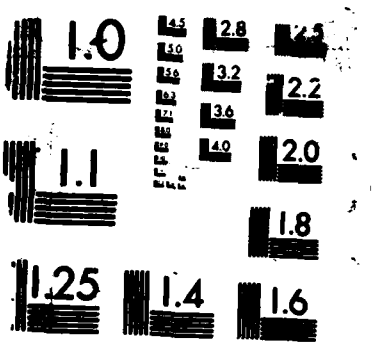

MICROCOPY RESOLUTION TEST CHART

TEST CASE CREATED FROM WPAFB TEST DATA FILE M18N9g0
LOAD = 140.1 LBS, ROLLING VELOCITY = 748 IN/SEC
AMBIENT TEMPERATURE = 183 DEG. F

IV. SURFACE ROUGHNESS VARIABLES

RQ1 - ROOT MEAN SQUARE SURFACE HEIGHT FOR BODY I = 2.00000 MICROINCH

RQ2 - ROOT MEAN SQUARE SURFACE HEIGHT FOR BODY II = 2.00000 MICROINCH

RQ - COMPOSITE ROOT MEAN SQUARE SURFACE HEIGHT = 2.82843 MICROINCH

DELQ1 - ROOT MEAN SQUARE PROFILE SLOPE FOR BODY I = .03500

DELQ2 - ROOT MEAN SQUARE PROFILE SLOPE FOR BODY II = .03500

DELQ - COMPOSITE ROOT MEAN SQUARE PROFILE SLOPE = .04950

FR11 - LOWER FREQUENCY LIMIT = 50.00000 1/IN

FR21 - UPPER FREQUENCY LIMIT = 10000.00000 1/IN

TEST CASE CREATED FROM WPAFB TEST DATA FILE M18N9g0
LOAD = 140.1 LBS, ROLLING VELOCITY = 748 IN/SEC
AMBIENT TEMPERATURE = 183 DEG. F

V. RUN CONTROL VARIABLES

DINC - INCREMENT FOR DELTAU = 1.00000 IN/SEC

DMAX - MAXIMUM VALUE FOR DELTAU = 10.00000 IN/SEC

ITHERM - TYPE OF ANALYSIS (0=ISOTHERMAL,1=THERMAL) = 0

VARIABLE NAME	PLOT SELECTION INDEX (1=PLOT VS U; 0=NO PLOT)
FX	1
FY	0
T	0
E(FX)	0
E(FY)	0
E(T)	0
FX + E(FX)	0
FY + E(FY)	0
T + E(T)	0
EL	0
ET	0
LF	0

TEST CASE CREATED FROM WPAFB TEST DATA FILE M18N9g0
LOAD = 140.1 LBS, ROLLING VELOCITY = 748 IN/SEC
AMBIENT TEMPERATURE = 183 DEG. F

H E R T Z C O N T A C T P A R A M E T E R S

AREA - AREA OF CONTACT ELLIPSE	=	5.62472E-04 INCHES**2
DELTA - TOTAL ELASTIC APPROACH	=	4.90480E-04 INCHES
SIGMA0 - MAXIMUM HERTZ CONTACT PRESSURE	=	3.73619E+05 LBS/IN**2
A - CONTACT ELLIPSE SEMIAXIS IN ROLLING DIRECTION	=	1.36275E-02 INCHES
B - CONTACT ELLIPSE SEMIAXIS IN TRANSVERSE DIRECTION	=	1.31381E-02 INCHES

TEST CASE CREATED FROM WPAFB TEST DATA FILE M18N9g0
LOAD = 140.1 LBS, ROLLING VELOCITY = 748 IN/SEC
AMBIENT TEMPERATURE = 183 DEG. F

F I L M T H I C K N E S S E S A N D R E D U C T I O N F A C T O R S

HCF - FULLY FLOODED CENTRAL FILM THICKNESS	=	6.48435E-06 INCHES
HMF - FULLY FLOODED CONSTRICTION FILM THICKNESS	=	3.80854E-06 INCHES
PHISC - CENTRAL FILM STARVATION FACTOR	=	1.00000E+00
HCS - STARVED CENTRAL FILM THICKNESS	=	6.48435E-06 INCHES
PHISM - CONSTRICTION FILM STARVATION FACTOR	=	1.00000E+00
HMS - STARVED MINIMUM FILM THICKNESS	=	3.80854E-06 INCHES
PHIT - INLET HEATING REDUCTION FACTOR	=	9.09253E-01
H - NET CENTRAL FILM THICKNESS	=	5.89592E-06 INCHES
HM - NET MINIMUM FILM THICKNESS	=	3.46293E-06 INCHES

TEST CASE CREATED FROM WPAFB TEST DATA FILE M18N9g0
LOAD = 140.1 LBS, ROLLING VELOCITY = 748 IN/SEC
AMBIENT TEMPERATURE = 183 DEG. F

T R A C T I O N V A R I A B L E S

D - DEBORAH NUMBER (BASED ON = .39807E+03
AVERAGE PRESSURE)

DELTAX - LOAD CENTER DISPLACEMENT = .53026E-04 INCHES

TEST CASE CREATED FROM WPAFB TEST DATA FILE M18N9g0
LOAD = 140.1 LBS, ROLLING VELOCITY = 748 IN/SEC
AMBIENT TEMPERATURE = 183 DEG. F

DEFINITION OF PARAMETERS

DELTAU - SLIDING VELOCITY (IN/SEC)

FX - FLUID SHEAR FORCE IN ROLLING DIRECTION (LBS)

FY - FLUID SHEAR FORCE IN TRANSVERSE DIRECTION (LBS)

T - TORQUE DUE TO FLUID SHEAR (IN-LBS)

EFX - EXPECTED ASPERITY FRICTIONAL TRACTION IN ROLLING DIRECTION (LBS)

EFY - EXPECTED ASPERITY FRICTIONAL TRACTION IN TRANSVERSE DIRECTION (LBS)

ET - EXPECTED TORQUE DUE TO ASPERITY FRICTION (IN-LBS)

EFX+FX - TOTAL TRACTION FORCE IN ROLLING DIRECTION (LBS)

EFY+FY - TOTAL TRACTION FORCE IN TRANSVERSE DIRECTION (LBS)

ET+T - TOTAL TRACTION TORQUE (IN-LBS)

EL - COMBINED FRICTIONAL POWER LOSS (HP)

ETR - POWER TRANSMITTED THROUGH CONTACT (HP)

LF - LOSS FACTOR

TEST CASE CREATED FROM WPAFB TEST DATA FILE M18N9g0
LOAD = 140.1 LBS, ROLLING VELOCITY = 748 IN/SEC
AMBIENT TEMPERATURE = 183 DEG. F

DELTAJ	FX	FY	T	EFX	EFY	ET	FX+EFX	FY+EFY	T+ET	EL	ETR	LF
.000	.00E+00	.00E+00	.00E+00	.00E+00	.00E+00	.00E+00	.00E+00	.00E+00	.00E+00	.00E+00	.00E+00	.00E+00
1.000	3.01E+00	.00E+00	-1.60E-19	1.86E-01	.00E+00	-9.96E-04	3.19E+00	.00E+00	-9.96E-04	4.83E-04	3.62E-01	1.34E-03
2.000	5.02E+00	.00E+00	3.34E-20	1.04E-04	.00E+00	.00E+00	5.02E+00	.00E+00	3.34E-20	1.52E-03	5.69E-01	2.67E-03
3.000	5.98E+00	.00E+00	-4.48E-19	5.87E-08	.00E+00	.00E+00	5.98E+00	.00E+00	-4.48E-19	2.72E-03	6.78E-01	4.01E-03
4.000	6.42E+00	.00E+00	-1.51E-18	3.30E-11	.00E+00	.00E+00	6.42E+00	.00E+00	-1.51E-18	3.89E-03	7.28E-01	5.35E-03
5.000	6.63E+00	.00E+00	-1.53E-18	1.86E-14	.00E+00	.00E+00	6.63E+00	.00E+00	-1.53E-18	5.03E-03	7.52E-01	6.68E-03
6.000	6.75E+00	.00E+00	2.29E-18	1.05E-17	.00E+00	.00E+00	6.75E+00	.00E+00	2.29E-18	6.13E-03	7.65E-01	8.02E-03
7.000	6.81E+00	.00E+00	1.71E-18	5.88E-21	.00E+00	.00E+00	6.81E+00	.00E+00	1.71E-18	7.22E-03	7.72E-01	9.36E-03
8.000	6.85E+00	.00E+00	-1.13E-18	3.31E-24	.00E+00	.00E+00	6.85E+00	.00E+00	-1.13E-18	8.30E-03	7.77E-01	1.07E-02
9.000	6.88E+00	.00E+00	2.03E-18	1.86E-27	.00E+00	.00E+00	6.88E+00	.00E+00	2.03E-18	9.38E-03	7.80E-01	1.20E-02
10.000	6.90E+00	.00E+00	1.16E-18	1.05E-30	.00E+00	.00E+00	6.90E+00	.00E+00	1.16E-18	1.04E-02	7.82E-01	1.34E-02

TEST CASE CREATED FROM WPAFB TEST DATA FILE M18N9g0
LOAD = 140.1 LBS, ROLLING VELOCITY = 748 IN/SEC
AMBIENT TEMPERATURE = 183 DEG. F

L O A D S H A R I N G D A T A A T H / S I G = 2.08452

ZNCON - EXPECTED NUMBER OF CONTACTS = .18778E-25

AVF - AVERAGE CONTACT FORCE = .64687E-03 LBS

TOTF - TOTAL CONTACT FORCE = .21555E+01 LBS

AVA - AVERAGE CONTACT AREA = .11518E-08 IN**2

TOTA - TOTAL CONTACT AREA = .21627E-34 IN**2

DSUM1 - NO. OF SUMMITS ON EQUIVALENT SURFACE = .33215E+05

M4 - MEAN SQUARE CURVATURE = .47234E+07 IN**(-2)

R - ASPERITY TIP RADIUS = .30575E-03 IN

K - SPECTRAL EXPONENT = .10879E+01

TEST CASE CREATED FROM WPAFB TEST DATA FILE M18N9g0
LOAD = 140.1 LBS, ROLLING VELOCITY = 748 IN/SEC
AMBIENT TEMPERATURE = 183 DEG. F

S U R F A C E F A T I G U E P A R A M E T E R S

ZNPLAS - EXPECTED NO. OF PLASTIC CONTACTS = .16354E+04

APLAS - EXPECTED AREA OF PLASTIC CONTACTS = .49911E-09 IN**2

PHIA - SURFACE FATIGUE INDEX = .81624E-06

FX VERSUS DELTAU

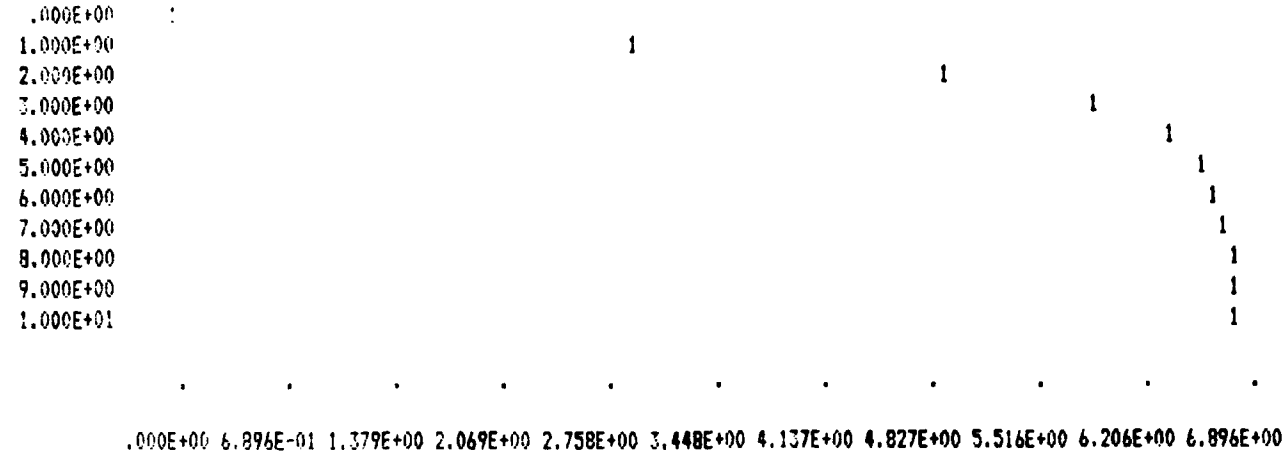

.000E+00 6.896E-01 1.379E+00 2.069E+00 2.758E+00 3.448E+00 4.137E+00 4.827E+00 5.516E+00 6.206E+00 6.896E+00

FX

2. Use a commercial editor or word processing package (such as WORDSTAR in non-document mode or WORD in non-formatted mode) to edit the data in the new file.

As already noted, the required input data file structure is illustrated in Fig. 8.3. In setting up the file structure, effort has been taken to make editing of the input data possible without reference to a manual. To this end, all of the headings, variable descriptions, units and symbols, and blank or dashed lines shown in Fig. 8.3 are built right into the data file. (**Important Note**: Since the program uses fixed format FORTRAN read statements, it is vital that the user edit only the data fields. None of the headings, variable descriptions, blank lines, etc. should be deleted or changed in length because the program expects to read the data in a specific location).

The input parameters are organized into 6 general categories: title information, material data, geometry and environmental data, lubricant data, surface data, and run control data. The input data fields are identified by the characters A (Alphanumeric) F (Floating Point) and I (Integer) indicating the type of data expected. Alphanumeric data consists of any combination of numbers letters or symbols. As noted, the program output produced by this input file is included as Fig. 8.4.

9.0 TRACTION TEST PROGRAM

As part of the contract effort, a set of four lubricants were selected, fluid samples were acquired and a traction test program was designed and performed within AFML, using an Air Force owned traction rig. The dual purpose of the traction test program was to provide input data for McFRIC and to evaluate its predictive accuracy.

9.1 Traction Rig and Test Variables

The parallel axis, two disc traction apparatus used in this study is shown schematically in Fig. 9.1. A full description is given in Smith [25]. A characteristic of the rig is that it requires only a small amount (400 ml) of the test fluid. The crowned discs are separately driven via independent drive transmissions and variable speed motors. A normal load is applied by means of a pneumatic load system. A variable speed pump is used to circulate the oil. A heat exchanger in the inlet line maintains the lubricant at the desired temperature.

The discs are made of 52100 vacuum degassed alloy steel with a hardness of 60-63 Rc. They are 1.5 in. in diameter. In the test program the disks had a lateral or crown radius of either 0.71 in., providing a nearly circular contact zone, or 6.22 in. providing a 4:1 aspect ratio, i.e., ratio of the major-to-minor axes of the contact ellipse.

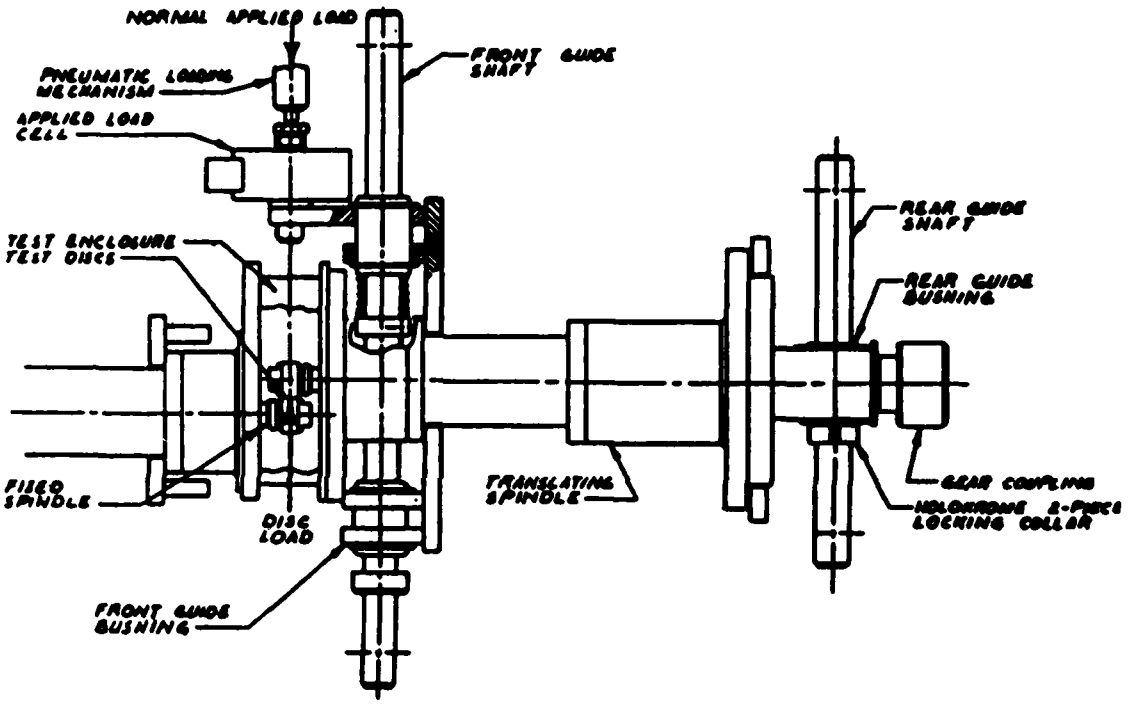

Fig. 9.1 AFML TRACTION RIG

The test variables employed were:

1. normal load
2. surface speed (rolling velocity)
3. temperature
4. aspect ratio (1:1 or 4:1)

When a test is performed a data acquisition system records the transmitted torque and speeds of the two spindles. The raw data is subsequently read on a mainframe computer and torque is converted to traction coefficient, and the rotational speeds are converted to sliding speed scaled by rolling speed. Fig. 9.2 is a plot and Table 9.1 the adjusted numerical data from a typical test.

9.2 Lubricant Selection

The lubricants selected after joint discussion with AFML were:

1. Mobil RL714 base stock, a synthetic hydrocarbon
2. Monsanto Santotrac 50, a traction fluid
3. Halocarbon Products SAFETOL-R-3.1, CTFE hydraulic fluid
4. Montedison Fomblin Z, a perfluoroalkylether

These oils were chosen for their chemical diversity consistent with being of intrinsic interest to AFML.

During the course of the test program it was discovered that Fluid No. 4 had an adverse effect on the test specimens. Testing was, therefore, suspended on this fluid.

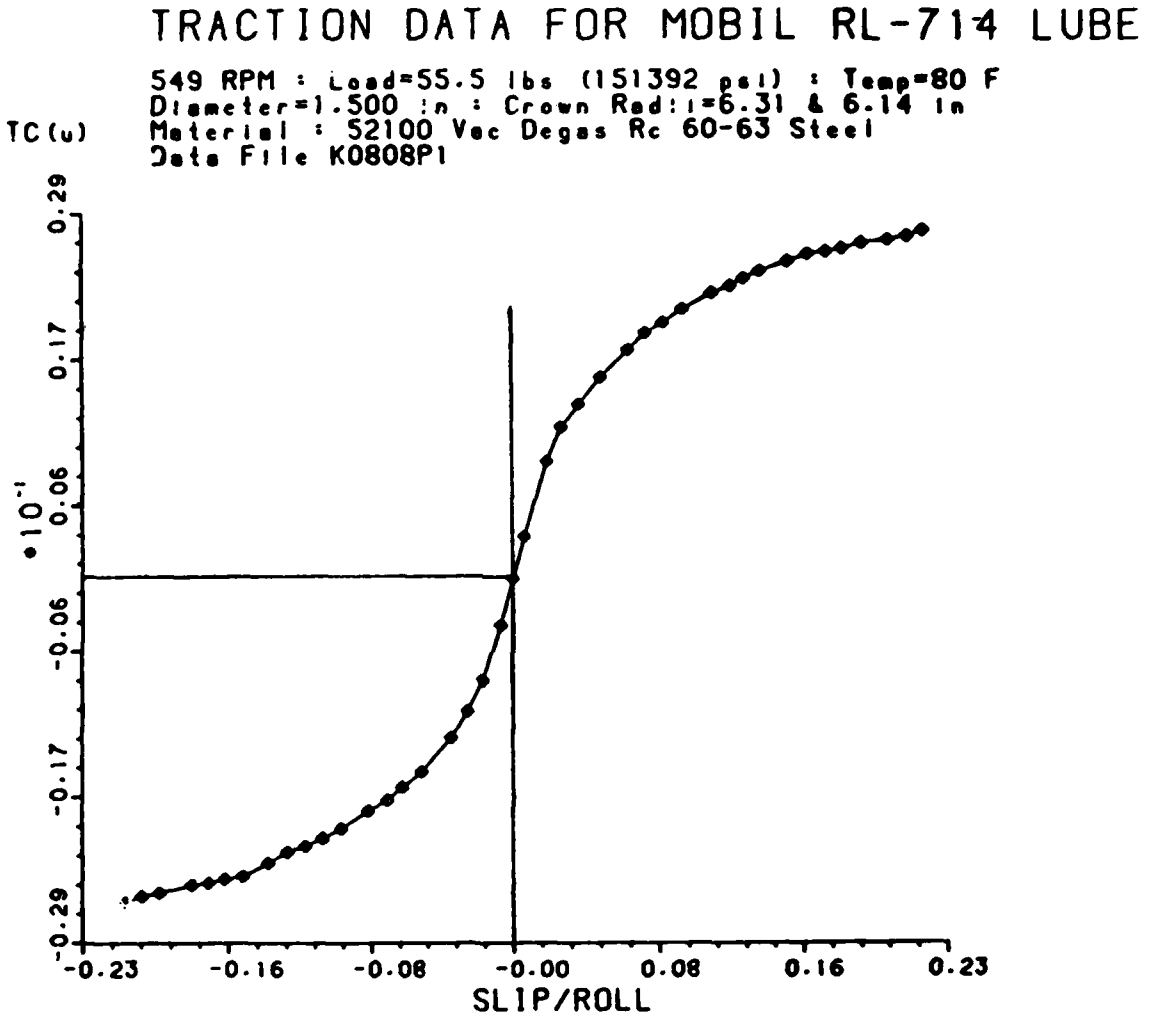

Fig. 9.2 EXPERIMENTAL TRACTION CURVE

TABLE 9.1 ADJUSTED TRACTION DATA POINTS

TRACTION DATA FOR MOBIL RL-714 LUBE
549 RPM : Load=55.5 lbs (151392 psi) : Temp=80 F
Diameter=1.500 in : Crown Radii=6.31 & 6.14 in
Material : 52100 Vac Degas Rc 60-63 Steel
Data File K0808P1

SLIP/ROLL	TRACTION COEFF.
+.223247936558	+.027674469013
+.214825449325	+.027223613875
+.204092902270	+.026952478819
+.189495552626	+.026637741805
+.178735834729	+.026205821547
+.170185391809	+.025993459509
+.160154092165	+.025806440712
+.149267595311	+.025203151580
+.134189667323	+.024448551508
+.125396658076	+.023883652569
+.118138554873	+.023285083033
+.108107322673	+.022682200608
+.091946167213	+.021420221116
+.081469149176	+.020380410023
+.071783689490	+.019564074996
+.062609428466	+.018179835505
+.047911851497	+.016020874931
+.035990053183	+.013874833549
+.026866994573	+.012077675182
+.018988376614	+.009338437182
+.006398940062	+.003345575069
+.000000000000	+.000000000000
-.007104808654	-.003715537039
-.016589580465	-.008085418931
-.025369241611	-.010586427440
-.034220311411	-.012687189245
-.050478183774	-.015424554585
-.061473280307	-.016647504835
-.069725784006	-.017679981813
-.080001743749	-.018523279248
-.094994514238	-.019916209915
-.105427538995	-.020679601353
-.114829477354	-.021301196610
-.124677192638	-.021769360058
-.135011059941	-.022631391080
-.148688057235	-.023688925032
-.158470937793	-.023926780125
-.167305547178	-.024241451783
-.176330178568	-.024387033208
-.193437713521	-.025009052262
-.202814322972	-.025277940731
-.211646783243	-.025753598940

9.3 Lubricant Properties

Shear Modulus G and Average Limiting Shear Stress $\bar{\tau}_c$

The extreme conditions of pressure, transit time and shear rate met in a typical EHL contact preclude the direct measurement by ordinary laboratory techniques of the properties G, τ_c and the average viscosity η under relevant conditions. They must, therefore, be deduced directly from traction measurements.

Following Tevaarwerk and Johnson [4] it is assumed that traction curves of the type shown in Fig. 9.3 are available at or close to the loads, speeds, aspect ratios and temperatures of interest. These tests are termed simple sliding tests because there is no imposed spinning velocity or transverse sliding velocity. Only the sliding velocity in the rolling direction, Δu, is varied. The maximum traction coefficient is reached at high sliding velocities. At sufficiently high sliding speeds the fluid will be plastic so that the traction force F_x will be the product of the average limiting shear force $\bar{\tau}_c$ and the contact area πab, i.e.,

$$F_x = \pi ab\bar{\tau}_c \tag{9.1}$$

Dividing F_x by the applied load P gives the maximum traction coefficient μ_{max}:

$$\mu_{max} = \pi ab\bar{\tau}_c/P \tag{9.2}$$

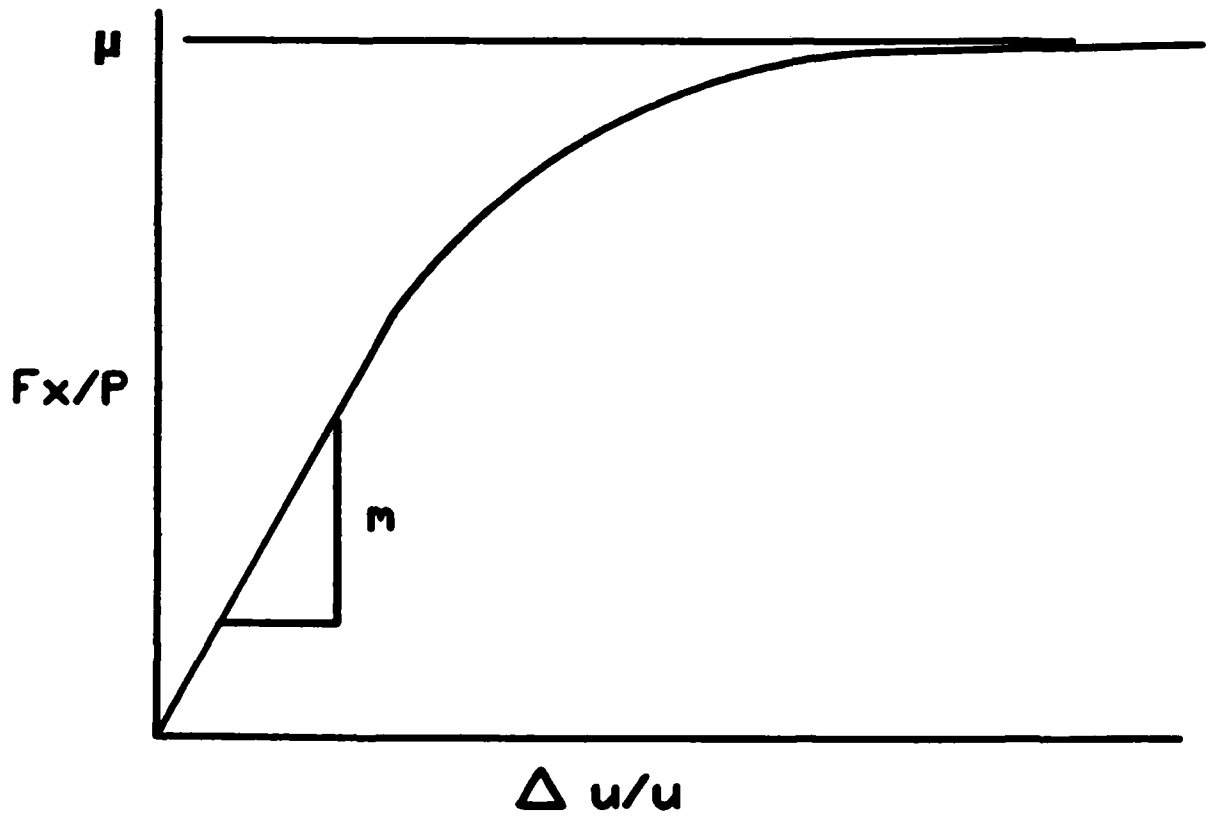

Fig. 9.3 A TYPICAL TRACTION CURVE

Using Eq. (9.2) $\bar{\tau}_c$ may be computed as:

$$\bar{\tau}_c = \mu_{max} P/\pi ab \tag{9.3}$$

For high Deborah numbers the oil will act purely elastically at low sliding rates. Tevaarwerk and Johnson [4] show that in this regime the resultant shear stress integrated over the elliptical contact area gives a force of

$$F_x = 8/3\ (a^2 b/Ph)\, G \bullet \Delta u/u \tag{9.4}$$

wherein G, the composite shear modulus of the fluid and contacting surfaces, is assumed to be constant through the contact. $\mu \equiv F_x/P$ is, therefore, linear with $\Delta u/u$ and has slope:

$$m \equiv 8/3\ a^2 b/Ph \bullet G \tag{9.5}$$

By measuring the slope m of the traction curve in the high Deborah number regime one may thus compute G as:

$$G = 3/8\ Phm/a^2 b \tag{9.6}$$

Inasmuch as the solid surfaces as well as the fluid deform elastically, this elastic modulus value represents the combined deformation of the composite fluid/solid system.

For low Deborah numbers the oil in the interface behaves as a Newtonian fluid, i.e., the shear stress is related to sliding velocity as:

$$\tau = \eta \, \Delta u/h \tag{9.7}$$

Considering isothermal conditions but using Barus' law for pressure dependence of viscosity, F_x is obtained as:

$$F_x = \iint \tau dx dy = \iint \eta(p) dx dy \bullet \Delta u/h \tag{9.8}$$

$$= \pi \, a \, b \, \bar{\eta} \, \Delta u/h$$

$$= u \, \pi \, a \, b \, \bar{\eta}/h \bullet \Delta u/u$$

where $\bar{\eta}$ is the average viscosity across the contact ellipse. In this case $\mu = F_x/P$ will also be linear with $\Delta u/u$, but with slope m given by

$$m = u \, \pi \, a \, b \, \bar{\eta}/hP \tag{9.10}$$

For intermediate Deborah numbers the traction curve at low shear rates will depend jointly on the viscosity and shear modulus.

At intermediate shear rates the shape of the traction curve will depend jointly on the values of $\bar{\eta}$, G and $\bar{\tau}_c$, with their relative influence a function of Deborah number. At high Deborah numbers the traction curve shape at intermediate sliding velocities depends on G and $\bar{\tau}_c$. At low Deborah numbers, intermediate sliding velocity behavior depends on $\bar{\eta}$ and $\bar{\tau}_c$.

One conceivable approach to estimating the lubricant parameters would be to use a least squares fit to an experimental trac-

tion curve. In this approach, $\bar{\eta}$, G and $\bar{\tau}_c$ are estimated as the values which minimize the sum of the squared deviations of the predicted and actual curves. This approach could be prohibitively time consuming inasmuch as the program would have to be run repeatedly for various trial values of the lubricant parameters.

As a practical alternative the following approach was adopted: 1) $\bar{\tau}_c$ is computed from Eq. (9.3), 2) G is computed from Eq. (9.5) on the assumption that the traction curve at low sliding speeds is elastic, 3) $\bar{\eta}$ is taken at the value based on its ambient viscosity value and Barus' equation integrated over the contact pressure.

These values are used in the computation of the Deborah number as discussed in Section 2.0. If the Deborah number is large enough, $\bar{\eta}$ is irrelevant since the initial slope depends on G only. If Deborah number is small, $\bar{\eta}$ can be adjusted as needed to agree with the measured slope m using Eq. (9.10).

9.4 Further Lubricant Properties

In addition to G and $\bar{\tau}_c$, it is necessary, both for the design of the traction tests and for input to McFRIC, to know six properties of each lubricant as a function of temperature. These properties are:

viscosity η

temperature viscosity coefficient β

pressure viscosity coefficient α

specific gravity SPGR

specific heat c

thermal conductivity Kf

A computer program entitled MATPROP and written in Fortran 77 for an IBM PC and compatibles, was developed to compute the required values at whatever temperatures T (°F) are of interest, for the three oils used in the test program. The relationships employed within MATPROP are given below.

9.4.1 Viscosity

The Walther-ASTM equation was used to relate viscosity η (cs) to temperature (°F) as follows:

$$\log(\eta+0.6) = \exp[K-c\ell nT] \qquad (9.11)$$

where **K** and **c** are fluid dependent constants. By substituting η at two temperatures, it was possible to solve for the constants **K** and **c** for each oil. The values thus determined are listed below:

Lubricant	K	c
RL-714	23.71805	3.55330
Santotrac 50	24.689883	3.7017861
CTFE	43.66862	6.82620

The viscosity values used in determining these constants were taken from [26], [37] and [28] respectively for the three oils.

9.4.2 Temperature Viscosity Coefficient

Given the viscosities η_1 and η_o, corresponding to the two temperatures T_1 and T_o, the pressure viscosity coefficient β is calculable as

$$\beta = -\ell n(\eta_1/\eta_2)/(T_1-T_o) \qquad (9.12)$$

To find β at an arbitrary temperature T, T_1 was taken as T+20° and T_o as T-20°. η_1 and η_2 at these two temperatures were then computed from Eq. (9.11) and β calculated from Eq. (9.12) as

$$\beta = \ell n[\eta(T+20)/\eta(T-20)]/40 \qquad (9.13)$$

9.4.3 Pressure Viscosity Coefficient

RL714

A graph of α vs. T supplied in [26], was fitted by the following equation:

$$\alpha = \exp\ [6.203294E\text{-}6\ T^2 - 0.00363T - 8.89978] \qquad (9.14)$$

SANTOTRAC 50

Values of α at three temperatures were given in [29] for a traction fluid known to be Santotrac 50. The following curve fit was developed:

$$\alpha = \exp[-0.0057T - 7.8858] \qquad (9.15)$$

CTFE

The following linear approximation was developed to a curve given in [31].

$$\alpha = 1.82287E\text{-}4 - 6.1598E\text{-}7 \bullet T \qquad (9.16)$$

This equation is used in program MATPROP. It does not reflect the change communicated in [30] that α at 275°F for CTFE is 4.276E-6 in^2/lb. The program is believed to be valid for T<180°F.

9.4.4 Specific Gravity

RL714

The equation given in [26] is:

$$SPGR = 8.177 - 1.13E\text{-}3 \bullet T \qquad (9.17)$$

The following equations were obtained as least square fits to data in [27] and [28].

SANTOTRAC 50

$$SPGR = 0.9237 - 3.45E\text{-}4T \qquad (9.18)$$

CTFE

$$SPGR = 1.9303 - 9.3091E\text{-}4T \qquad (9.19)$$

9.4.5 Conductivity

RL714

The following equation was given in [26].

$$K = (0.813/(12*SPGR)*(1.0-3E-4(T-32)*0.2161 \text{ lb-sec/°F} \quad (9.20)$$

The following equations were obtained as least squares fits:

SANTOTRAC 50

$$K = 0.061-1E-5T \quad ; \quad T < 200°F$$
$$= 0.065-3E-5T \quad ; \quad T > 200°F$$

CTFE

$$K = 0.01016 - 81.647E-6T$$

9.4.6 Specific Heat

RL714

The following piecewise linear fit was obtained:

$$c = 1.175E-3T + 0.405 \qquad T<200°F$$
$$c = 0.210E-3T + 0.598 \qquad T>200°F$$

SANTOTRAC 50

$$c = 6.15E-4T + 0.3840$$

CTFE

The value c = 0.20 was used independently of temperatures.

9.5 Test Design

The range of variables used in the tests was limited by the maximum load that could be safely applied to the rig (140 lbs), and by upper and lower limits on the rotational speeds (500 rpm and 10000 rpm). Three temperatures were chosen: 80°F, 180°F and 280°F. Three values of the maximum Hertz stress were used: 50 ksi, 206 and 366 ksi. These stresses were achieved using loads of 24.7 and 139 lbs with the two specimen crown radii. Using the lubricant properties relevant to the temperature, the rolling speeds were calculated using computer program TRIBOS [19] so as to give three values of constant film thickness for each temperature regardless of load or aspect ratio. This could not always be achieved because of the physical constraints cited above.

Tables 9.2 through 9.4 show for each combination of load, temperature and aspect ratio the test number assigned by AFML, the required rolling speed (in/sec) and the computed film thickness (μin). The entire set of tests at 280°F were eliminated for the CTFE fluid because of concern about disk damage at the low calculated film thickness. A few other tests had to be discontinued for various reasons accounting for some missing cells in the test matrices.

TABLE 9.2 TRACTION DATA TEST MATRIX MOBIL RL-714

MAX HERTZ PRESSURE (KSI)	ASPECT RATIO	LOAD (LBS.)	T1 = 80°F			T2 = 180°F			T3 = 280°F		
			U1	U2	U3	U4	U5	U6	U7	U8	U9
150	0.25	P1 = 54	K08O8P1	K08A5P1	K08C7P1	K18C3P1	K18F0P1	K18J7P1	–	–	K28K9P1
			43	78	190	170	300	540	90	340	600
			10	15	28	7	10	15	2	4.8	7
205.6	0.25	P2=139	K08O8U6	K08A6U6	K08D3U6	K18C7U6	K18F3U6	K18K9U6	–	–	K28N0U6
			45	83	2801	190	320	600	91	380	700
			10	15	28	7	10	15	2	4.8	7
205.6	1.0	P3 = 24.7	K07A1V9	K0781V9	K07E1V8	K17E1V6	K18I0V7	–	–	–	K2809V6
			58	110	260	260	450	800	120	450	800
			10	15	28	7	10	15	2	4.8	7
366	1.0	P4 = 139	K08A3G0	K07B6G0	K17F2G0	K08F9G0	K18J3G0	K1809G0	–	–	K2809G0
			70	135	350	314	520	800	150	560	800
			10	15	28	7	10	13	2	4.8	6.2

ENTRIES IN EACH CELL ARE: 1) AFML TEST NO.

2) ACTUAL ROLLING SPEED (IN/SEC)

3) NOMINAL FILM THICKNESS (μIN)

TABLE 9.3 TRACTION DATA TEST MATRIX SANTOTRAC 50

MAX HERTZ PRESSURE (KSI)	ASPECT RATIO	LOAD (LBS.)	T1 = 80°F			T2 = 180°F		
			U1	U2	U3	U4	U5	U6
150	0.25	P1 = 54	M07A1P1 60 5	M08B0P1 105 7	M08C5P1 180 10	M18D1P1 209 3	M18H3P1 418 5	M18L7P1 638 7
205.6	0.25	P2=139	M08A3U6 66 5	M08B3U6 115 7	M08C9U6 197 10	M18D6U6 230 3	M18I2U6 460 5	M18N0U6 701 7
205.6	1.0	P3 = 24.7	M08A9V7 97 5	M08C1V7 160 7	M08E5V8 277 10	M18E0V7 252 3	M18K4V7 570 5	M18L5V7 629 5.4
366	1.0	P4 = 139	M08B2G0 115 5	M08C7G0 190 7	M08F5G0 329 10	M18E9G0 299 3	M18M5G0 678 5	M18N9G0 750 5.4

ENTRIES IN EACH CELL ARE: 1) AFML TEST NO.
2) ACTUAL ROLLING SPEED (IN/SEC)
3) NOMINAL FILM THICKNESS (μIN)

TABLE 9.4 TRACTION DATA TEST MATRIX HF-CTFE

MAX HERTZ PRESSURE (KSI)	ASPECT RATIO	LOAD (LBS.)	T1 = 80°F			T2 = 180°F			T3 = 280°F		
			U1	U2	U3	U4	U5	U6	U7	U8	U9
150	0.25	P1 = 54	–	–	–	L18A9P1	L17H9P1	L18J7P1	–	–	L28H7P1
			41	48	80	100	450	540	80	290	440
			18	20	28	6.4	18	20	2	4.8	6.4
205.8	0.25	P2=139	–	–	–	L18B0U6	L18I9U6	L18K9U6	–	–	L28I6U6
			42	50	84	105	500	600	88	310	480
			18	20	28	6.4	18	20	2	4.8	6.4
205.8	1.0	P3 = 24.7	L08A2W0	L08A4W0	L08B4W0	–	–	L1809V8	–	–	L28M1W0
			82	72	120	140	680	800	112	420	660
			18	20	28	6.4	18	20	2	4.8	6.4
366	1.0	P4 = 139	–	–	–	–	L18B1G1	L1809G2	–	–	L2809G1
			74	84	140	170	110	800	140	520	800
			18	20	28	6.4	4.8	18	2	4.8	6.4

ENTRIES IN EACH CELL ARE: 1) AFML TEST NO.

2) ACTUAL ROLLING SPEED (IN/SEC)

3) NOMINAL FILM THICKNESS (μIN)

10.0 TRACTION DATA REDUCTION, ANALYSIS AND DISCUSSION

10.1 Traction Data Base

For each traction test performed at AFML, the value of μ_{max} was read from the printed traction data output. The traction curve slope **m** in the vicinity of zero sliding velocity ($\Delta u=0$) was determined using the method of least squares and pairs of values of F_x/P and $\Delta u/u$ in the vicinity of $\Delta u=0$.

The model assumed is:

$$y_i = mx_i+\varepsilon_i \tag{10.1}$$

where y_i is the traction coefficient measured for the i-th point, x_i is the associated slide-to-roll ratio $(\Delta u/u)_i$ and ε_i is a random error having an expected value of zero.

The least squares estimate of **m**, designated **m**, is the value which minimizes the quantity:

$$s = \sum_{i=1}^{n} (y_i-mx_i)^2 \tag{10.2}$$

Setting $\partial s/\partial m = 0$ and solving gives,

$$\hat{m} = \sum_{i=1}^{n} x_iy_i / \sum_{i=1}^{n} x_i^2 \tag{10.3}$$

A program called TRSLOPE was written in BASIC to perform this calculation and is included with the executable Diskette No. 1 (cf. Section 8.4.1).

Table 10.1 is a data form used to compile the data for each traction test into a data base. With the data base software system used to store and manipulate these data, it was possible to specify certain fields by a formula relating the value of the field to the values specified in one or more of the other fields. The calculated fields are denoted by an asterisk in Table 10.1. The formula used to compute these fields is given to the right of the colon at the end of the field name. Specifically, the shear strength and shear modulus are computed from Eqs. (9.3) and (9.6) under the supposition that the fluid behaves elastically in the low slip region and plastically at high slip. It is further assumed that the asperity contribution to traction is negligible. Based on the computed film thicknesses relative to the surface roughness (roughly 2 μin) this was almost certainly the case for all but a few of the CTFE tests.

Tables 10.2 through 10.4 give the complete data base contents for each oil. The column headings correspond to the field names on the data form, but have been truncated in some cases.

These data were used to prepare input files for program McFRIC. The program was run primarily in the isothermal mode unless the AFML plots showed a clear indication that traction diminished with sliding speed. After a series of trial runs showed that the results changed negligibly for larger values of NX and NY, the number of divisions of the contact ellipse were taken as NX = NY = 41.

TABLE 10.1

TRACTION DATA FORM

LUBRICANT:

FILE NO.:

ROTATIONAL SPEED:

* ROLLING VELOCITY: 0.0785 * ROTATIONAL SPEED

LOAD:

TEMPERATURE:

* ASPECT RATIO: SEMIAXIS IN ROLLING DIR. / SEMIAXIS TRANVERSE

SEMIAXIS IN ROLLING DIR.:

SEMIAXIS TRANVERSE:

VISCOSITY:

* DYNAMIC VISCOSITY: VISCOSITY * SP GR * 0.000000145

PRES VISC INDX:

SP GR:

TEMP VISC INDX:

CONDUCTIVITY:

SP HEAT:

* DENSITY: SP GR * 62.5 / 1728

FILM THICKNESS:

* HERTZIAN PRESSURE: 1.5 * LOAD / (3.14159 * SEMIAXIS IN ROLLING DIR. * SEMIAXIS TRANVERSE)

SLOPE OF TRACTION CURVE:

MAX TRAC COEF:

* SHEAR MODULUS: 0.7854 * FILM THICKNESS * HERTZIAN PRESSURE * SLOPE OF TRACTION CURVE / SEMIAXIS IN ROLLING DIR.

* SHEAR STRENGTH: HERTZIAN PRESSURE * MAX TRAC COEF / 1.5

DEBORAH NO:

* Computed Automatically

TABLE 10.2 MOBIL RL-714 DATABASE

LUBRICANT	ROTATIONAL SP	ROLLING VEL	LOAD	TEMP	ASPR	SEMIAXIS	SEMIAXIS	VISC	PRES VISC INDX	SP GR	TEMP VISC INDX	CONDUCTI
MOBIL RL-714	549.00	43.10	55.5	80	0.25	6.67E-03	2.67E-02	49	1.06E-04	0.821	0.02391	0.01758
MOBIL RL-714	996.00	78.19	55.9	80	0.25	6.69E-03	2.67E-02	40	1.06E-04	0.821	0.02391	0.01758
MOBIL RL-714	2423.00	190.21	55.9	80	0.25	6.69E-03	2.67E-02	49	1.06E-04	0.821	0.02391	0.01758
MOBIL RL-714	574.00	45.06	141	80	0.25	9.10E-03	3.64E-02	49	1.06E-04	0.821	0.02391	0.01758
MOBIL RL-714	1059.00	83.13	141	80	0.25	9.10E-03	3.64E-02	49	1.06E-04	0.821	0.02391	0.01758
MOBIL RL-714	2804.00	220.11	141	83	0.25	9.10E-03	3.64E-02	49	1.06E-04	0.821	0.02391	0.01758
MOBIL RL-714	2173.00	170.58	55.1	181	0.25	6.65E-03	2.66E-02	8.2	8.84E-05	0.786	0.01427	0.0178
MOBIL RL-714	3830.00	300.66	55.7	181	0.25	6.68E-03	2.67E-02	8.2	8.84E-05	0.786	0.01427	0.0178
MOBIL RL-714	6883.00	540.32	55.7	183	0.25	6.68E-03	2.67E-02	8.2	8.84E-05	0.786	0.01427	0.0178
MOBIL RL-714	2425.00	190.36	141	180	0.25	9.10E-03	3.64E-02	8.2	8.84E-05	0.786	0.01427	0.0178
MOBIL RL-714	4080.00	320.28	141	181	0.25	9.10E-03	3.64E-02	8.2	8.84E-05	0.786	0.01427	0.0178
MOBIL RL-714	7654.00	600.84	141	184	0.25	9.10E-03	3.64E-02	8.2	8.84E-05	0.786	0.01427	0.0178
MOBIL RL-714	7654.00	600.84	55.7	283	0.25	6.68E-03	2.67E-02	3	8.00E-05	0.751	0.00903	0.018
MOBIL RL-714	8926.00	700.69	141	285	0.25	9.10E-03	3.64E-02	3	8.00E-05	0.751	0.00903	0.018
MOBIL RL-714	739.00	58.01	26.7	78	1	7.85E-03	7.56E-03	49	1.06E-04	0.821	0.02391	0.01758
MOBIL RL-714	1401.00	109.98	26.9	78	1	7.87E-03	7.58E-03	49	1.06E-04	0.821	0.02391	0.01758
MOBIL RL-714	3314.00	260.15	26.6	79	1	7.84E-03	7.56E-03	49	1.06E-04	0.821	0.02391	0.01758
MOBIL RL-714	892.00	70.02	140	80	1	1.36E-02	1.31E-02	49	1.06E-04	0.821	0.02391	0.01758
MOBIL RL-714	1721.00	135.10	140	79	1	1.36E-02	1.31E-02	49	1.06E-04	0.821	0.02391	0.01758
MOBIL RL-714	4460.00	350.11	140	80	1	1.36E-02	1.31E-02	49	1.06E-04	0.821	0.02391	0.01758
MOBIL RL-714	3316.00	260.31	25.7	177	1	7.75E-03	7.47E-03	8.2	8.84E-05	0.786	0.01427	0.0178
MOBIL RL-714	5740.00	450.59	26	182	1	7.78E-03	7.50E-03	8.2	8.84E-05	0.786	0.01427	0.0178
MOBIL RL-714	10198.00	800.54	26	182	1	7.78E-03	7.50E-03	8.2	8.84E-05	0.786	0.01427	0.0178
MOBIL RL-714	4006.00	314.47	140	178	1	1.36E-02	1.31E-02	8.2	8.84E-05	0.786	0.01427	0.0178
MOBIL RL-714	6632.00	520.61	140	183	1	1.36E-02	1.31E-02	8.2	8.84E-05	0.786	0.01427	0.0178
MOBIL RL-714	10199.00	800.62	140	183	1	1.36E-02	1.31E-02	8.2	8.84E-05	0.786	0.01427	0.0178
MOBIL RL-714	3827.00	300.42	140	182	1	1.36E-02	1.31E-02	8.2	8.84E-05	0.786	0.01427	0.0178
MOBIL RL-714	10200.00	800.70	25.6	286	1	7.74E-03	7.46E-03	3	8.00E-05	0.751	0.00903	0.018
MOBIL RL-714	10198.00	800.54	140	287	1	1.36E-02	1.31E-02	3	8.00E-05	0.751	0.00903	0.018

TABLE 10.2 MOBIL RL-714 DATABASE (CONDT)

SP HEAT	DENSITY	FILM THI	HERTZIAN	SLOPE	MAX TRAC	SHEAR MO	SHEAR ST	DYNAMIC	FILE NO.	DEBORAH
0.5	2.97E-02	1E-05	148984.27	0.846	0.0277	148.42	2751.24	5.83E-06	K0808P1	9.4873
0.5	2.97E-02	1.5E-05	149342.25	0.604	0.0257	158.95	2558.73	4.76E-06	K08A5P1	16.443
0.5	2.97E-02	2.8E-05	149342.25	0.583	0.0223	286.39	2220.22	5.83E-06	K08C7P1	22.201
0.5	2.97E-02	1E-05	203512.84	1.295	0.0352	227.41	4775.77	5.83E-06	K0808U6	223.65
0.5	2.97E-02	1.5E-05	203512.84	1.33	0.032	350.34	4341.61	5.83E-06	K08A6U6	266.14
0.5	2.97E-02	2.8E-05	203512.84	0.827	0.0246	406.63	3337.61	5.83E-06	K08D3U6	610.69
0.617	2.84E-02	7E-06	148624.88	0.122	0.0131	14.98	1297.99	9.35E-07	K18C3P1	10.184
0.617	2.84E-02	1E-05	149163.43	0.1298	0.0138	22.77	1372.30	9.35E-07	K18F0P1	12.146
0.617	2.84E-02	1.5E-05	149163.43	0.181	0.0126	47.63	1252.97	9.35E-07	K18J7P1	10.435
0.617	2.84E-02	7E-06	203416.37	0.348	0.0195	42.78	2644.41	9.35E-07	K18C7U6	73.506
0.617	2.84E-02	1E-05	203416.37	0.363	0.0173	63.74	2346.07	9.35E-07	K18F3U6	83.005
0.617	2.84E-02	1.5E-05	203368.23	0.354	0.0159	93.25	2155.70	9.35E-07	K18K9U6	106.16
0.657	2.72E-02	7E-06	149163.43	0.06082	0.0052	7.47	517.10	3.27E-07	K28K9P1	11.218
0.657	2.72E-02	7E-06	203512.84	0.0932	0.00859	11.46	1165.45	3.27E-07	K28N0U6	113.54
0.5	2.97E-02	1E-05	214769.91	2.172	0.039	466.92	5584.02	5.83E-06	K07A1V9	360.41
0.5	2.97E-02	1.5E-05	215306.08	2.198	0.035	708.77	5023.81	5.83E-06	K07B1V9	466.36
0.5	2.97E-02	2.8E-05	214501.05	2.36	0.034	1420.54	4862.02	5.83E-06	K07E1V8	521.91
0.5	2.97E-02	1E-05	373440.94	4.45	0.0462	958.22	11501.98	5.83E-06	K08A3g0	9099700
0.5	2.97E-02	1.5E-05	373529.98	5.193	0.0377	1677.31	9388.05	5.83E-06	K07B6g0	10030000
0.5	2.97E-02	2.8E-05	373708.22	2.831	0.0323	1706.88	8047.18	5.83E-06	K08F9g0	25854000
0.617	2.84E-02	7E-06	212049.00	0.977	0.0256	147.01	3618.97	9.35E-07	K17E1V6	57.129
0.617	2.84E-02	1E-05	212872.59	0.871	0.0256	187.24	3633.03	9.35E-07	K1810V7	81.188
0.617	2.84E-02	1.5E-05	212872.59	3.255	0.0195	1049.58	2767.34	9.35E-07	K1809V7	25.732
0.617	2.84E-02	7E-06	373440.94	3.133	0.0344	472.24	8564.25	9.35E-07	K17F2g0	165120
0.617	2.84E-02	1E-05	373262.50	2.707	0.0348	582.90	8659.69	9.35E-07	K18J3g0	219250
0.617	2.84E-02	1.3E-05	373529.98	3.32	0.0331	929.36	8242.56	9.35E-07	K1809g0	214690
0.617	2.84E-02	7E-06	373708.22	3.45	0.0368	520.02	9168.31	9.35E-07	K18F0g0	145420
0.657	2.72E-02	7E-06	211773.00	1.196	0.0189	179.97	2668.34	3.27E-07	K2809V6	15.1
0.657	2.72E-02	6.2E-06	373173.07	1.32	0.0226	176.23	5622.47	3.27E-07	K2809g0	47984

TABLE 10.3 SANTOTRAC-50 DATABASE

LUBRICANT	ROTATIONAL SP	ROLLING VEL	LOAD	TEMP	ASPR	SEMIAXIS	SEMIAXIS	VISC	PRES VISC INDX	SP GR	TEMP VISC INDX	CONDUCTI
SANTOTRAC 50	1276.00	100.01	55.8	181	0.25	6.68E-03	2.67E-02	8	1.64E-04	0.862	0.01182	0.0127
SANTOTRAC 50	5737.00	450.35	55.6	179	0.25	6.67E-03	2.67E-02	8	1.64E-04	0.862	0.01182	0.0127
SANTOTRAC 50	6884.00	540.39	55.7	181	0.25	6.68E-03	2.67E-02	8	1.64E-04	0.862	0.01182	0.0127
SANTOTRAC 50	1338.00	105.03	141.2	183	0.25	9.10E-03	3.64E-02	8	1.64E-04	0.862	0.01182	0.0127
SANTOTRAC 50	6374.00	500.36	141.1	181	0.25	9.10E-03	3.64E-02	8	1.64E-04	0.862	0.01182	0.0127
SANTOTRAC 50	7644.00	600.05	141	182	0.25	9.10E-03	3.64E-02	8	1.64E-04	0.862	0.01182	0.0127
SANTOTRAC 50	5610.00	440.39	55.6	281	0.25	6.67E-03	2.67E-02	3	1.28E-04	0.828	0.00626	0.0121
SANTOTRAC 50	6117.00	480.18	140.8	282	0.25	9.09E-03	3.64E-02	3	1.28E-04	0.828	0.00626	0.0121
SANTOTRAC 50	791.00	62.09	27.2	82	1	7.90E-03	7.61E-03	57	2.33E-04	0.896	0.0264	0.013
SANTOTRAC 50	918.00	72.06	27.3	81	1	7.90E-03	7.62E-03	57	2.33E-04	0.896	0.0264	0.013
SANTOTRAC 50	1530.00	120.11	27.4	81	1	7.91E-03	7.63E-03	57	2.33E-04	0.896	0.0264	0.013
SANTOTRAC 50	10195.00	800.31	26.5	183	1	7.83E-03	7.55E-03	8	1.64E-04	0.862	0.01182	0.0127
SANTOTRAC 50	8670.00	680.60	26.6	181	1	7.84E-03	7.56E-03	8	1.64E-04	0.862	0.01182	0.0127
SANTOTRAC 50	1402.00	110.06	141.2	184	1	1.37E-02	1.32E-02	8	1.64E-04	0.862	0.01182	0.0127
SANTOTRAC 50	10187.00	799.68	141.7	183	1	1.37E-02	1.32E-02	8	1.64E-04	0.862	0.01182	0.0127
SANTOTRAC 50	8414.00	660.50	27.2	282	1	7.90E-03	7.61E-03	3	1.28E-04	0.828	0.00626	0.0121
SANTOTRAC 50	10193.00	800.15	141.3	285	1	1.37E-02	1.32E-02	3	1.28E-04	0.828	0.00626	0.0121

TABLE 10.3 SANTOTRAC-50 DATABASE (CONTD)

SP HEAT	DENSITY	FILM THI	HERTZIAN	SLOPE	MAX TRAC	SHEAR MO	SHEAR ST	DYNAMIC	FILE NO.	DEBORAH
0.495	3.12E-02	6.4E-06	149252.83	9.479	0.0789	1064.34	7850.70	1.00E-06	L18A9P1	171.79
0.495	3.12E-02	1.8E-05	149074.10	14.29	0.0739	4512.75	7344.38	1.00E-06	L17N9P1	179.13
0.495	3.12E-02	2E-05	149163.43	16.516	0.0673	5795.23	6692.47	1.00E-06	L18J7P1	169.92
0.495	3.12E-02	6.4E-06	203512.84	7.81	0.0882	877.75	11966.55	1.00E-06	L18B0U6	60551
0.495	3.12E-02	1.8E-05	203464.50	26.54	0.0759	8389.05	10295.30	1.00E-06	L18I9U6	30031
0.495	3.12E-02	2E-05	203416.37	16.936	0.0632	5948.13	8570.61	1.00E-06	L18K9U6	50538
0.556	2.99E-02	6.4E-06	149074.10	5.884	0.0426	660.68	4213.83	3.60E-07	L28N7P1	12.04
0.556	2.99E-02	6.4E-06	203319.97	9.81	0.0513	1102.52	6953.54	3.60E-07	L2816U6	591.28
0.433	3.24E-02	1.8E-05	216104.98	21.763	0.1268	8421.36	18268.07	7.41E-06	L08A2W0	2.62E+09
0.433	3.24E-02	2E-05	216370.06	21.909	0.1194	9419.88	17223.06	7.41E-06	L08A4W0	2.83E+09
0.433	3.24E-02	2.8E-05	216634.31	13.4	0.11	8065.98	15886.52	7.41E-06	L08B4W0	5.73E+09
0.495	3.12E-02	2E-05	214231.30	21.741	0.0655	9347.36	9354.77	1.00E-06	L1809V8	162650
0.495	3.12E-02	1.8E-05	214501.05	15.343	0.082	5936.98	11726.06	1.00E-06	L18M5V8	224000
0.495	3.12E-02	4.8E-06	374596.37	30.064	0.0754	3107.38	18829.71	1.00E-06	L1881g1	1.59E+12
0.495	3.12E-02	1.8E-05	375038.80	17.42	0.0576	6751.94	14401.49	1.00E-06	L1809g2	5.56E+12
0.556	2.99E-02	6.4E-06	216104.98	15.868	0.0737	2183.20	10617.96	3.60E-07	L28N1W0	1408.4
0.556	2.99E-02	6.4E-06	374684.89	22.952	0.068	3163.06	16985.71	3.60E-07	L2809g1	350.15

TABLE 10.4 HF-CTFE DATABASE

LUBRICANT	ROTATIONAL SP	ROLLING VEL	LOAD	TEMP	ASPR	SEMIAXIS	SEMIAXIS	VISC	PRES VISC INDX	SP GR	TEMP VISC INDX	CONDUCTI
HF-CTFE	1230.00	96.56	26.1	81	1	7.79E-03	7.51E-03	7.22	1.33E-04	1.8558	0.0286	0.0095
HF-CTFE	2035.00	159.75	26.3	81	1	7.81E-03	7.53E-03	7.22	1.33E-04	1.8558	0.0286	0.0095
HF-CTFE	3530.00	277.11	26.4	82	1	7.82E-03	7.54E-03	7.22	1.33E-04	1.8558	0.0286	0.0095
HF-CTFE	1462.00	114.77	140	82	1	1.36E-02	1.31E-02	7.22	1.33E-04	1.8558	0.0286	0.0095
HF-CTFE	2414.00	189.50	140	81	1	1.36E-02	1.31E-02	7.22	1.33E-04	1.8558	0.0286	0.0095
HF-CTFE	4196.00	329.39	140	84	1	1.36E-02	1.31E-02	7.22	1.33E-04	1.8558	0.0286	0.0095
HF-CTFE	763.00	59.90	55.1	79	0.25	6.65E-03	2.66E-02	7.22	1.33E-04	1.8558	0.0286	0.0095
HF-CTFE	1334.00	104.72	55.3	81	0.25	6.66E-03	2.66E-02	7.22	1.33E-04	1.8558	0.0286	0.0095
HF-CTFE	2287.00	179.53	55.3	82	0.25	6.66E-03	2.66E-02	7.22	1.33E-04	1.8558	0.0286	0.0095
HF-CTFE	837.00	65.70	140	83	0.25	9.08E-03	3.63E-02	7.22	1.33E-04	1.8558	0.0286	0.0095
HF-CTFE	1466.00	115.08	140	83	0.25	9.08E-03	3.63E-02	7.22	1.33E-04	1.8558	0.0286	0.0095
HF-CTFE	2515.00	197.43	141	84	0.25	9.09E-03	3.63E-02	7.22	1.33E-04	1.8558	0.0286	0.0095
HF-CTFE	3211.00	252.06	26	181	1	7.78E-03	7.50E-03	1.31	7.14E-05	1.7627	0.0101	0.0086
HF-CTFE	7274.00	571.01	26.1	182	1	7.79E-03	7.51E-03	1.31	7.14E-05	1.7627	0.0101	0.0086
HF-CTFE	8021.00	629.65	26	181	1	7.78E-03	7.50E-03	1.31	7.14E-05	1.7627	0.0101	0.0086
HF-CTFE	3812.00	299.24	140	186	1	1.36E-02	1.31E-02	1.31	7.14E-05	1.7627	0.0101	0.0086
HF-CTFE	8641.00	678.32	140	185	1	1.36E-02	1.31E-02	1.31	7.14E-05	1.7627	0.0101	0.0086
HF-CTFE	9531.00	748.18	140	183	1	1.36E-02	1.31E-02	1.31	7.14E-05	1.7627	0.0101	0.0086
HF-CTFE	2673.00	209.83	55.1	185	0.25	6.65E-03	2.66E-02	1.31	7.14E-05	1.7627	0.0101	0.0086
HF-CTFE	5341.00	419.27	55.2	185	0.25	6.66E-03	2.66E-02	1.31	7.14E-05	1.7627	0.0101	0.0086
HF-CTFE	8142.00	639.15	55.1	186	0.25	6.65E-03	2.66E-02	1.31	7.14E-05	1.7627	0.0101	0.0086
HF-CTFE	2938.00	230.63	141	181	0.25	9.09E-03	3.63E-02	1.31	7.14E-05	1.7627	0.0101	0.0086
HF-CTFE	5865.00	460.40	140	186	0.25	9.08E-03	3.63E-02	1.31	7.14E-05	1.7627	0.0101	0.0086
HF-CTFE	8944.00	702.10	141	187	0.25	9.09E-03	3.63E-02	1.31	7.14E-05	1.7627	0.0101	0.0086

TABLE 10.4 HF-CTFE DATABASE (CONTD)

SP HEAT	DENSITY	FILM THI	HERTZIAN	SLOPE	MAX TRAC	SHEAR MO	SHEAR ST	DYNAMIC	FILE NO.	DEBORAH
0.2	6.71E-02	5E-06	213145.71	11.095	0.0997	1192.53	14167.08	1.94E-06	M08A9V7	3258.8
0.2	6.71E-02	7E-06	213689.84	21.8	0.0942	3280.43	13419.72	1.94E-06	M08C1V7	2051.6
0.2	6.71E-02	1E-05	213960.89	25.12	0.0651	5400.05	9285.90	1.94E-06	M08E5V8	2211.7
0.2	6.71E-02	5E-06	373797.19	32.86	0.0848	3537.86	21132.00	1.94E-06	M08B2g0	1.15E+09
0.2	6.71E-02	7E-06	374071.55	13.965	0.0624	2108.05	15561.38	1.94E-06	M08C7g0	3.17E+09
0.2	6.71E-02	1E-05	373797.19	33.812	0.0604	7280.72	15051.57	1.94E-06	M08F5g0	1.60E+09
0.2	6.71E-02	5E-06	148624.88	2.567	0.0813	225.18	8055.47	1.94E-06	M07A1P1	41.062
0.2	6.71E-02	7E-06	148804.89	6.38	0.0609	783.52	6041.48	1.94E-06	M08B0P1	20.938
0.2	6.71E-02	1E-05	148804.89	3.968	0.0515	696.15	5108.97	1.94E-06	M08C5P1	40.4
0.2	6.71E-02	5E-06	203078.62	18.38	0.0618	1613.81	8366.84	1.94E-06	M08A3U6	575.39
0.2	6.71E-02	7E-06	203126.89	10.15	0.0644	1247.68	8720.91	1.94E-06	M08B3U6	1308.9
0.2	6.71E-02	1E-05	203175.26	11.77	0.0353	2066.88	4781.39	1.94E-06	M08C9U6	1361
0.2	6.38E-02	3E-06	212872.61	13.7	0.0928	883.51	13169.72	3.35E-07	M18E0V7	0.75984
0.2	6.38E-02	5E-06	213145.71	14.57	0.0655	1566.04	9307.36	3.35E-07	M18K4V7	0.39948
0.2	6.38E-02	5.4E-06	212872.61	13.121	0.066	1523.11	9366.39	3.35E-07	M18L5V7	0.44764
0.2	6.38E-02	3E-06	373886.00	40.833	0.0514	2637.77	12811.83	3.35E-07	M18E9g0	149.28
0.2	6.38E-02	5E-06	373618.92	26.772	0.0552	2882.39	13749.18	3.35E-07	M18M5g0	305.97
0.2	6.38E-02	5.4E-06	373618.92	21.016	0.0506	2443.69	12603.41	3.35E-07	M18N9g0	398.07
0.2	6.38E-02	3E-06	148624.88	2.336	0.043	122.95	4260.58	3.35E-07	M18D1P1	0.10147
0.2	6.38E-02	5E-06	148714.88	1.907	0.0341	167.28	3380.78	3.35E-07	M18H3P1	0.80691
0.2	6.38E-02	7E-06	148624.88	1.942	0.0301	238.49	2982.41	3.35E-07	M18L7P1	0.15934
0.2	6.38E-02	3E-06	203239.04	5.328	0.0604	280.78	8183.76	3.35E-07	M18D6U6	0.4798
0.2	6.38E-02	5E-06	203078.62	5.557	0.0432	487.92	5848.66	3.35E-07	M18I2U6	0.54892
0.2	6.38E-02	7E-06	203175.26	3.93	0.0437	483.09	5919.17	3.35E-07	M18N0U6	0.84895

10.2 Predicted Traction Curves

The friction force F_x predicted by MCFRIC as well as the measured friction force were plotted against the sliding speed Δu, for all of the experimental traction data. The complete set of these curves are on file at AFML.

All of the isothermal fits for RL714 fluid were judged to be acceptable even though some of the tests had low Deborah numbers in the range (9-22). Figs. 10.1 and 10.2 are examples of two distinctly different traction curve slopes which the model nonetheless appears capable of accommodating. Case K18FOP1 had a Deborah number of 12.14. Case K07BIV9 had a Deborah number of 466.

Fig. 10.3 is an example of a thermal run with RL714. It is seen that the program grossly overestimates the magnitude of the thermal effect. Fig. 10.4 shows the same overestimate of the thermal effect for a CTFE test. The program was accordingly modified to remove the effect of temperature on the limiting shear stress while leaving the effect of temperature on viscosity intact.

The revised plots are shown as Figs. 10.5 and 10.6. (The "bump" in the predicted curve is an artifact of the plotting program's spline fitting routine). The fits are seen to be greatly improved. For the RL714 fluid, there remains a graphically discernible thermal effect on the predicted traction curve.

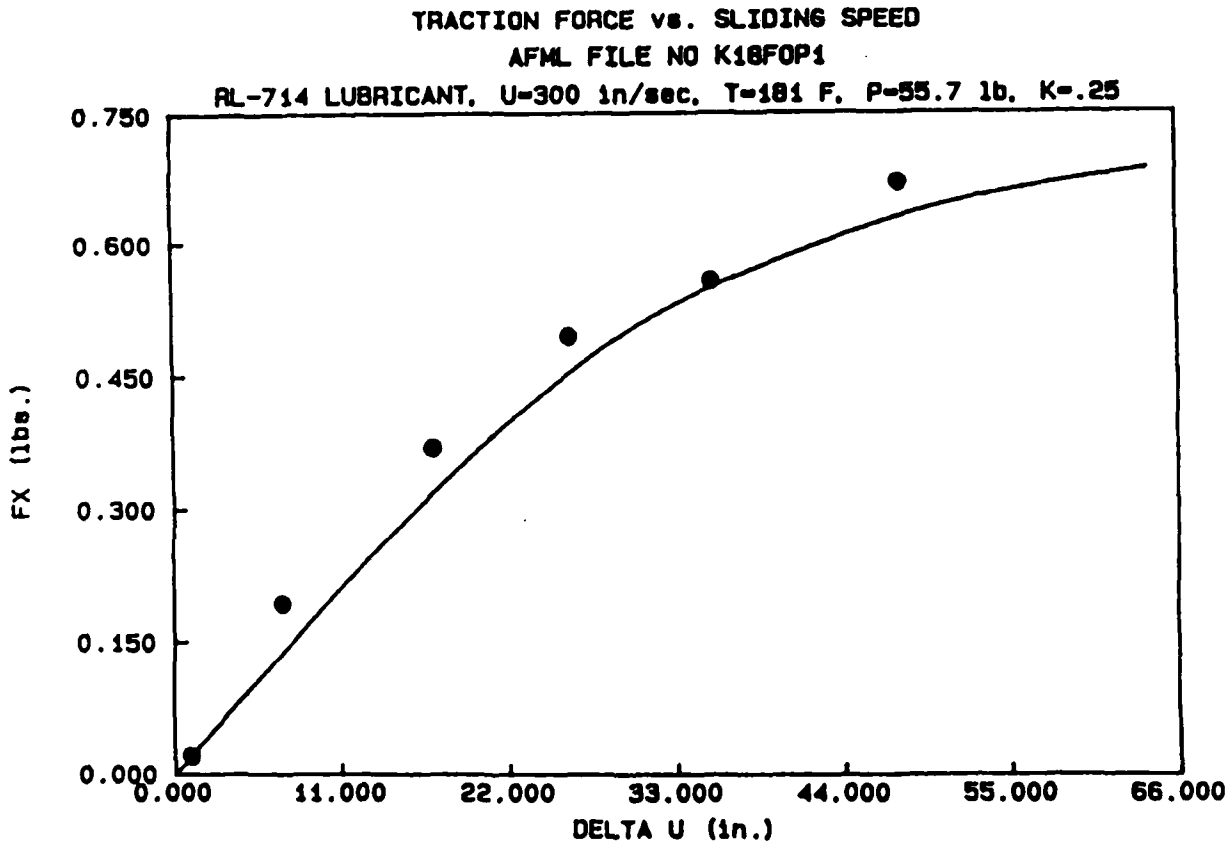

Fig. 10.1

TRACTION FORCE VS. SLIDING SPEED
AFML FILE NO. K18FOP1

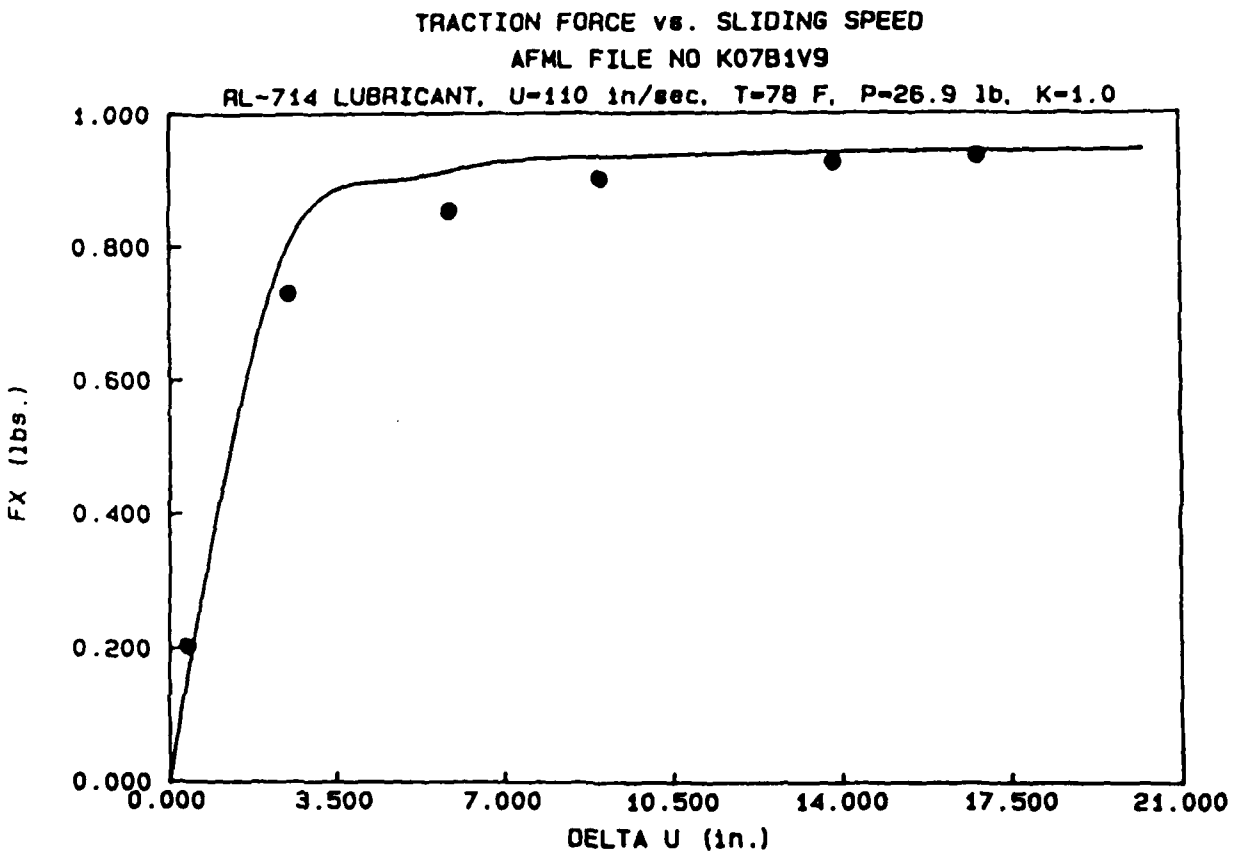

Fig. 10.2

TRACTION FORCE VS. SLIDING SPEED
AFML FILE NO. K07B1V9

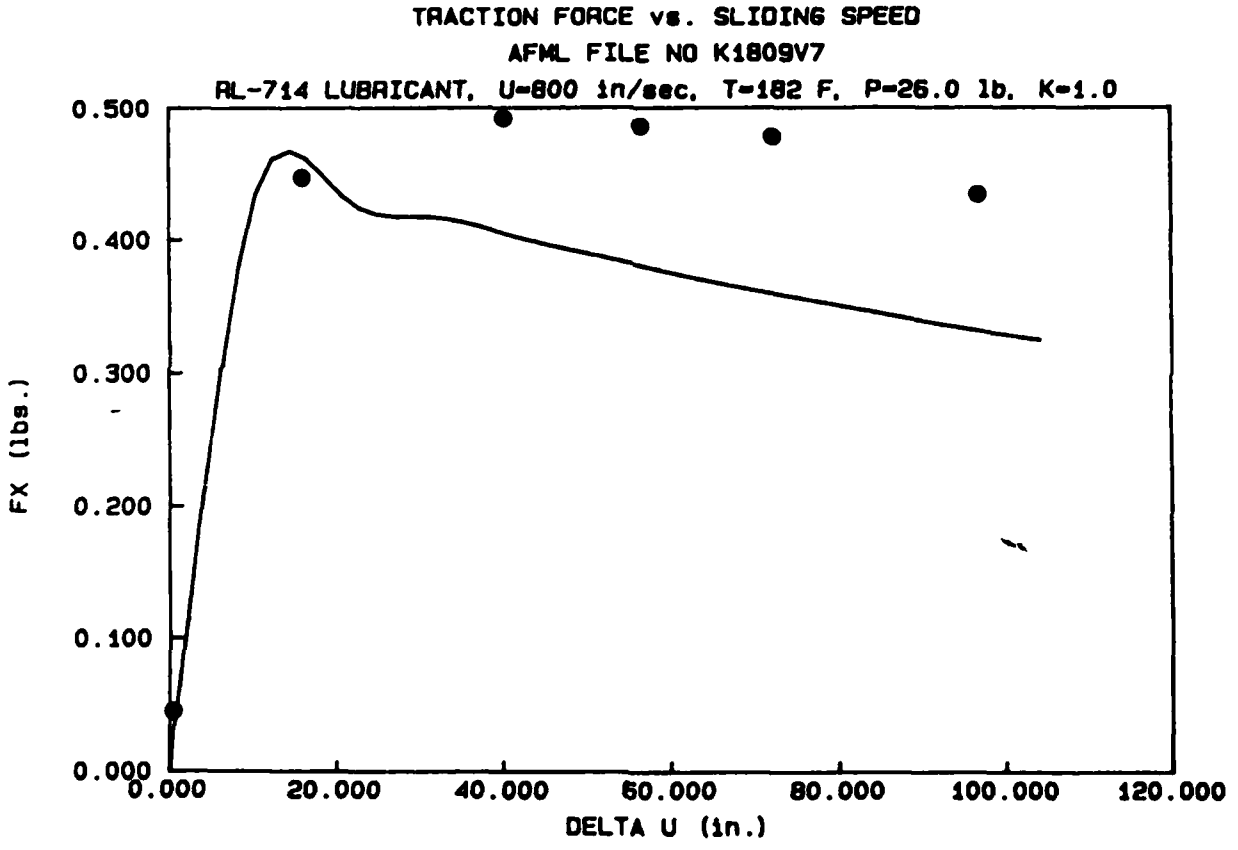

Fig. 10.3

TRACTION FORCE VS. SLIDING SPEED
AFML FILE NO. K1809V7

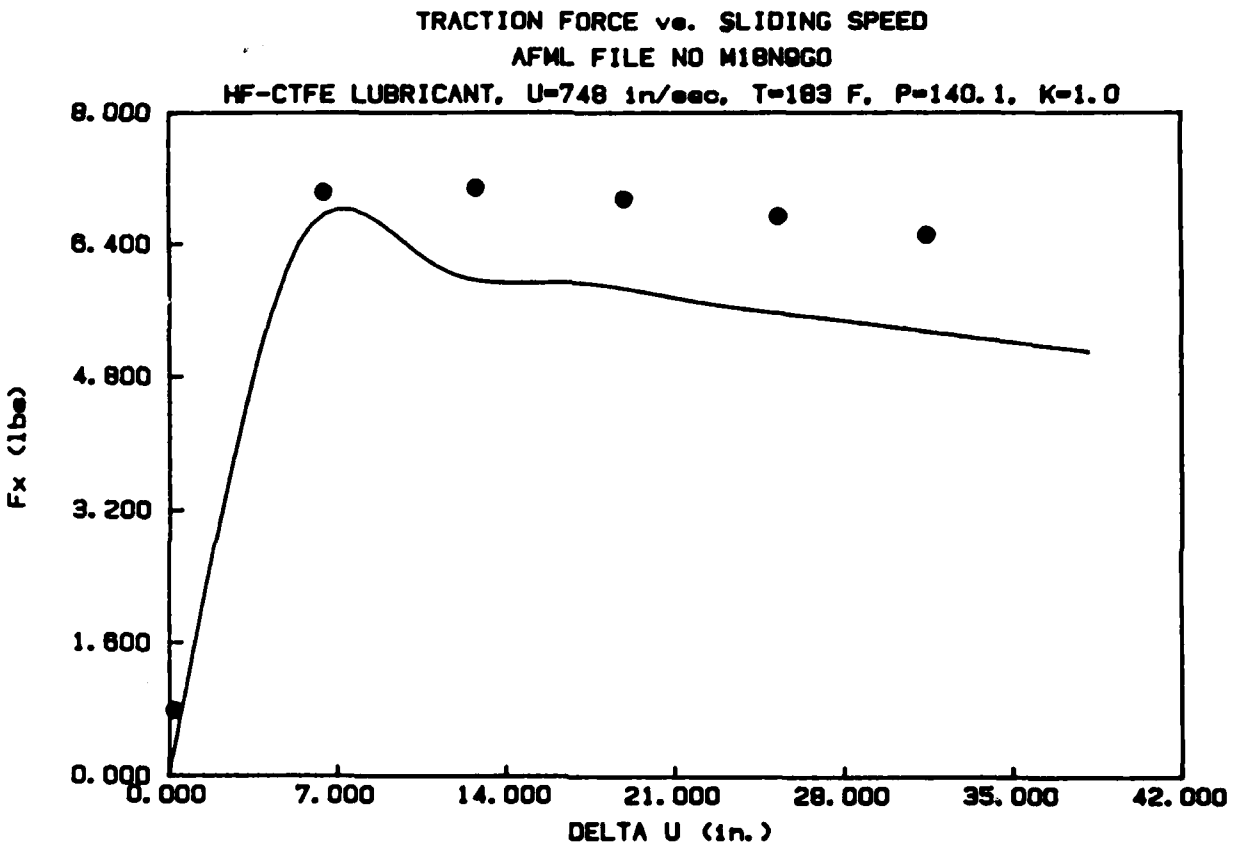

Fig. 10.4

TRACTION FORCE VS. SLIDING SPEED
AFML FILE NO. M18N9GO

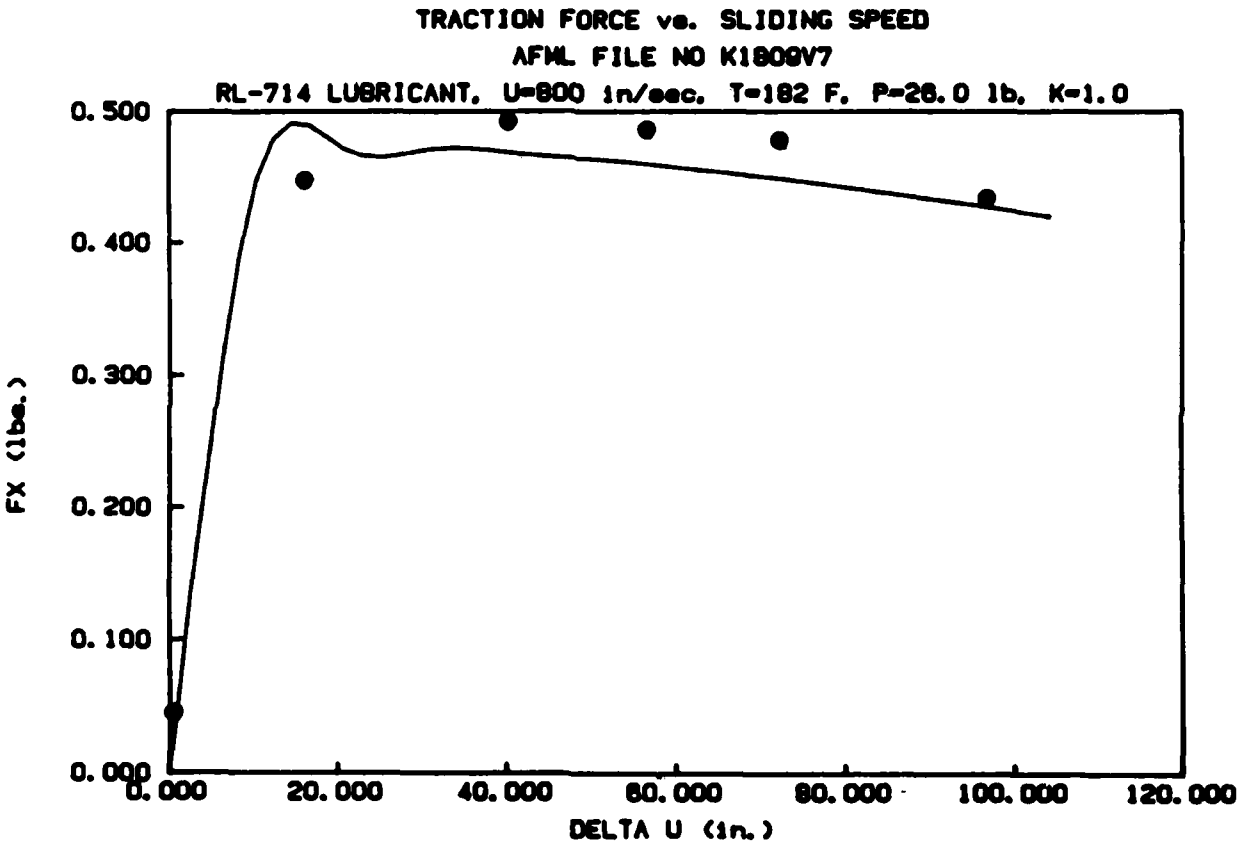

Fig. 10.5

TRACTION FORCE VS. SLIDING SPEED
AFML FILE NO. K1809V7

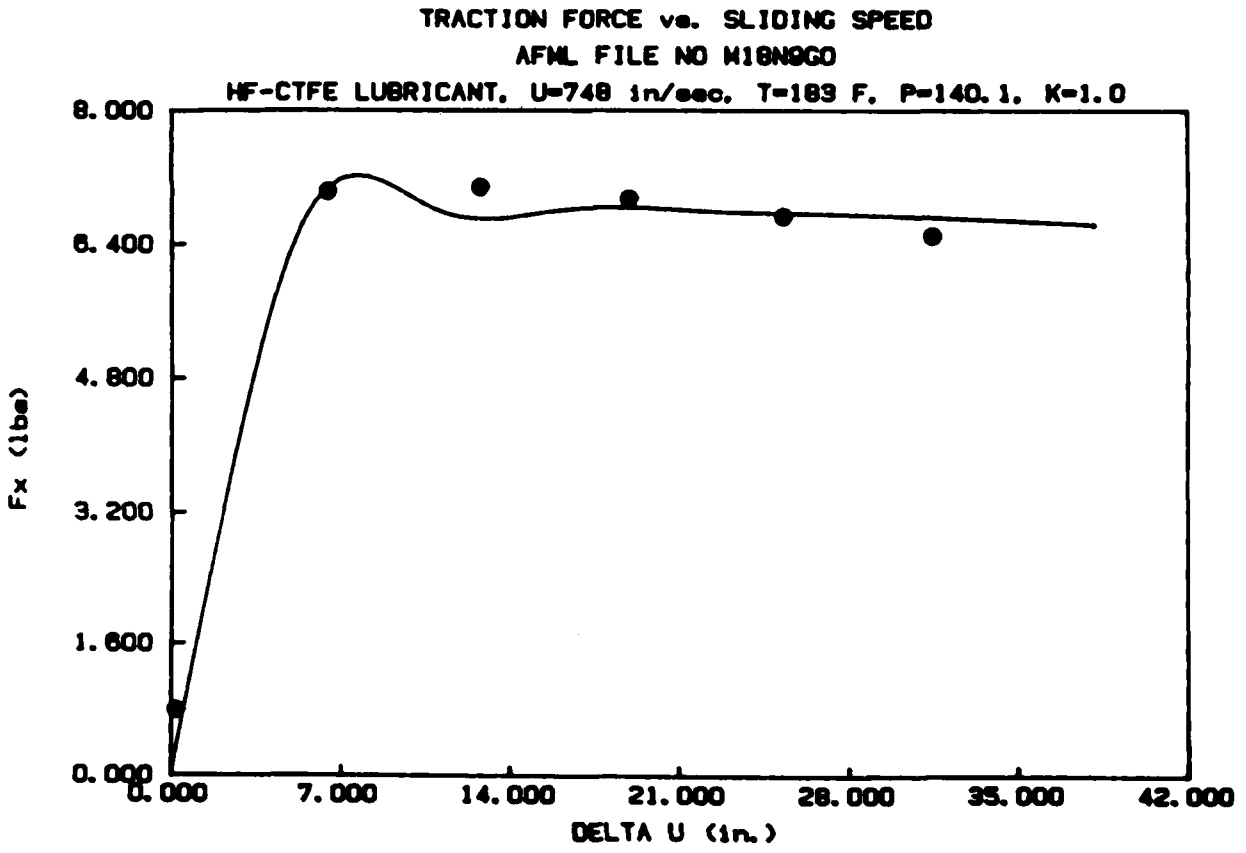

Fig. 10.6

TRACTION FORCE VS. SLIDING SPEED
AFML FILE NO. M18N9GO

The experimental traction data for Santotrac did not exhibit a decrease at high sliding speeds suggestive of a thermal effect.

Figs. 10.7 and 10.8 show, respectively, the experimental and isothermally predicted results for case L28H7P1 which had the lowest calculated Deborah number among the Santotrac tests (12.04), and for case LO8B4WO which had the largest Deborah number value. Both fits are judged to be acceptable.

Fig. 10.9 shows a plot of the results of a thermal run applied to Santotrac case L17H9P1 (Deborah No. = 179) using the original version of the program. Fig. 10.10 shows a thermal run with the modified program. The program output does show a temperature decrease at high sliding, but it is too small to be graphically perceptible.

10.3 Viscoplastic Regime

The most serious discrepancy between predicted traction and experimental traction force values occurred in the 9 CTFE tests for which the Deborah number was less than unity.

These tests were all performed at a nominal temperature of 180°F at which the pressure viscosity index is 7.14E-5 in^2/lb. Fig. 10.11 shows the isothermally predicted and experimental data for File No. M18EOV7 for which the Deborah number value is 0.76. The predicted curve appears to have too low an initial slope and fails to become asymptotic over the range of sliding speeds represented by the experimental data.

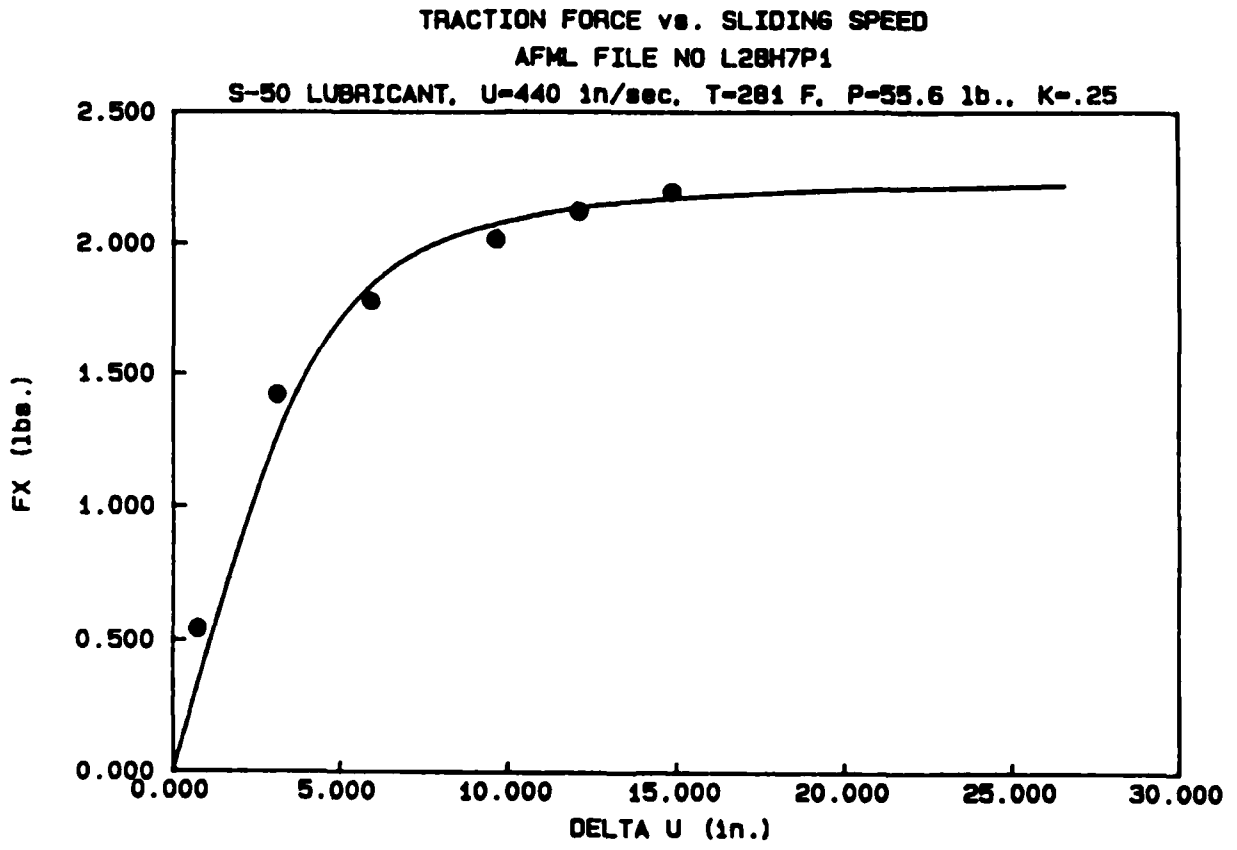

Fig. 10.7

TRACTION FORCE VS. SLIDING SPEED
AFML FILE NO. L28H7P1

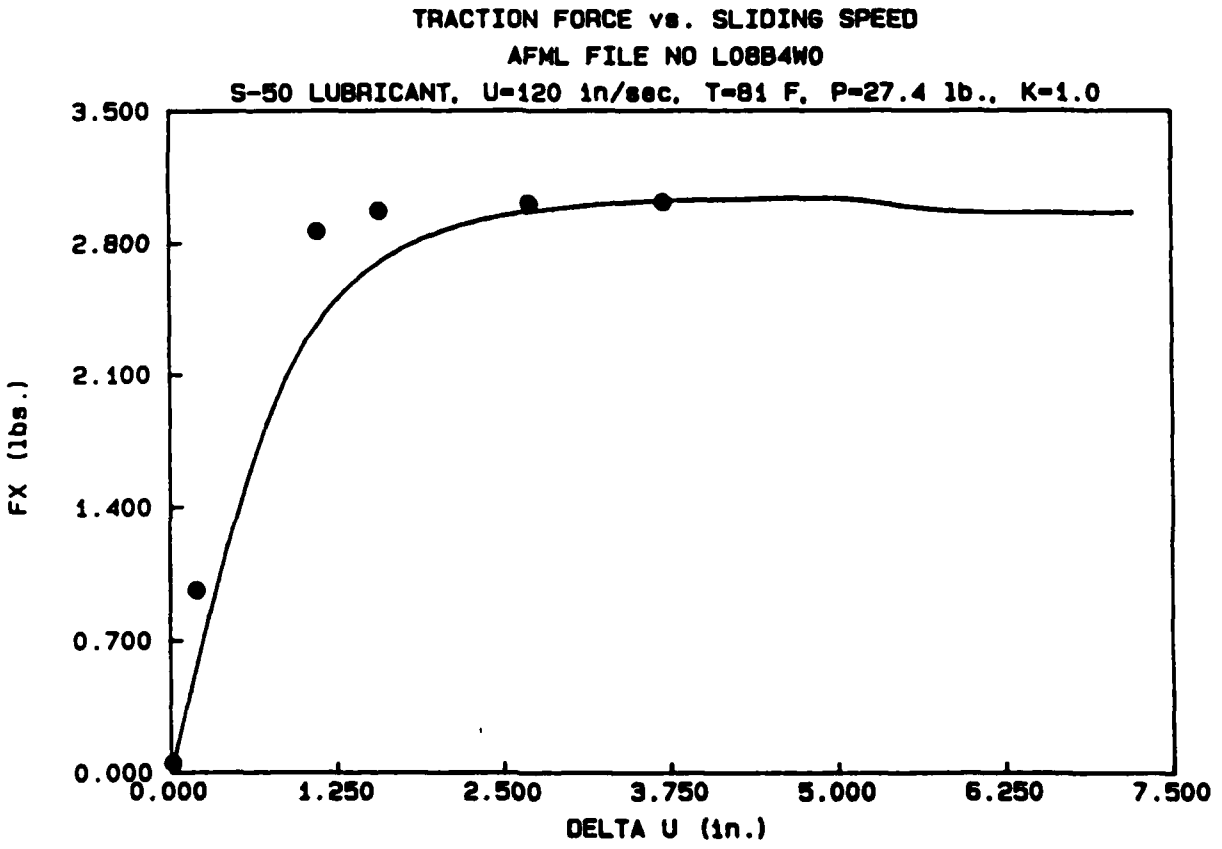

Fig. 10.8

TRACTION FORCE VS. SLIDING SPEED
AFML FILE NO. L08B4WO

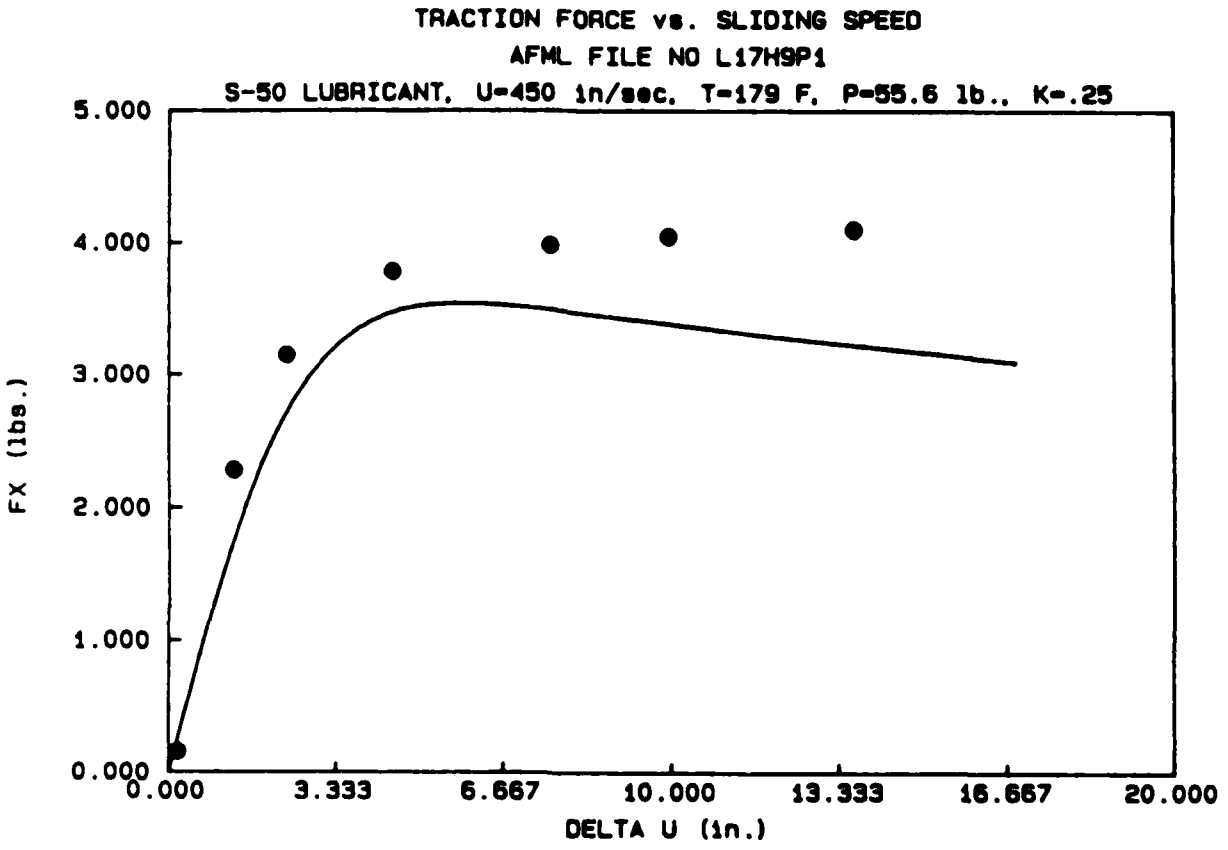

Fig. 10.9

TRACTION FORCE VS. SLIDING SPEED
AFML FILE NO. L17H9P1

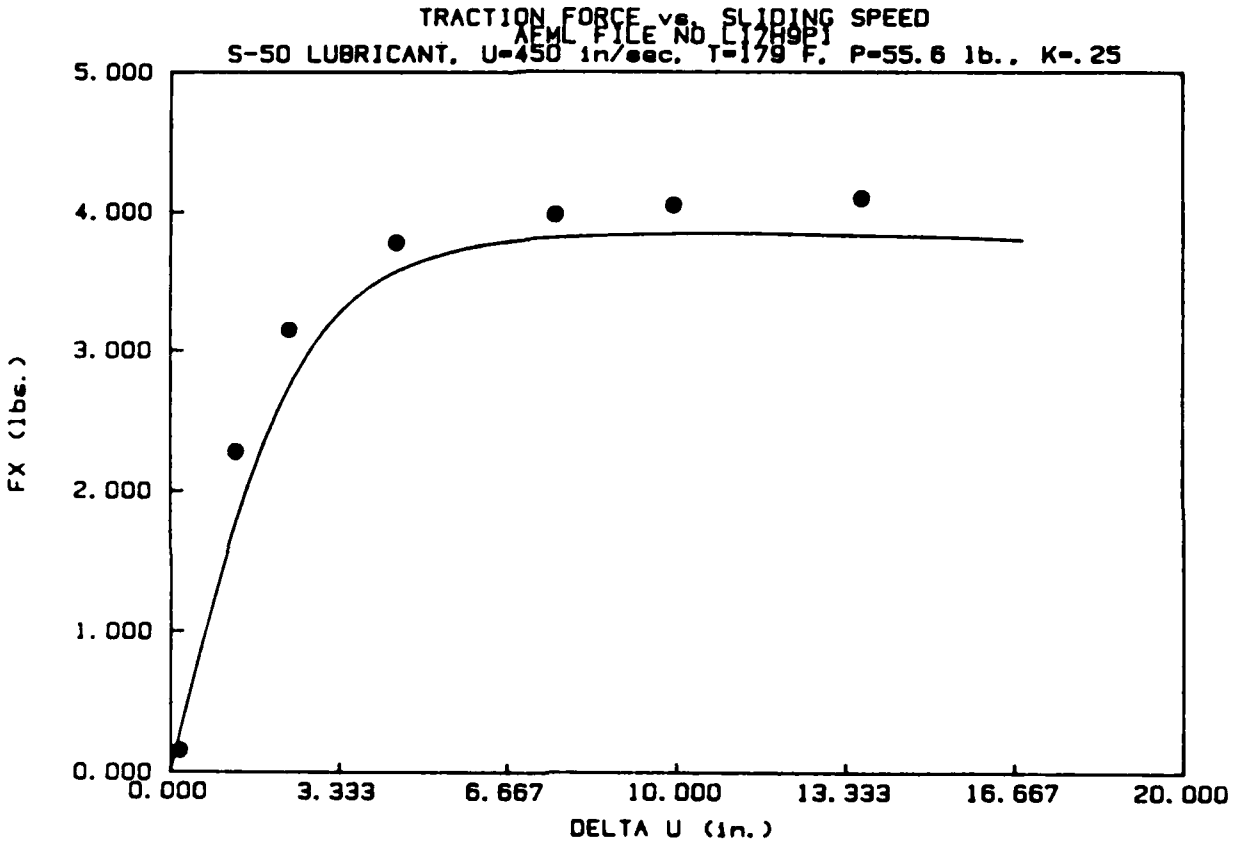

Fig. 10.10

TRACTION FORCE VS. SLIDING SPEED
AFML FILE NO. L17H9P1

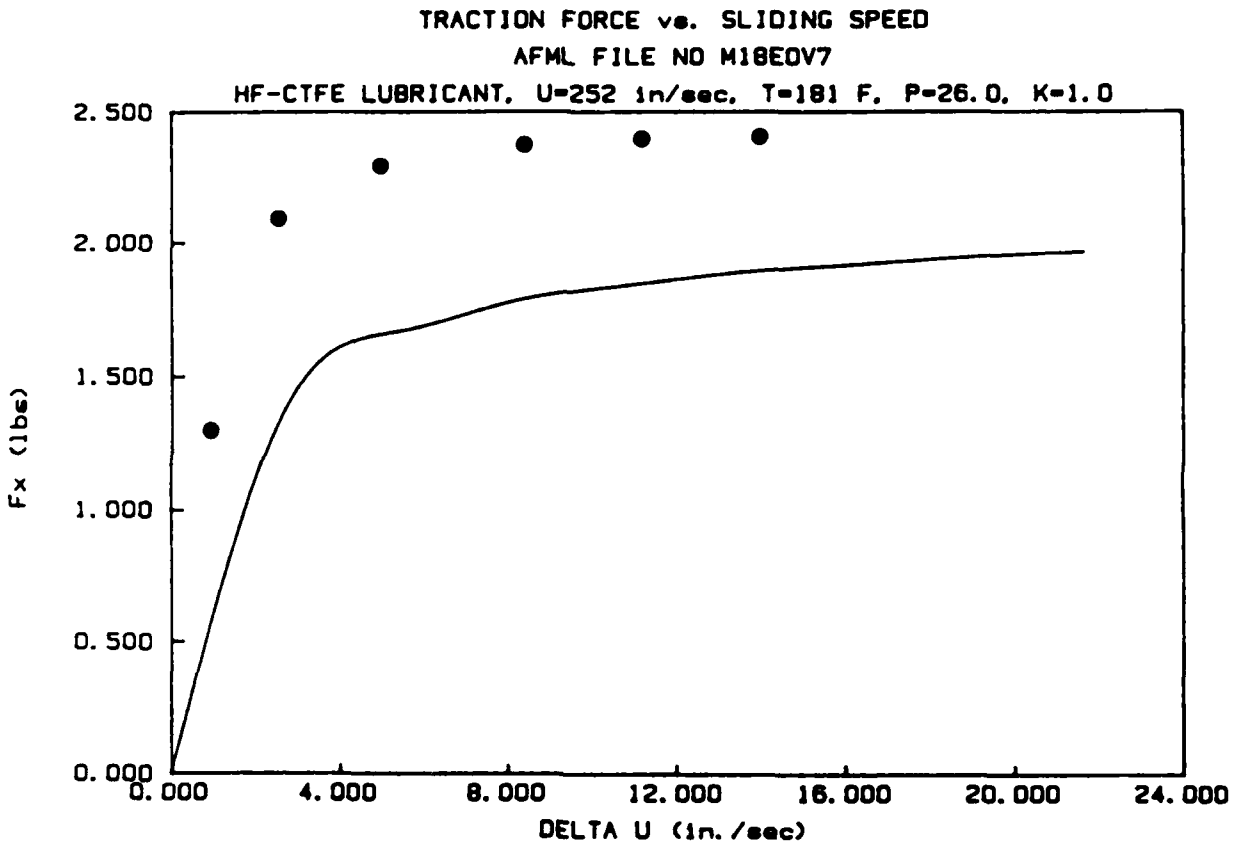

Fig. 10.11

TRACTION FORCE VS. SLIDING SPEED
AFML FILE NO. M18EOV7

As noted in Section 9.4, when operating in the elastic/plastic regime (high Deborah Nos.) the model essentially depends on the two values (slope and maximum coefficient) that come from the experimental curve. The predicted values, therefore, cannot help but reasonably approximate the data. For low Deborah numbers the predicted curve depends, as noted in Section 9.4, on the viscosity $\bar{\eta}$ averaged over the contact area and thus on the ambient viscosity and more problematically, on the relation (Barus' Law) linking pressure and viscosity. An approach was accordingly developed to correct the average viscosity to yield the empirically observed traction behavior in the low Deborah number regime at low sliding rates.

Using Eq. (9.4), one may calculate $\bar{\eta}$ giving the experimentally determined traction curve slope **m**, as:

$$\bar{\eta} = (h\ P/u\ \pi\ a\ b) \bullet m \tag{10.4}$$

Under Barus' Law,

$$\bar{\eta} = 1/\pi\ ab \int_{-b}^{b} \int_{-a(y)}^{a(y)} \eta(x,y)dxdy = 1/\pi\ ab \int_{-b}^{b} \int_{-a(y)}^{a(y)} \eta_o \exp\ [\alpha p(x,y)]dxdy \tag{10.5}$$

where

$$p(x,y) = \sigma_o\ [1-(x/a)^2 - (y/b)^2]^{1/2} \tag{10.6}$$

and

$$a(y) = a[1-(y/b)^2]^{1/2} \tag{10.7}$$

Transforming to

$$Y = y/b$$

and $X = x/a$

gives $\bar{\eta} = \eta_o I_1/\pi$ (10.8)

where

$$I_1 = I_1(\alpha\sigma_o) = \int_{-1}^{1} \int_{-[1-Y^2]^{1/2}}^{1+[1-Y^2]^{1/2}} \exp\ [\alpha\sigma_o[1-X^2-Y^2]^{1/2} dxdy \tag{10.9}$$

For $\alpha = 0$, $I_1(o)$ is the area of the unit circle, i.e. π, so that $\bar{\eta}$ in this case reduces to

$$\bar{\eta} = \eta_o$$

I_1 was evaluated by numerical integration over the range of $\alpha\sigma_o$ from 1.0 to 100. The relationship between I_1 and $\alpha\sigma_o$ was approximated as follows:

$$\ell n I_1 = a + b\ (\alpha\sigma_o) + c(\alpha\sigma_o)^2 \tag{10.10}$$

The values of **a**, **b** and **c** found by least squares over four subintervals from $\alpha\sigma_o$ = 1 to 50, are summarized below:

RANGE OF $\alpha\sigma_o$	a	b	c
1-10	1.0681	0.7390	0.0099
10-20	0.4215	0.8816	0.0018
20-30	-0.0101	0.9257	7.150E-4
40-50	-0.4848	0.9549	2.6146E-4

Using Eq. (10.5) in (10.1), the value of η_o required to make the initial traction curve slope agree with the measured value **m** is

$$\eta_o = (h\ P/I_1\ u\ a\ b) \bullet m \qquad (10.11)$$

Using the data from Table 10.3 for File M18EOV7, the product of $\alpha\sigma_o$ is,

$$\alpha\sigma_o = 212{,}900 \bullet 7.14E\text{-}5 = 15.2$$

The approximate value of I_1 may be computed from Eq. (10.10):

$$\ell n I_1 = 0.4215 + (.8816) \bullet 15.2 + .0018(15.2)^2 = 14.24$$

which gives,

$$I_1 = e^{14.24} = 1.525E6$$

Using this value of I_1 and other variable values from Table 10.3 in Eq. (10.11), the new value of η_o to match the experimental traction curve slope **m** is

$$\eta_o = \frac{3E\text{-}6 \bullet 26 \bullet 13.7}{1.52E6 \bullet 252 \bullet 7.78E\text{-}3 \bullet 750E\text{-}3}$$

$$= 4.765E\text{-}8$$

This value is lower than the value 3.35E-7 of the ambient viscosity η_o listed in Table 10.3 and obtained from viscometer readings.

The average viscosity is thus not the source of the low initial slope of the traction curve in Fig. 10.11.

10.4 The Trachman-Cheng Viscous Model

The problem appears to be inherent in the Trachman-Cheng nonlinear viscous law which, written in terms of the average viscosity and yield strength is:

$$\tau = \bar{\eta} / (\bar{\eta}/\bar{\tau}_c + 1/\dot{\gamma}) \qquad (10.12)$$

As noted τ approaches $\bar{\tau}_c$ as $\dot{\gamma}$ increases, but the rate of approach appears too slow. This may be seen in Fig. 10.12 which is a replot of Fig. 10.11 with a wider range of sliding velocities. The rate of change of τ with respect to $\dot{\gamma}$ is, in fact,

$$d\tau/d\dot{\gamma} = \bar{\eta} / (\bar{\eta}/\tau_c\dot{\gamma} + 1)^2 \qquad (10.13)$$

At $\gamma = 0$,

$$d\tau/d\dot{\gamma} = \bar{\eta} \qquad (10.14)$$

Even if the slope $\bar{\eta}$ is correct at low $\dot{\gamma}$ values, it decreases with $\dot{\gamma}$ at a rate which can be quite slow if $\bar{\eta}/\bar{\tau}_c$ is large.

An approach that might be usefully pursued is to develop a lubricant dependent convergence factor k such that the above relationship becomes

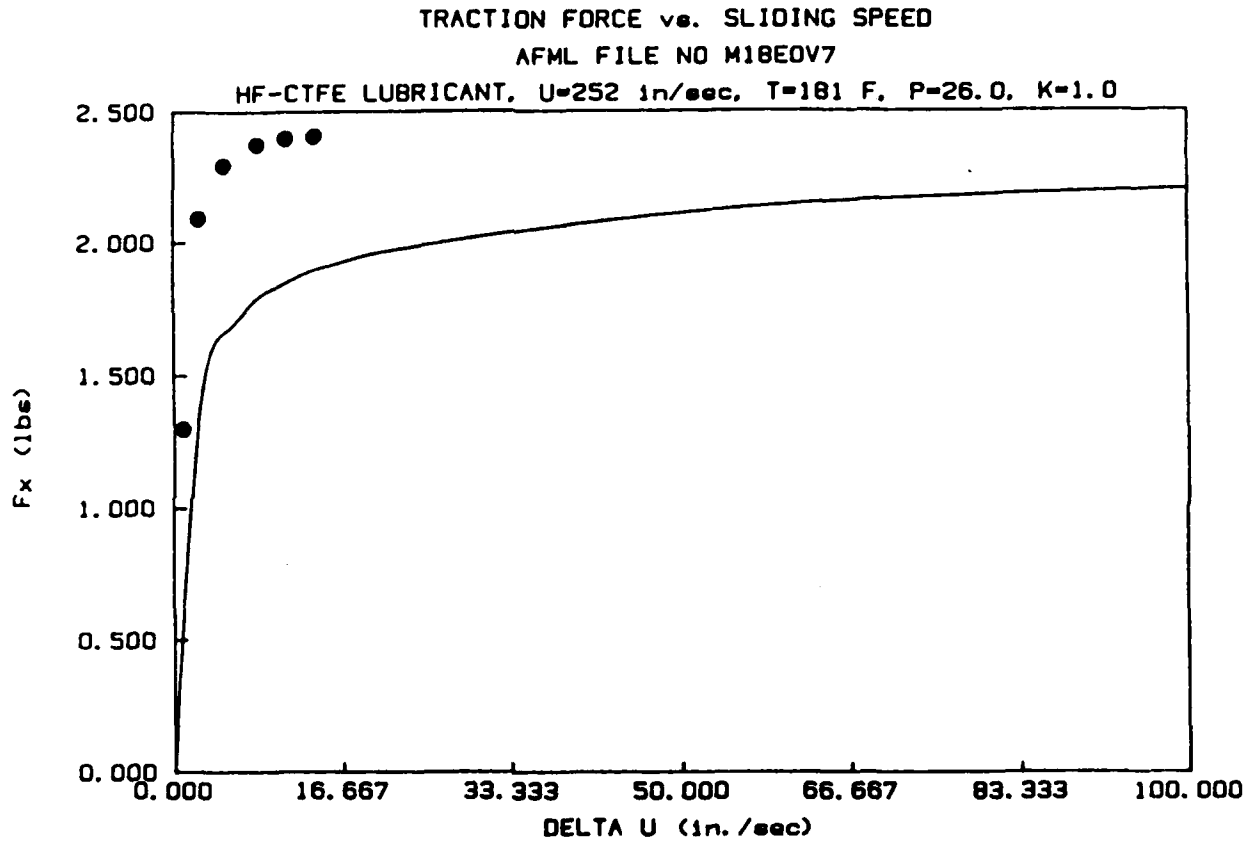

Fig. 10.12

TRACTION FORCE VS. SLIDING SPEED
AFML FILE NO. M18EOV7

$$\tau = \bar{\eta}/(\bar{\eta}/\bar{\tau}_c + 1/k\dot{\gamma}) \qquad (10.15)$$

This value could "tune" the approach to the asymptotic limiting stress τ_c. Such a factor would be analogous to the parameter τ_o which appears in the Ree-Eyring model and determines where nonlinearity sets in. It is recommended that this or comparable alternative approaches for modulating the rate of convergence to $\bar{\tau}_c$ in the viscoplastic regime be examined in future work.

10.5 Alternative Approach to Speeding Convergence Rate

A different approach that does not involve a fundamental change in the rheological model was considered for restraining the viscoplastically predicted traction curve from becoming asymptotic too slowly with strain rate.

As discussed, the empirically measured traction curve has a slope m at low Δu and approaches an asymptote at which $\tau = \tau_c$. Projecting the straight line portion of the traction curve it can be deduced that the traction curve becomes horizontal at a slide-to-roll ratio $\Delta u/u$ in the vicinity of:

$$\Delta u/u = \mu_{max}/m \qquad (10.16)$$

The shear rate at this point is thus

$$\dot{\gamma} = \Delta u/h = u\ \mu_{max}/mh \qquad (10.17)$$

It is reasonable to require that τ given by the T-C relation has risen to nearly the value $\tau = \bar{\tau}_c$ at this shear rate. Taking $\tau = 0.99\bar{\tau}_c$ and using Eq. (10.17) in (10.12) gives

$$0.99\ \bar{\tau}_c = \bar{\eta}/(\bar{\eta}/\bar{\tau}_c + mh/u\ \mu_{max}) \tag{10.18}$$

Solving for $\bar{\eta}$ gives,

$$\bar{\eta} = 99\bar{\tau}_c\ m\ h/u\ \mu_{max} \tag{10.19}$$

Using $\mu_{max} = F_x/P$ where

$$F_x = \bar{\tau}_c \bullet \pi ab \tag{10.20}$$

and **P** may be written

$$P = 2/3\ \sigma_o \bullet \pi ab \tag{10.21}$$

so that

$$\mu_{max} = 1.5\ \bar{\tau}_c/\sigma_o \tag{10.22}$$

giving

$$\bar{\eta} = 99\ mh\sigma_o\ /(u \bullet 1.5) \tag{10.23}$$

It is recalled that the G value input to the program is deduced from the empirically measured value of **m** under the assumption that the linear portion of the traction curve is due to elastic deformation. From Eq. (9.6), **m** may be re-expressed as

$$m = 8\ a^2\ bG/3Ph = 4\ aG/\pi\ h\ \sigma_o \tag{10.24}$$

Using (10.24) in (10.19) results in

$$\bar{\eta} = (8 \bullet 99)/3 \bullet (aG/\pi\, u) \qquad (10.25)$$

Using Eq. 10.5, this gives the modified ambient viscosity value η_o' of

$$\eta_o' = 264\ aG/u\ I_1$$

Using the values from Table 10.3, this calculates out to,

$$\eta_o' = \frac{264 \bullet 7.78E\text{-}3 \bullet 883.5}{252 \bullet 1.52E6} = 4.74E\text{-}6 \qquad (10.26)$$

Using this value of η_o in the traction calculation (but not in the film thickness calculation) results in the excellent fit shown in Fig. 10.13. A recomputation in this manner has been incorporated into McFRIC and is used wherever the Deborah number falls below unity.

The nature of this "fix" is revealed by Eq. (10.25) which may be written as

$$\eta u/aG = 84$$

This, except for the difference in computation of η, is the Deborah number. The fix, therefore, amounts to changing low Deborah numbers to large Deborah numbers, thereby causing the traction curve slope at low slip to be determined by the elastic modulus.

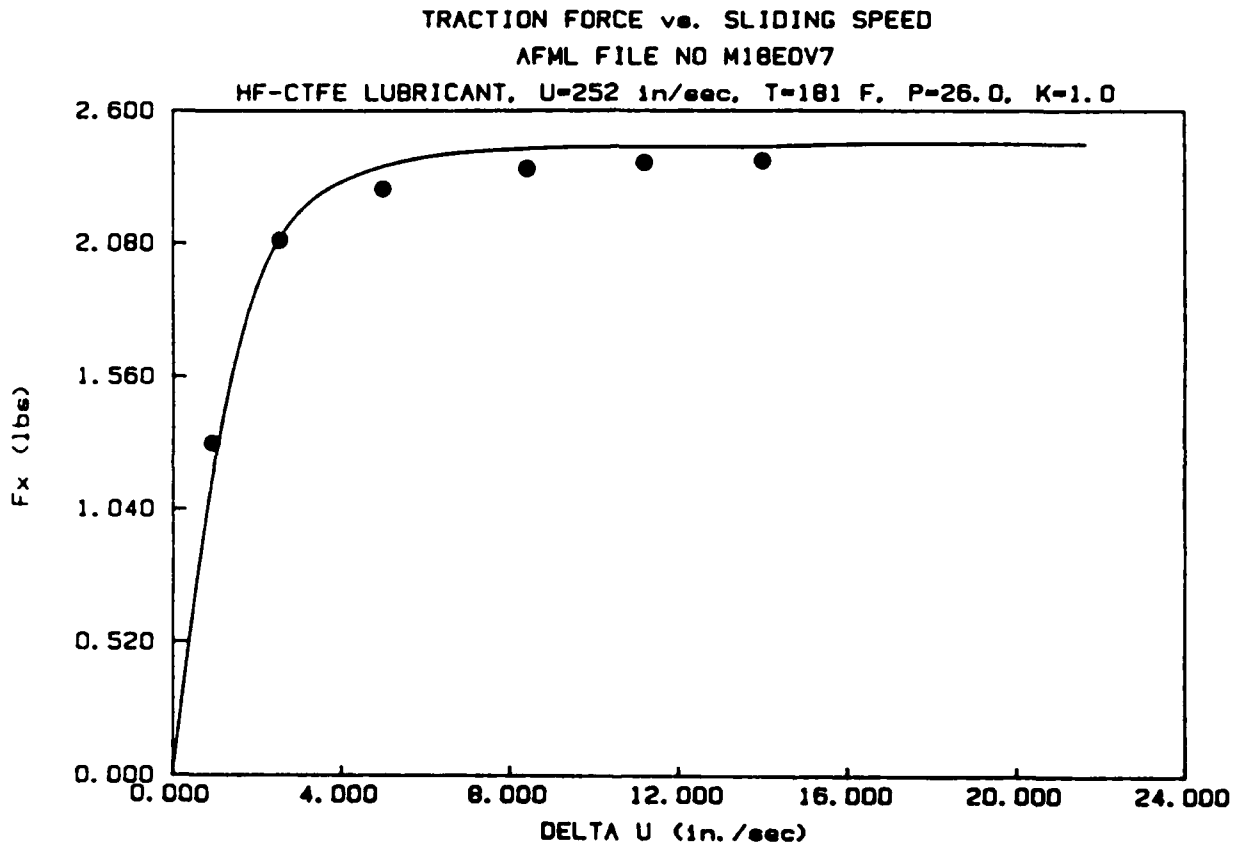

Fig. 10.13

TRACTION FORCE VS. SLIDING SPEED
AFML FILE NO. M18EOV7

Whether this is correct cannot be judged with the present data. It is necessary, following Johnson and Roberts [14] to measure lateral force in the presence of spin to distinguish elastic and viscous behavior. As it stands the program as modified is capable of predicting the results of simple traction tests for all three test oils.

10.6 Estimating G and $\bar{\tau}_c$

McFRIC requires input data namely **G** and $\bar{\tau}_c$, that must be deduced from traction tests conducted at the contact conditions of interest.

To overcome this, equations were fitted to the traction data using stepwise linear regression in order to express the limiting shear stress and shear modulus as functions of temperature **T** (°F), maximum Hertz pressure **p** (psi), aspect ratio (AR), and rolling velocity **U** (in/sec).

The coefficients in the relationships thus determined are tabled below for each of the three oils.

LUBRICANT	CONSTANT	U	T	AR	p
RL-714	365.7	1.05	-6.28	379.3	0.0018
Santotrac 50	11576	7.97	-53.4	0	0
CTFE	651.4		-12.8	1627	0.0079

Coefficients for G Equation

LUBRICANT	CONSTANT	U	T	AR	p
RL-714	-1736	-1.926	-7.987	0	0.0334
Santotrac 50	3937	-7.846	0	5538	0.0322
CTFE	1599	-7.017	0	6258	0.0272

Coefficients for $\bar{\tau}_c$ Equation

Application of these equations to the data used in their development gave reasonably good predictions. If, however, G or $\bar{\tau}_c$ was small, the above equations occasionally gave negative values.

The equations may be expected to be most reliable for conditions which fall between the extremes of the data used in their development.

REFERENCES

1. Hamrock, B. J. and Dowson, D., "Isothermal Elastohydrodynamic Lubrication of Point Contacts, Part III - Fully Flooded Results," J. Lub. Technology, Vol. 99, No. 2, pp. 264-276 (April 1977).

2. Murch, L. E. and Wilson, W.R.D., "A Thermal Elastohydrodynamics Inlet Zone Analysis," Trans. ASME, J. Lub. Tech., 97F, No. 2, p. 272 (1975).

3. Hertz, H., "On the Contact of Rigid Elastic Solids and on Hardness," Miscellaneous Papers, MacMillan & Co., London, pp. 163-183 (1896).

4. Tevaarwerk, J. L. and Johnson, K. L., "The Influence of Fluid Rheology on the Performance of Traction Drives," ASME J. Lub. Tech., Vol. 101, p. 266 (1979).

5. Bair, S. and Winer, W. O., "Some Observations in High Pressure Rheology of Lubricants," J. Lub. Tech., Vol. 104, No. 3, pp. 357-364 (1982).

6. Greenwood, J. A. and Williamson, J., "Contact of Two Nominally Flat Rough Surfaces," Proc. Roy. Soc. London, Ser. A, 295, pp. 300-319 (1966).

7. McCool, J. I., "Relating Profile Instrument Measurements to the Functional Performance of Rough Surfaces," ASME J. of Tribology, Vol. 109, No. 2, pp. 264-270 (1987).

8. McCool, J. I., "Comparison of Models for the Contact of Rough Surfaces," Wear, 107, pp. 37-60 (1986).

9. Longuet-Higgins, M. S., "The Statistical Analysis of a Random, Moving Surface," Philos. Trans. Royal Soc., Ser. A, 249, pp. 321-387 (1957).

10. Bush, A. W., Gibson, R. D. and Keogh, G., "The Limit of Elastic Deformation in the Contact of Rough Surfaces," Mec. Res. Commun., 3, pp. 169-174 (1976).

11. Sayles, R. S. and Thomas, T. R., "Thermal Conductance of a Rough Elastic Contact," Appl. Energy, 2, pp 249-267 (1976).

12. Wedeven, L. D. and Cusano, C., "Elastohydrodynamic Contacts - Effects of Dents and Grooves on Traction and Local Film Thickness," NASA Technical Paper 2175, June 1983.

13. McCool, J. I., "Traction Model Development," Air Force Materials Lab, Technical Report No. AFWAL-TR-85-4142, (May 1986).

14. Johnson, K. L. and Roberts, A. D., "Observations of Viscoelastic Behavior of an Elastohydrodynamic Lubricant Film," Proc. Roy. Soc. London, Ser. A., Vol. 337, No. 1609, pp. 217-242 (March 1974).

15. Gentle, C. and Boness, R., "Prediction of Ball Motion in High Speed Thrust Loaded Ball Bearings," ASME Trans., J. Lub. Tech., pp. 463-470 (1976).

16. Johnson, K. L. and Tevaarwerk, J. L., "Shear Behavior of Elastohydrodynamic Oil Films," Proc. Roy. Soc. London, Ser. A., Vol. 356, No. 1685, pp. 215-236 (Aug. 1977).

17. Trachman, E. G. and Cheng, H. S., "Thermal and Non-Newtonian Effects on Traction in Elastohydrodynamic Contacts," Proc. Inst. Mech. Engrs., Elastohydrodynamic Lubrication: 1972 Symposium, p. 142 (1974).

18. Trachman, E. G. and Cheng, H. S., "Traction in Elastohydrodynamic Line Contacts for Two Synthesized Hydrocarbon Fluids," ASLE Transactions, Vol. 17, No. 4, pp. 271-279 (1974).

19. McCool, J. I. "TRIBOS: A Performance Evaluation Tool for Traction Transmitting Partial EHD Contacts," ASLE Trans., Vol. 29, No. 3, pp. 432-440 (1986).

20. Houpert, L., "Fast Numerical Calculations of EHD Sliding Traction Forces; Application to Rolling Bearings," ASME Trans., J. of Tribology, Vol. 17, pp. 234-240 (1985).

21. Houpert, L., "Contribution a`l'étude frottement dans un contact élastohydrodynamique," These de Docteur Ingenieur No. IDI.3-8019, I.N.S.A., Lyon, (1980).

22. Archard, J. F., "The Temperature of Rubbing Surfaces," Wear, Vol. 2, pp. 438-455 (1958).

23. Lingard, S., "Tractions at the Spinning Point Contacts of a Variable Ratio Friction Drive," Tribology International, pp. 228-234 (1974).

24. L. Houpert, Personal Communication

25. Smith, R. L., "Development of a Lubricant Traction Measuring Device," Technical Report No. AFWAL-TR-81-4102, Air Force Materials Laboratory, Wright-Patterson AFB, OH (1981).

26. Kresge, K.C., Mobil Research and Development Co., Private Communication to S. Sharma, March 8, 1984.

27. Anonymous, SANTOTRAC, Monsanto Corporation, Trade Pubication IC/FP-28R (undated).

28. Sharma, S. K., "Ambient Properties of CTFE," unpublished memorandum, (1984).

29. Jones, W., Johnson, R., Winer, W. O., and Sanborn, D., "Pressure Viscosity Measurements for Several Lubricants to 5.5×10^8 Newtons Per Square Meter (8×10^4 psi) and 149°C (300°F)," ASLE Trans., Vol. 18, No. 4, pp. 249-262.

30. Sharma, S. K., "Traction Data/Ambient Properties," Personal Communication, (June 5, 1986).

U.S. GPO 548-054

END
DATE
FILMD
3-88
DTIC